

Aus dem
Walter-Brendel Zentrum für experimentelle Medizin
Direktor: Prof. Dr. med. dent Reinhard HICKEL

**ENDOTHELIAL ACTIN DYNAMICS IN
ANGIOGENESIS ASSESSED THROUGH
ACTIN VISUALIZATION *IN VIVO* &
FUNCTIONAL α -PARVIN CHARACTERIZATION**



Dissertation
Zum Erwerb des Doktorgrades der Medizin
An der Medizinischen Fakultät der Ludwig-Maximilians-Universität München

Alessia Fraccaroli
(Bruneck, Italien)
2017

Mit Genehmigung der Medizinischen Fakultät
der Universität München

Berichterstatter: Prof. Dr.med. Ulrich Pohl

Mitberichterstatter: PD Dr. Annette Müller-Taubenberg
Univ.-Prof. Dr. med Christian Weber
PD Dr. rer. nat. Gerald Schmid

Mitbetreuung durch den
promovierten Mitarbeiter: Dr. Eloi Montanez

Dekan: Prof. Dr. med. dent. Reinhard Hickel

Tag der mündlichen Prüfung: 19.10.2017

Eidesstattliche Erklärung

Die Versuche zur vorgelegten Dissertation wurden in der Zeit von Februar 2012 bis Februar 2015 in der Arbeitsgruppe „*vascular biology*“ von Dr. Eloi Montanez am Walter-Brendel Zentrum für experimentelle Medizin der LMU München durchgeführt.

Hiermit erkläre ich, dass ich diese Arbeit selbstständig und nur unter Verwendung der angegebenen Quellen und Hilfsmittel angefertigt habe. Alle Erkenntnisse, die aus dem Schrifttum ganz oder annähernd übernommen sind, wurden als solche kenntlich gemacht und nach ihrer Herkunft unter Bezeichnung der Fundstelle einzeln nachweisbar gemacht. Die Abbildungen im Ergebnisteil, welche die Lifeact-EGFP Daten präsentieren sind aus Fraccaroli et al., Plos One 2012 entnommen worden. Ebenso die Abbildungen (Fig.) 18, 19, 20, und 21 aus Fraccaroli et al., Circulation Research 2015.

Weiteres erkläre ich, dass die hier vorgelegte Dissertation nicht in gleicher oder in ähnlicher Form bei einer anderen Stelle zur Erlangung eines akademischen Grades eingereicht wurde.

München, den

Alessia Fraccaroli

An meine Großmutter...

TABLE OF CONTENTS:

Eidesstattliche Erklärung	I
Table of contents	III
Abbreviations	VI
List of tables, illustrations and figures	XI
1. Introduction	1
1.1 Vessel development	1
1.1.1 Hallmarks of sprouting angiogenesis	3
1.2 The cytoskeleton – a cell’s framework	5
1.2.1 The actin cytoskeleton in angiogenesis	5
1.2.2 The actin cytoskeleton and its dynamics	7
1.2.3 Impaired actin dynamics in vascular dysfunctions	9
1.2.4 Visualization of the Actin cytoskeleton	10
1.3 The Integrins – integrating the outside with the inside	11
1.3.1 Integrin signaling – bidirectional, across the membrane	12
1.3.2 Integrin signaling in angiogenesis	15
1.4 The IPP complex in angiogenesis	17
1.4.1 Integrin linked kinase in angiogenesis	17
1.5 The Parvin	18
2. Aims	21
3. Materials and Methods	22
3.1 Materials	22
3.1.1 Reagents and Chemicals	22

TABLE OF CONTENTS

3.1.2 Kits	23
3.1.3 Antibodies	24
3.1.4 Solutions	25
3.1.5 Media	27
3.1.6 Oligonucleotides	27
3.1.7 Equipment and disposals	28
3.2 Animals	29
3.2.1 Lifeact-EGFP transgenic mice	29
3.2.2 Inducible α -pv knockout mice	29
3.3 Postnatal mouse retina as an angiogenesis model	31
3.3.1 Whole retina immunohistochemistry	33
3.3.2 Proliferation assay	34
3.4 Immunohistochemistry in other tissues	35
3.4.1 Whole embryo immunohistochemistry	35
3.4.2 Skin immunohistochemistry	35
3.4.3 Skeletal muscle IHC/cremaster <i>in vivo</i> microscopy	35
3.5. Molecular biology methods	36
3.5.1 DNA isolation of mouse ear biopsies	36
3.5.2 Polymerase chain reaction	36
3.5.3 Agarose gel electrophoresis	37
3.6 Cell culture	37
3.6.1 Freezing and thawing of cells	37
3.6.2 Cell lines	38
3.6.3 siRNA Transfection	38
3.6.4 Protein lysis	38
3.6.5 Protein quantification: Bicinchoninic acid assay	39
3.6.6 SDS page	39
3.6.7 Immunoblot	39
3.6.8 Immunofluorescence of cells	40
3.7 Microscopic models	40
3.7.1 Confocal microscopy	40
3.7.2 <i>In vivo</i> microscopy	41
3.8 Statistical analysis	41
4 Results	42

TABLE OF CONTENTS

4.1 Imaging of endothelial actin cytoskeleton	42
4.2 Functional α -pv characterization	54
5. Statement of contributions	66
6. Discussion	67
7. Summary	76
8. Zusammenfassung	78
9. References	80
Danksagung	84

ABBREVIATIONS:

Aa	Amino acid
a.k.a	Also known as
ABD	Actin binding domain
ABP	Actin binding protein
AC	Astrocyte
ADP	Adenosine diphosphate
AJ	Adherent junction
Arp2/3 complex	Actin related protein 2/3 complex
ATP	Adenosine triphosphate
ATPase	Adenosine triphosphatase
AV	Arterial-venous
BCA	Bicinchoninic acid
BM	Basement membrane
BrdU	Bromodeoxyuridine
BSA	Bovine serum albumin
CAG	Chicken- β -actin
CD31	Cluster of differentiation glycoprotein 31
Cdc42	Cell division cycle 42
CdGAP	Cdc42 GTPase activating protein
Cdh5	Cadherin 5
CH (domain)	Calponin homology (domain)
Coll	Collagen
CMV	cytomegalovirus

ABBREVIATIONS

CVS	Cardiovascular system
Cy3	Cyanine dye 3
Dll-4	Delta like ligand-4
DMSO	Dimethyl sulfoxide
DNA	Deoxyribonucleic acid
E	Embryonic day
EC	Endothelial cell
ECM	Extracellular matrix
EDTA	Ethylenediaminetetraacetic acid
EGFP	Enhanced green fluorescent protein
EPC	Endothelial precursor cell (angioblast)
ERK	Extracellular signal regulated kinase
EtBr	Ethidiumbromide
F-actin	Actin filaments
FA	Focal adhesions
FCS	Fetal calf serum
FITC	Fluorescein-5-isothiocyanat
Fl	floxed
FN	Fibronectin
FX	Focal complex
G-actin	Globular actin
GAP	GTPase activating protein
GAPDH	Glycerinaldehyd-3-phosphate-dehydrogenase encoding gene
GDI	Guanine nucleotide dissociation inhibitor
GDP	Guanosine diphosphate
GEF	Guanine nucleotide exchange factor
Gel	Gelatin
GFAP	Glial fibrillar protein
GFP	Green fluorescent protein
GSK3 β	Glykogen synthase kinase 3 beta
GTP	Guanosine triphosphate
GTPase	Guanosine triphosphatase
H&E	Hematoxylin and eosin stain

ABBREVIATIONS

HUVEC	Human umbilical vein endothelial cell
IB4	Isolectin B4
ICAM-2	Intercellular adhesion molecule 2
IF	Immunofluorescence
Ig	Immunoglobulin
ILK	Integrin-linked kinase
OP	intraperitoneal
IPP complex	ILK-PINCH-Parvin complex
JAIL	Junction-associated intermittent lamellipodia
JNK	Jun-amino-terminal kinase
kDa	Kilo Dalton
KO	Knockout
LN	Laminin
M	molar
MAPK	Mitogen activated protein kinase
MMP	metalloproteases
MRTF	Myocardin related transcription factor
mTOR	Mammalian target of rapamycin
nM	nanomolar
n.s	Non significant
NG2	Anti-neuron glial 2
NFκB	Nuclear-factor κB
OD	Optical density
ORF	Open reading frame
P	Postnatal day
Pax	Paxillin
PBS	Phosphate buffered saline
PC(s)	Pericyte(s)
PCR	Polymerase chain reaction
PECAM-1	Platelet endothelial cell adhesion molecule-1
PFA	Paraformaldehyde
PI3K	Phosphoinositide-3-kinase
PINCH	Particularly interesting Cys-His-rich protein
PKB	Protein-kinase B

ABBREVIATIONS

PM	Plasmamembrane
PS	Penicillin/Streptomycin
Pv	Parvin
Rac1	Ras-related C3 botulinum toxin substrate 1
Ras	Rat sarcoma
RGD	Arginine-glycine-aspartatic acid
RhoA	Ras homologous
RNA	Ribonucleic acid
RIPA	Radioimmunoprecipitation assay
RNA	Ribonucleic acid
ROCK	Rho associated kinase
RPM	Rounds per minute
RT	Room temperature
RTK	Receptor tyrosine kinase
s	second
Scr siRNA	Scrambled small interfering RNA
SD	Standard deviation
SDS	Sodium dodecyl sulfate
SDS-PAGE	Sodium dodecylsulfate polyacrylamide gel electrophoresis
SEM	Standard error of the mean
siRNA	Small interfering RNA
SRF	Serum response factor
SSC	Saline-sodium-citrate
TAE	Tris-acetate-EDTA
TBS	Tris-buffered saline
TBST	Tris-buffered saline and Tween 20
Tie2	Tyrosine kinase with immunoglobuline-like and EGF-like domains -2
TM	Tissue macrophages
U	unit
UV	ultraviolet
VE-Cad	Vascular endothelial-cadherin
VEGF	Vascular endothelial growth factor

ABBREVIATIONS

VEGFR-2	VEGF Receptor-2
vMC	Vascular mural cells
VN	vitronectin
vs.	versus
vSMC	Vascular smooth muscle cells
WASP	Wiskott Aldrich syndrome protein
WB	Western Blot
WHO	World health organization
WT	Wildtype
YS	Yolk sacs
α -pv	Alpha-parvin
α -pv ^{fl/fl}	α -pv ^{floxed/floxed}
α -pv ^{ΔEC}	Endothelial specific knockout of α -pv gene
α SMA	Alpha smooth muscle actin
β -cat	Beta-catenin
β -pv	Beta-parvin
γ -pv	Gamma parvin
dNTPs	Deoxynucleotides
μ M	Micromolar
cm	Centimeter
2D	Two dimensional
μ g	Microgram

LIST of ILLUSTRATIONS, TABLES AND FIGURES:

Illustrations

- | | |
|---------|--|
| III. 1 | The vascular cell types |
| III. 2 | The tip and the stalk cell |
| III. 3 | Hallmarks of sprouting angiogenesis |
| III. 4 | Specialized actin structures in migrating ECs |
| III. 5 | Actin polymerization |
| III. 6 | Actin dynamics regulate gene expression via SRF |
| III. 7 | Integrin receptor family |
| III. 8 | Bidirectional integrin signaling |
| III. 9 | Integrin signaling |
| III. 10 | The IPP complex |
| III. 11 | Integrins in angiogenesis – a hypothetical model |
| III. 12 | Vector fragment containing Lifeact-EGFP |
| III. 13 | Site-specific recombinase technology |
| III.14 | 2D-Imaging of retinal angiogenesis |
| III. 15 | Postnatal mouse retina angiogenesis model |

Tables

LIST OF ILLUSTRATIONS, TABLES AND FIGURES

Table 1	Reagents and chemicals
Table 2	Kits
Table 3	Antibodies
Table 4	Solutions
Table 5	Media
Table 6	Oligonucleotides
Table 7	Equipment and disposals

Figures

Fig. 1	Lifact-EGFP is ubiquitously expressed during embryogenesis
Fig. 2	Lifact-EGFP is highly expressed in EC but practically absent from AC in the postnatal retina of Lifact EGFP mice
Fig. 3	Lifact-EGFP expression is nearly absent in retinal tissue macrophages
Fig. 4	Lifact-EGFP is weakly expressed in vMC of the retinal vasculature
Fig. 5	Lifact-EGFP mice allow visualization of F-actin structures in vMC in skin and cremaster muscle
Fig. 6	Postcapillary venues in the cremaster muscle from Lifact-EGFP mouse
Fig. 7	Lifact-EGFP colocalizes with phalloidin
Fig. 8	Lifact-EGFP labels cortical actin, filopodia and stress fibers in retinal tip and stalk EC
Fig. 9	Visualization of endothelial actin cytoskeleton in a sprout
Fig. 10	Lifact-EGFP is a marker for apical-basal cell polarity
Fig. 11	Identification of α -pv ^{iΔEC} mice
Fig. 12	Loss of endothelial α -pv leads to impaired vessel sprouting and hypovascularization
Fig. 13	Depletion of endothelial α -pv alters vessel morphology and patterning
Fig. 14	Loss of endothelial α -pv results in a proliferation deficit
Fig. 15	Loss of endothelial α -pv results in increased vessel regression
Fig. 16	Abnormal vessel integrity in absence of endothelial α -pv
Fig. 17	Mural cell coverage of retinal vessels in α -pv ^{iΔEC} mice

LIST OF ILLUSTRATIONS, TABLES AND FIGURES

- Fig. 18 Depletion of endothelial α -pv does not affect stability or maintenance of established vessels
- Fig. 19 Severe persistent retinal vascular pathology in α -pv^{iΔEC} mice
- Fig. 20 Depletion of α -pv impairs formation of FXs and migration of ECs
- Fig. 21 Loss of α -pv does not alter VEGF-A mediated ERK activation

1 INTRODUCTION:

Blood vessels are the components of the cardiovascular system (CVS) that permit blood to circulate throughout the body. Forming an extensive network of arteries, capillaries and veins, they supply nutrients (such as amino acids (aas) and electrolytes), oxygen and hormones to all tissues in the body, and concurrently remove metabolic waste products (such as carbon dioxide and lactate) in order to maintain homeostasis [6].

The CVS is crucial in embryonic development (organogenesis), and remains of central importance throughout postnatal life, with its blood vessels participating in processes such as tissue regeneration occurring in wound healing, and tissue growth. Hence, it is not surprising that structural or functional vessel abnormalities contribute to many diseases, including cancer, ischemic retinopathies, stroke and metabolic disorders [14, 15].

Closer insights in the regulation of vascular morphogenesis are therefore of fundamental importance in medicine. Understanding the processes involved in new blood vessel development as well as vessel stabilization might eventually lead to new therapeutic strategies for disease control [14].

1.1 Vessel development

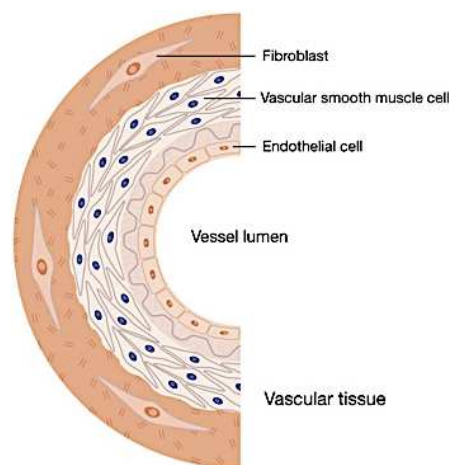
There are two distinct mechanisms describing how vessel formation and growth take place. Whereas vasculogenesis mainly takes place during embryogenesis and refers to the *de novo* formation of vessels from mesoderm derived endothelial precursor cells (EPCs) (angioblasts)

giving rise to a first primitive vascular plexus, angiogenesis describes the formation of new blood vessels from pre-existing ones, allowing the expansion of a vascular network by sprouting of endothelial cells (ECs) [6].

The expansion of the vascular network is a highly dynamic, closely regulated process, involving coordinate interactions between ECs, extracellular matrix (ECM) components as well as soluble pro-angiogenic factors and chemokines constantly adjusting their crosstalk to organ tissue needs [6].

The vascular network consists of small and large vessels. Arteries vary in levels of blood flow and pressure through diameter changes and supply organs with oxygenated blood. Veins return blood back to the heart. Capillaries allow gas exchange and nutrients as well as waste substances to pass across their walls. The vascular cell types involved in this tight regulation are: ECs, vascular smooth muscle cells (vSMC), pericytes (PC), fibroblasts (FB), and other connective tissue cell types. Each of them has distinct functions (III.1) [6, 16, 17].

ECs cover the inner layer of a vessel and play a critical role in tissue homeostasis and growth. They form a semi-selective barrier for bioactive molecules; they mediate angiogenesis and interact with adjacent vSMC during vessel growth and transition of molecules as well as white blood cells from the blood into the interstitial fluid. vSMCs and PCs envelope the surface of a vascular tube, have contractile function and stabilize vessels. They do not just serve as scaffolds, but communicate with ECs by direct physical contact and paracrine signaling pathways. Alterations in function result in vascular disease [18].

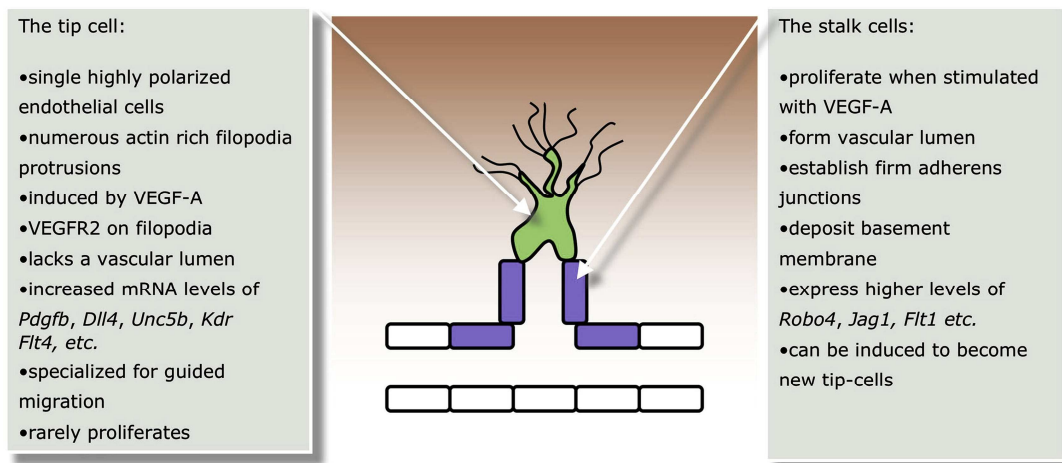


III.1 The vascular cell types within the vessel wall. For more information regarding the distinct cell types see text. III. Taken from <https://www.thermofisher.com/de/de/home/life-science/cell-culture/primary-cell-culture/pcc-misc/vascular-biology.html>

1.1.1 Hallmarks of sprouting angiogenesis

ECs play a key role in angiogenesis. They line the inner surface of the vessel creating a barrier between blood and tissue thereby controlling the extravasation of macromolecules. When nutritional and oxygen demands within the tissue exceed the supply provided by the vessels, the tissue releases signals to stimulate the formation of new blood vessels [16]. These signals are sensed by ECs and promote sprouting angiogenesis.

The main tissue-derived pro-angiogenic factor is the vascular endothelial growth factor (VEGF) [17]. Signals as hypoxia induce the release of growth factors as VEGF. Upon binding to its cognate receptors on the endothelium (VEGFR), ECs detach from vessel walls and ECs are activated. VEGF as well as integrin signaling allow EC specification into distinct cellular fates: the tip and the stalk phenotype (III.2). Depending on their position they adopt distinct functions in the forming sprout [17, 19, 20].



III.2 The tip (in green) and the stalk cell (in blue). Phenotypic and molecular differences upon EC activation by growth factors (extracellular gradient in orange) [9].

By Neuropilin, VEGF/VEGFR, NOTCH / delta like 4 (DLL4) and JAGGED-1 signaling a tip cell is selected in sprout formation. The tip cell releases metalloproteases (MMPs) to degrade the surrounding basement membrane (BM) and so frees the way through the ECM for the growing vessel.

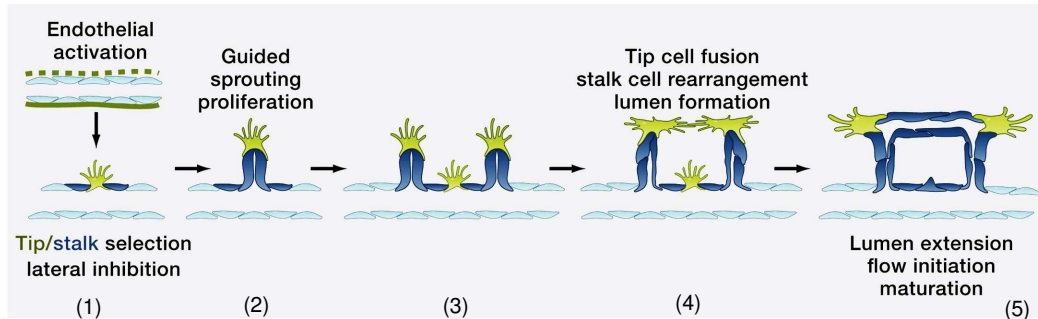
The tip cells show high planar polarity. They are located on the tip of the forming vessel and lead the new sprouts. By protruding filopodia and lamellipodia they scan the microenvironment for

chemotactic signals while migrating towards the angiogenic stimulus. The tip cells are primarily migratory and do not proliferate [6, 8].

The stalk cells trail behind the tips. They proliferate, elongate the sprouting vessel, form the lumen, deposit a basement membrane, and establish tight cell-cell junctions to stabilize the stalk. When two tip cells from neighboring sprouts meet, they anastomose in order to form new vessel branches. EC proliferation ceases and PCs are recruited to stabilize the new vessels (PDGFR/PDGF-B, Ang-1 signaling) [6].

Once blood flow is initiated the activated ECs transit into a quiescent phenotype, the phalanx cells (III.3). The endothelium establishes apical-basal polarity, with the luminal (apical) side faced to blood and the abluminal (basal) side facing the vascular tissue. The sprouting process iterates until pro-angiogenic signals abate.

The initial vascular plexus is remodeled through extensive pruning and selective branch regression, ultimately establishing an efficient and mature hierarchical vascular network in order to allow optimized blood flow for tissue perfusion and oxygenation [6].



III.3 Hallmarks of sprouting angiogenesis adapted from [6]. (1) EC activation and tip/stalk cell selection; (2) tip cell migration and stalk cell proliferation allowing elongation of the sprout; (3) branching coordination; (4) anastomosis, stalk elongation and lumen formation; (5) perfusion and maturation.

The key pathway in tip/stalk cell specification is the Notch signaling pathway, an evolutionary conserved cell-cell contact-dependent communication mechanism. Notch is the receptor and is mainly expressed by stalk cells, whereas delta like ligand-4 (DLL-4) as Notch-Ligand characterizes a tip cell [17].

VEGF-A release is induced by hypoxia and amongst others binds to VEGF-receptor-2 (VEGFR-2) on ECs. Through downstream pathways DLL-4 expression is induced. The

respective cells thereafter acquire a tip cell phenotype. Through DLL-4 binding to its receptor (Notch) on the adjacent cells, the Notch intracellular domain is released and translocated to the nucleus where it stimulates the transcription of Notch target genes [6]. Thereafter the cell acquires a stalk cell signature [6, 9, 19]. Through lateral inhibition the tip cell prevents its immediate neighbor to adopt the same phenotype.

Sprouting angiogenesis involves coordinate EC specification, adhesion, migration, polarization and proliferation. Its regulation involves physical interactions of ECs to ECM as well as the establishment of homotypic adhesions between adjacent ECs.

The cellular and molecular machinery underlying EC dynamics largely depends on the organization and dynamic rearrangement of the endothelial actin cytoskeleton. The cytoskeleton provides a structural framework of a cell that determines a cell's shape. It is a dynamic structure that is frequently reorganized, when cells move, change shape or divide. It enables a cell to migrate, to form spike-like protrusions and to polarize their actin cytoskeleton in the direction of migration [8, 20].

1.2 The Cytoskeleton - a cell's framework

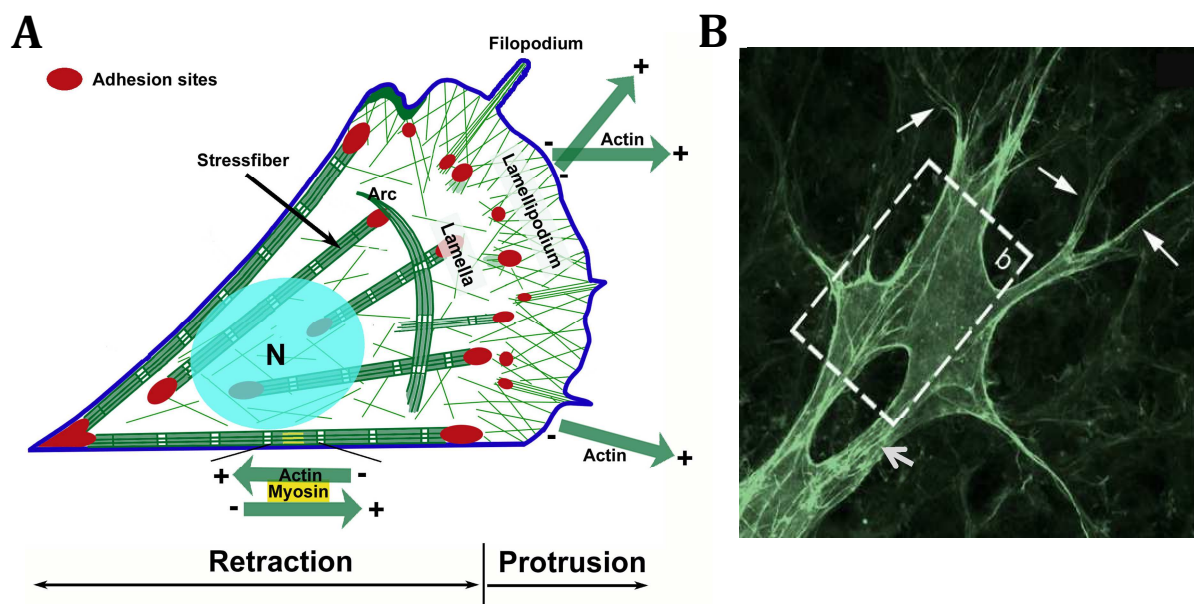
The cytoskeleton is a network of fibers of proteins contained within a cell's cytoplasm. It represents a dynamic structure providing cell stability by parts of it constantly being destroyed, renewed or newly constructed. There are three types of cytosolic filaments within a eukaryotic cell: (1) the actin filaments (a.k.a. microfilaments), (2) the intermediate filaments and (3) microtubules. Their main functions consist in maintaining cell structure, enabling cells to respond to mechanical forces as well as allowing cell movement. They are critical in cell division (1,2), in intracellular transport (1,2), in stabilization of the nucleus by connecting it to the plasma membrane (PM) and in regulation of signal transduction (3) [21].

1.2.1 The actin cytoskeleton in angiogenesis

A pro-angiogenic factor can induce F-actin polymerization enabling the arrangement of actin structures with fundamental roles in cell movement: (1) lamellipodial actin network at the

leading edge of a cell, (2) unipolar filopodial bundles beneath the plasma membrane and (3) contractile actin stress fibers in the cytoplasm (III.4) [8].

Lamellipodia are sheet-like cytoplasmic protrusions that form at the leading edge of migrating cells and contain a short-branched network of actin filaments that produce the physical force for the protrusion of the leading edge [8, 20, 22]. Filopodia on the other hand, are spike-like membrane projections that contain long parallel actin filaments arranged into tight bundles. These particular structures act as sensors of motile stimuli and elongation of these filaments - in response to these stimuli - pushes the leading edge forward and promotes cell migration [8, 20, 22]. Through integrin receptors lamellipodial and filopodial protrusions adhere to their surrounding ECM. Integrins so form focal contact points that connect the cytoskeleton to the ECM, allowing stress fibers - consisting of short actin/myosin filaments with mixed polarity along their length - to contract, thus pulling the cell towards these anchors, and inducing forward movement by retraction of the trailing edge [8, 20, 22].



III.4: Specialized actin structures in migrating EC. (A) Schematic showing polarized cell with lamellipodia, filopodia and stress fibers (from: <http://mcdb3280colorado.pbworks.com/w/page/15225500/-Actin>). (B) Migrating retinal endothelial tip cell. Arrowheads point to F-actin filaments (Lifeact-EGFP:green) depicting filopodia, lamellipodium and stress fibers [11].

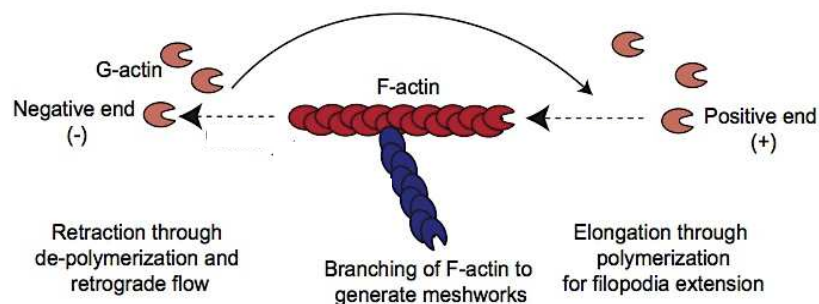
Cell receptors are responsible for cell-cell junction formation. The latter allow the establishment of a dynamic link to the actin cytoskeleton, via the formation of actin filament

associated protein complexes along transmembrane adhesion sites. The cytoplasmic domain of the core cell-cell contact molecule vascular endothelial (VE)-Cadherin interacts with proteins associated with the actin cytoskeleton, thereby anchoring the junctions to the cellular scaffold. This provides stabilization of newly formed vessels and regulates vessel permeability [23]. Angiogenesis requires a fast and local remodeling of EC-cell junctions [24]. Therefore, they represent highly dynamic structures that are disrupted and reformed at high frequency by local spatiotemporal rearrangements of the actin cytoskeleton [25].

1.2.2 The actin cytoskeleton and its dynamics

The major cytoskeletal component of ECs (and other cells) is the actin, which orchestrates the multiple steps in angiogenesis (III.3). It provides the framework for the formation of specialized cellular structures crucial for cell motility, polarization and proliferation.

Actin is composed of 43-kDA monomeric globular subunits (G-actin) that polymerize to form twisted strings of filamentous actin (F-actin). Actin filaments are polar with a fast-growing and slow-growing end, the assembly of which is tightly associated with the hydrolysis of ATP by intrinsic ATPase activity. ATP-bound monomeric G-actin is incorporated into growing filaments at the barbed end and ATP hydrolyzed to ADP as actin monomers are shifted along the filaments towards the pointed end [26, 27]. Most cells keep a large pool of G-actin to maintain the ability to quickly reorganize the cytoskeleton when exposed to environmental changes (III.5).



III.5 Actin polymerization. Schematic representation. (Adapted from [8])

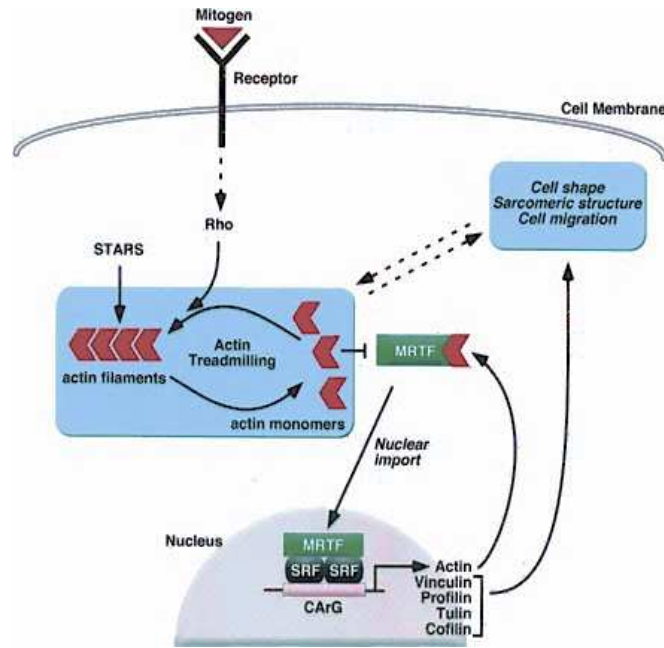
Tight spatiotemporal control of actin dynamics is indispensable in order to assure the assembly and disassembly of actin fibers, such as bundles, and for controlled rearrangement or breakdown of these structures. Regulation involves integrin signaling (*Integrins and their associated proteins will be discussed in detail in a separate chapter*), Rho GTPases and numerous additional proteins, collectively referred to as actin-binding proteins (ABPs).

Upon the above mentioned, the Rho GTPases function as key regulators of actin dynamics. The best-studied three representatives of the family that comprises more than 22 members are Ras homologous (RhoA), Ras- related C3 botulinum toxin substrate 1 (Rac1) and cell division cycle 42 (Cdc42). As all G proteins, they “molecularly switch” between inactive GDP bound and active GTP bound state. In the latter Rho GTPases specifically interact with diverse effector proteins inter alia, to control cytoskeletal dynamics [28]. RhoA thereby promotes stress fiber formation and maturation of nascent adhesions (NA) through its effector, the Rho-associated serine/threonine kinase (ROCK) [29]. Rac1 and Cdc42 instead promote membrane protrusions at the leading edge of migrating cells. Rac1 has been shown to be associated with lamellipodia formation by promoting actin related protein 2/3 complex (Arp2/3) activity, whereas Cdc42 is responsible for filopodia extension through activation of Wiskott Aldrich syndrome protein (WASP) [30]. The tight regulation of these processes includes spatiotemporal control of the Rho GTPases, which respectively is mediated by three classes of regulatory proteins: guanine nucleotide exchange factors (GEFs), GTPase activating proteins (GAPs) and guanine nucleotide dissociation inhibitors (GDIs) [31]. GEFs facilitate the exchange of GDP for GTP and thus are required for the activation of Rho GTPases [31]. GDIs instead inhibit the nucleotide exchange and sequester Rho GTPases in an inactivated state in the cytosol [32].

By controlling both the recruitment and activity of multiple GEFs and GAPs, integrins are critically involved in the regulation of Rho GTPases and hence in cytoskeleton dynamics [33]. This is one of the many aspects explaining how integrins interact with actin dynamics.

F-actin dynamics itself contribute to the control of gene expression on a nuclear level by regulating myocardin-regulated transcription factors (MRTFs), which function as cofactors of serum response factor (SRF) in the regulation of cytoskeletal genes [5, 34].

SRF is a ubiquitously expressed transcription factor that regulates transcription of genes involved in cell proliferation, cell motility and cell adhesion over environmental stimuli (III.6).



III.6 Actin dynamics regulate gene expression via SRF.

For details see text. G-actin in red, MRTF in green [5].

Activated by Rho GTPases, actin polymerization starts and leads to the incorporation of G-actin into the growing filaments, resulting in a consumption of G-actin and liberation of G-actin-bound MRTFs. The dissociated MRTFs translocate to the nucleus where they bind to SRF and so initiate the transcription of actin/actin regulating genes and rearrange cell shape. Once the growth-factor receptor signal abates nuclear G-actin facilitates the nuclear export of MRTFs to terminate the MRTF-SRF mediated transcription [35].

1.2.3 Impaired actin dynamics in vascular dysfunctions

Recent studies associate deregulation of actin dynamics to retinal vascular pathologies leading to blindness [34, 36]. Mostly this seems caused by retinal hypovascularization due to altered SRF–MRTF mediated signals in ECs, which compromises the motility of these cells. Changes in the dynamic rearrangement of actin filaments upon VEGF signaling are transmitted to the genome by actin-directed release of MRTF and induce deranged response of gene expression. As a consequence to impaired endothelial SRF-MRTF signaling, vessel

homeostasis is altered. The respective mouse lines show impaired endothelial tip cell filopodia protrusion, resulting in incomplete angiogenesis with less vascularized areas. They seem similar to those found in familial exudative vitreoretinopathies, such as the Norrie Disease (ND), where the hypovascularizations primarily affecting the retina, cause excessive neovascularization ultimately culminating in vision loss [36].

In summary this results highlight the importance of the actin cytoskeleton in vascular biology as well as in medicine. Hence, it is essential to be able to visualize these actin dependent processes *in vitro* and *in vivo* in order to get distinct perception of physiological as well as pathological angiogenesis and allied disease.

1.2.4 Visualization of the actin cytoskeleton

A lack of tools for *in vivo* imaging of F-actin structures in individual ECs in mammals has so far precluded an understanding of how ECs regulate their actin cytoskeleton during angiogenesis. Our knowledge on the organization and regulation of the endothelial actin cytoskeleton is mainly based on *in vitro* studies, which are missing essential physiological features, such as composition of the ECM, blood flow and mechanical input from the tissue.

It is thus a purpose of this thesis to describe a tool, found during analysis of Lifeact-EGFP mice, which overcomes this enduring problem and might help to get deeper understanding of actin dynamics and their regulation.

There are diverse *in vitro* approaches enabling the visualization of the actin cytoskeleton, relying on the use of fluorescent markers.

Historically, one of the first compounds used to visualize the actin cytoskeleton was the fungal toxin Phalloidin, originating from the mushroom *Amanita phalloides*. For immunostaining purposes it is coupled to different fluorophores. By selectively binding along the sides of actin filaments it inhibits their depolymerization leading to cell death by paralyzing the cell's cytoskeleton, yet allowing F-actin imaging only in fixed cells [37].

A widely used alternative for visualizing the F-actin network without disturbing actin dynamics and functionality is to express green fluorescent protein (GFP)-actin in cells, thus allowing live cell imaging of the cytoskeletal processes. However GFP fusions to actin binding domains have certain limitations of use as they show reduced functionality compared to endogenous protein, they compete with their cellular counterparts, change the subset of F-

actin structure and do not label all actin within the cell. Moreover their use is restricted to cells that can be transfected [38, 39].

The marker Lifeact overcomes these limitations. It does not interfere with cytoskeletal dynamics *in vitro* or *in vivo*. Up to now, the 17-aa long peptide is the shortest actin marker for living cells. It has low binding affinity for F-actin and seems to be the best marker available to study F-actin dynamics [38]. (For more information see materials and methods).

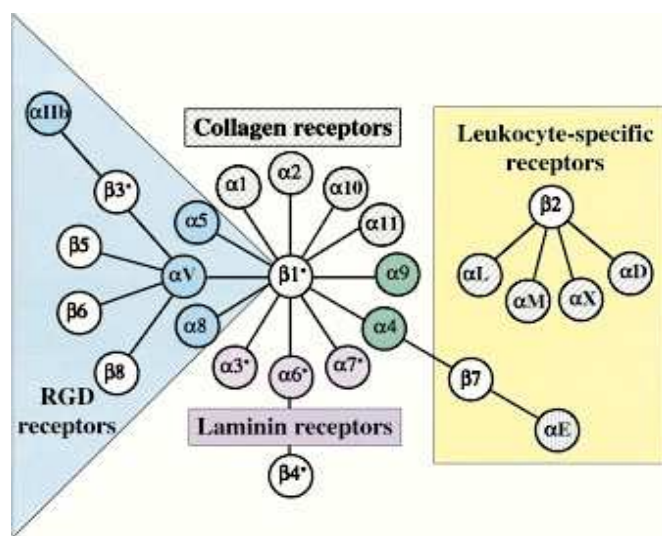
Although the markers mentioned above are extensively been used to investigate actin dynamics in various cell types and experimental models, they are still of restricted utility when looking at primary cells, tissues and whole animals. Transgenic mouse strategies are significant tools in addressing those limitations. Several transgenic mouse lines that express the GFP-actin gene under the control of tissue specific promoters have been created and described in literature: GFP-actin mice [40, 41]. They should permit to study actin dependent processes in the mouse and visualize actin expression patterns throughout embryonic development [41]. It is being argued though, that there is notable variability in GFP expression patterns within transgenic strains, with none of them giving ubiquitous GFP expression [42].

This being the case, the structural organization, dynamics and regulation of F-actin in mammals *in vivo* are still not well understood.

1.3 The Integrins - integrating the outside with the inside

Integrins are considered one of the main regulators of the endothelial actin cytoskeleton during angiogenesis. Together with growth factor receptors, they function as mediators between the surrounding tissue and cell behavior by sensing environmental changes and propagating many intracellular signals thereby orchestrating multiple steps in angiogenesis (see above). Integrins are the main cell-ECM receptors. They show remarkable plasticity as they constantly remodel in response to changes in the ECM and adapt cytoskeletal organization, cell migration and signaling processes according to environmental changes.

Integrins are a family of glycosylated heterodimeric transmembrane cell adhesion receptors that contain an α and a β subunit each, that associate to form different receptors in order to be able to bind to distinct ECM components [13]. Both subunits contribute to the binding specificity of a given integrin heterodimer for its extracellular ligand. So far 18 α - and 8 β -subunits have been described in mammals and are known to form 24 different heterodimers with overlapping substrate specificity and cell type specific expression patterns (Ill.7) [13, 43].



Ill.7: The Integrin receptor family.

Schematic representation of the integrin heterodimers sorted by their main ligand binding specificity and leukocyte-specific expression, resulting in a classification into four major groups:

- Integrins binding to tripeptide sequence RGD (arginine-glycine-aspartic acid). Ligands for this group include fibronectin (FN) and Vitronectin (VN)
 - Collagen binding $\beta 1$ heterodimers
 - Laminin (LN) binding $\beta 1$ heterodimers
 - Leukocyte specific integrins.
- (Ill. from [13])

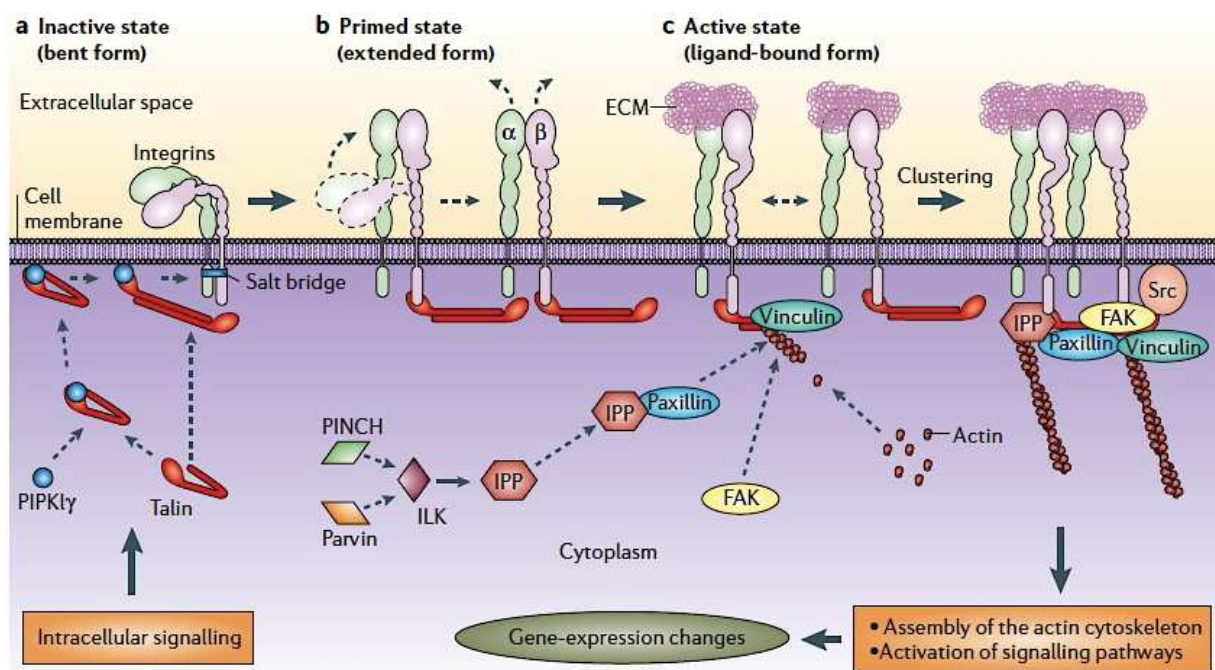
1.3.1 Integrin signaling – bidirectional, across the membrane

Most of the integrins are not constitutively active. They can be expressed in an inactive state on cell surfaces, where they neither show a ligand binding nor a signaling activity. Thenceforward, they are able to undergo conformational changes and switch to states with high ligand binding affinity and signaling activity. The conformational changes are induced by intracellular signals. Cytoplasmic proteins bind to the β integrin tails and thereby enable the separation of α - and β -transmembrane and cytoplasmic segments, facilitating ligand binding to the extracellular domain [44].

This concept of regulation of integrin function from within the cell has commonly been called “inside-out signaling” and has to be distinguished from “outside-in signaling” [13]. Affinity

modulation is essential to control ligand binding and integrate cues from the extracellular environment across the PM with the cell's interior organization.

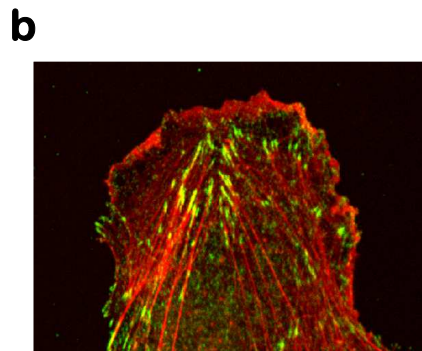
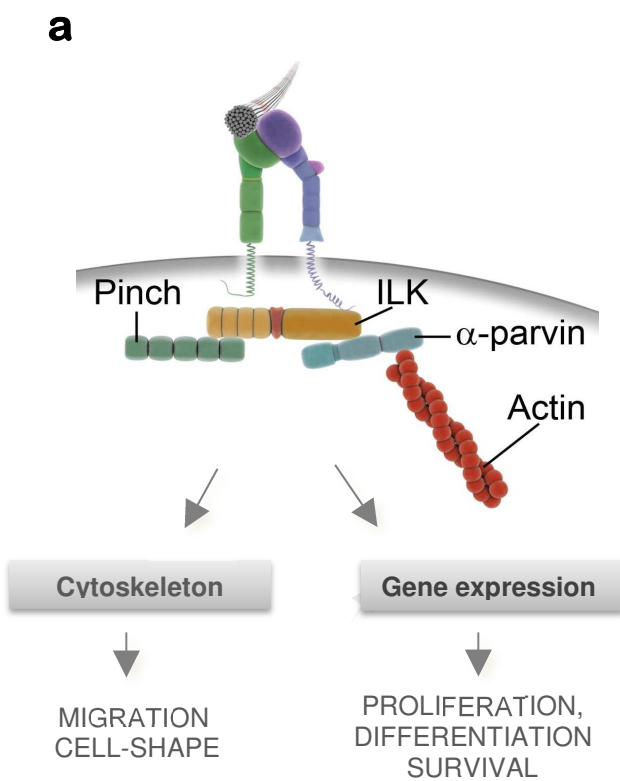
Upon binding to ECM components integrins switch to an activated state and cluster in order to provide a firm adhesion to the ECM. The synergistic effect of multiple weak interactions is known as avidity and requires collective binding of multiple integrin interactions, each resting upon single weak ligand-receptor engagement. Based on size, morphology, localization and protein composition, several types of such adhesive units can be distinguished. A vast number of cytoplasmic adaptor and signaling molecules are recruited to the adhesion sites and allow their maturation starting from nascent adhesion [45], over focal complexes (FX) to focal adhesions (FA) and fibrillar adhesions [46] (III.8).



III.8 Bidirectional integrin signaling. Schematic depicts conformational changes of the receptors, the biogenesis of FA illustrating the connection of the integrins with the actin cytoskeleton and signaling properties. For more information see text. Taken from [1]

FAs are sites of tight adhesion between the membrane and the ECM on one hand, and the membrane and actin cytoskeleton on the other. Their assembly follows Integrin-mediated recruitment of signaling molecules, whereupon they sense mechanical forces, transduce survival and growth signals between ECM and interacting cell. They provide a structural link

allowing the anchorage of stress fibers to the membrane as well as to integrins, hence allowing cell migration [1, 43, 47] (III.9).



III.9: Integrin signaling. **A** Signals converge on actin polymerization enabling cellular contractility and cell migration. Receptor activation further leads to changes in transcriptional program and protein expression affecting cell behavior. (Ill adapted from [2]) **B** FA in HUVECs. Immunostaining in green α pv marking FA, red Phalloidin marking F-actin.

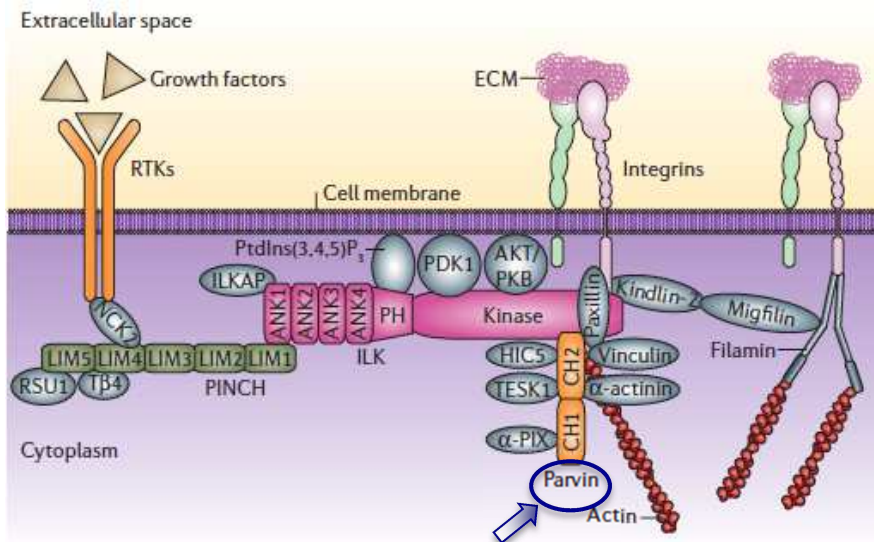
Integrins themselves

do not possess own enzymatic activity; rather their signaling properties rely on their ability to recruit specific signaling and adaptor proteins to their cytoplasmic domain at the adhesion site. Over 180 molecules are found to be associated with the integrin adhesions [48]. Among a wide array of proteins involved in the "integrin adhesome", three have been shown to have major impact on vascular development; the integrin-linked kinase (ILK), PINCH and parvin (pv). Taken together they form the ternary IPP-complex (named after its components in order of their discovery) [1, 47]. IPP signaling is achieved through its direct interaction with factors that function as upstream regulators of many different signaling pathways (III.10). Along these lines the complex acts through phosphorylation of downstream targets and/or through binding upstream effectors. In this way the IPP is able to influence cell invasion, proliferation, tissue morphogenesis, survival, spreading, migration, motility and last but not least angiogenesis [1].

However, little is known about how exactly signals initiated by integrins are molecularly integrated by ECs to assure the appropriate endothelial actin cytoskeleton organization required for successful angiogenesis.

To solve this question recent efforts concentrate on the specific roles of the individual integrin associated proteins. So far in the mammalian system loss of expression of $\beta 1$ integrin, ILK, PINCH1 and pv was shown to cause early embryonic death in mice, even so these mutants display subtle differences in their phenotypes, which provide allusive hint that distinct defects might underlie these phenotypes [1].

In this thesis we will focus on the IPP partner pv, and analyze its functions within the angiogenic process.

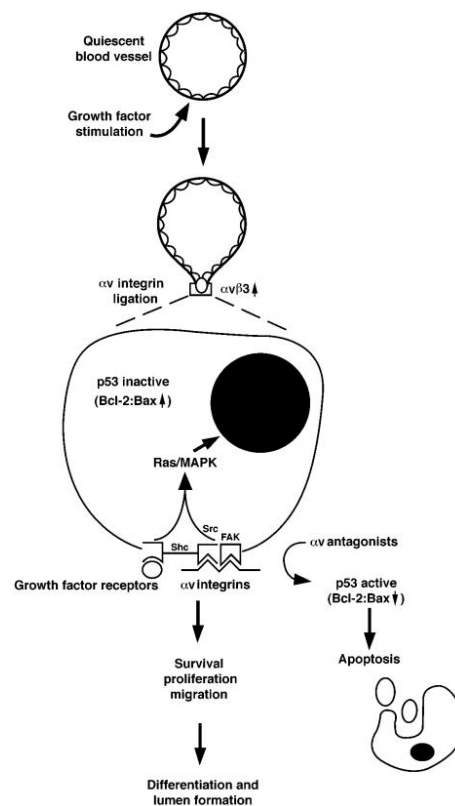


III.10 The IPP-complex with some interaction partners. Arrow marks Parvin. III. form [1]

1.3.2 Integrin signaling in angiogenesis

In sprouting angiogenesis filopodia (through integrins on their surface) make contact with ECM components and initiate the formation of FA. These FA grant stress fibers an anchoring point through which they induce a cell's forward movement by pulling the cell body towards these sites. On molecular level FA are sides of transduction from the ECM to the EC involved in various intracellular signaling cascades [49].

Integrin expression is dynamically regulated in response of tissue alterations induced by growth factors or changes in the surrounding stroma. Depending on activation status EC express several integrins, including the $\beta 1$ integrins $\alpha 1\beta 1$, $\alpha 2\beta 1$, $\alpha 3\beta 1$, $\alpha 4\beta 1$, $\alpha 5\beta 1$, $\alpha 6\beta 1$ and $\alpha 9\beta 1$, the αV integrins $\alpha v\beta 3$ and $\alpha v\beta 5$, as well as $\alpha 6\beta 4$ [49, 50]. Numerous genetic and pharmaceutical studies revealed their critical function within the vasculature. Among them the $\alpha v\beta 3$ has been shown to be unregulated after growth factor stimulation and plays a key role in the initial steps of angiogenesis. On EC surface it co-localizes with proteolytically active MMP-2 and so enables cell-mediated degradation of the surrounding ECM, facilitating tip cell migration. On molecular level $\alpha v\beta 3$ assists growth factor signaling via extracellular signal regulated kinase (ERK) signaling, it also activates the small GTPases Rac 1 and Cdc 42 during spreading and migration. For regulated proliferation and survival it facilitates the interaction with signaling cascades including focal adhesion kinase (FAK) – phosphoinositide-3-kinase (PI3K) - Akt, ERK and nuclear factor (NF) κ B. By recruitment of caspase-8 to the plasma membrane it also plays a crucial role in apoptosis regulation [4, 51] (III.11).



III.10 Integrins in angiogenesis – a hypothetical model.[4] Growth factors bind to their receptors and activate multiple signaling cascades. They induce αV integrin expression allowing cells to invade the surrounding tissue and activate Ras/MAP kinase signaling cascades. Inhibition of αV integrin raises p53 activity and facilitates apoptosis.

$\beta 1$ subunit (thus all $\beta 1$ integrin heterodimers) was shown to have major impact on vascular development and angiogenesis. While EC lacking $\beta 1$ integrin displayed impaired proliferation and vessel branching [43], endothelial-specific deletion of the $\beta 1$ subunit in mice resulted in embryonic lethality due to multiple vascular defects. Although vasculogenesis and the formation of larger vessels did not seem to be affected, angiogenesis was severely compromised in those mice [50].

1.4 The IPP complex in angiogenesis

Integrin receptor activation through ligand binding results in the formation of an integrin adhesion complex transducing signals into the cellular machinery. Part of the integrin intracellular molecular rearrangement is the IPP complex, which supports integrin activation through stabilization of active conformation and provides a linkage to cytoskeletal proteins and signaling molecules. Its components: the ILK, the PINCH and the pvs function as a stable structural and functional unit controlling cell adhesion, migration and spreading [1, 52]. They act by modification of Akt/protein kinase B (PKB), glycogen-synthase-kinase 3 beta (GSK3 β)/ β -catenin, jun-amino-terminal kinase (JNK), α -PIX/Rac1 signaling pathways [1]. Deletion of a single partner of the heterotrimeric complex disturbs mechanical anchorage and signaling properties, thus leading to proteasome-mediated degradation as well as to embryonic lethality if knocked out *in vivo* [53].

It is appealing to understand which role every single partner plays in angiogenesis. The best-characterized regarding angiogenesis is the ILK. The role of pv still remains uncertain.

1.4.1 Integrin linked kinase in angiogenesis

One of the best functionally characterized components of the IPP-complex is the ILK, a serin-threonin protein kinase containing a catalytic domain at the C-terminus, a central pleckstrin homology-like domain and 4 ankyrin-like repeats at the N-terminus. ILK functions as an important component in the focal adhesion complex, which anchors actin filaments to integrin receptors and the cell membrane [54].

Several studies were made to identify ILK's function within ECs. Most of them were *in vitro* studies using small interfering (si)RNA to knockdown ILK expression. Loss of endothelial ILK thereby resulted in disruption of mechanical anchoring as well as in changes of EC shape in respective cells. To that effect Guo L. et al. reported disordered F-actin assembly and severely compromised cell morphology characterized by reduced lamellipodia and filopodia formation in ILK depleted ECs. These might be reasons for altered EC-migration [54].

Besides alteration in structure in ILK depleted cells, many up- and downstream signaling pathways controlling migration, cell growth, survival, invasion, cell motility and contraction in vascular development and in angiogenesis were affected by the loss of ILK [54].

Regarding these molecular signaling pathways, the best analyzed in angiogenesis are the VEGF-dependent signaling cascades.

It has been shown that ILK knockdown inhibited VEGF mediated angiogenesis by interfering with VEGF-induced cell-attachment and spreading as well as VEGF induced cell migration. [55] Most likely this is due to functional and structural disruption of the actin cytoskeleton. The small GTPases Rac and Cdc42 involved in actin dynamics are decreased by ILK knockdown [56] through alterations in PAK-interactive exchange factor α [57].

Downregulation of ILK inhibited VEGF stimulated proliferation [55] by inducing a cell cycle arrest in G1/S phase through reduction of cyclin D1 [58].

Even so VEGF levels per se were lower in transfected cells, thereby limiting all VEGF-VEGFR-2 dependent cell functions. ILK depleted cells showed significantly suppressed VEGF-induced phosphorylation of p38 mitogen-activated-protein-kinase (MAPK) and PI3K/Akt in ECs. JNK and ERK phosphorylation was not affected [55].

ILK is an important regulator of EC during angiogenesis, which provides a functional link between growth factor signaling and actin cytoskeleton [55].

1.5 The Parvins

Pvs are a family of adaptor proteins that localize to FAs and facilitate the interaction of integrins with the actin cytoskeleton. Three members have been identified so far, that differ from each other in expression patterns and binding partners. Whereas α -pv shows

ubiquitous expression, β -parvin (β -pv) is enriched in heart and skeletal muscle and γ -parvin's (γ -pv) occurrence is restricted to hematopoietic cells.

The most prominent structural feature the members of the pv-family share, are two tandem arranged calponin homology (CH) domains in the C-terminal region (Ill.10). This tandem arrangement recurs in many actin-binding proteins (ABPs) [59] and facilitates microfilament binding [60]. One interaction partner all pv members share is the ILK, to which they bind using the second of the two CH domains (CH2). Direct actin binding instead could only be demonstrated for α -pv [60]. β -pv and γ -pv were shown to just indirectly link the IPP complex to the cytoskeleton via α -actinin [61], a further ABP, the latter never binding to α -pv, though [62]. Both, α - and γ -pv bind paxillin with their CH2 domain, which through its interaction with vinculin provides an additional link to the actin cytoskeleton, leading to further stabilization of the FA.

Moreover, pvs interact with other important regulatory proteins, including regulators of the Rho GTPases, coupling the integrin- to the receptor tyrosine kinase (RTK) signaling, Hic5, Cdc42 GTPase activating protein (CdGAP), α PIX (Ill.9). This again highlights the prominent functions of α -pv in integrin mediated adhesion and actin dependent processes such as cell shape regulation and cell migration [1].

Montanez et al. in 2009 analyzed the functions of α -pv *in vivo* generating α -pv mutant mice. The ubiquitous deletion of α -pv gene in mice led to embryonic lethality around embryonic day (E) 10.5-E14.5, largely associated with severe cardiovascular defects. The group was able to show that loss of α -pv results in aberrant vascular network formation, impaired vessel maturation as well as abnormal heart development. Studies mainly focused on the function of α -pv in vascular mural cells (vMC) and revealed its contribution to RhoA/ROCK signaling. Interestingly Montanez et al. also found that the other members of the IPP complex remained unaffected by disruption of α -pv, as the occurring upregulation of β -pv levels seem to stabilize ILK and PINCH levels and localize them into FAs also in absence of α -pv. They claim that α -pv and β -pv exist in two different complexes containing ILK. However, shape and spreading defects are solely attributable to the absence of α -pv and cannot be compensated by β -pv [2].

Further it has been shown that α -pv is upregulated during the angiogenic process.

All together these findings underline α -pv's importance in vascular development. Yet its specific role in EC has not been studied. It remains unclear how α -pv functions in the regulation of endothelial actin cytoskeleton during sprouting angiogenesis.

2 HYPOTHESIS & AIMS:

I. Lifeact-EGFP

We first hypothesized that endothelial expression of Lifeact-EGFP may allow to study actin dynamics in a model of angiogenesis. We therefore performed a careful analysis of the expression patterns of Lifeact-EGFP - in respective mice - in the vascular system throughout the body, searching for areas where there was a preferential endothelial Lifeact-EGFP expression allowing analysis of actin dynamics.

By using Lifeact-EGFP mice, we aimed to establish a fast and easily applicable tool for *in/ex vivo* visualization of actin dependent processes in ECs during angiogenesis.

II. α - Parvin

Disrupted β 1 integrin signaling, as well as impaired ILK signaling has a major impact on vascular development through compromised EC-proliferation and branching during the angiogenic process. Pv is involved in this integrin signaling. In 2009 Montanez et al. first demonstrated, that ubiquitous deletion of α -pv in mice led to embryonic lethality, mostly due to aberrant vascular network formation. Here, we hypothesized that endothelial α -pv itself might have an independent and crucial role in vascular development. Thus, we aimed to characterize the role of α -pv on the regulation of endothelial actin cytoskeleton in sprouting angiogenesis.

3 MATERIAL & METHODS:

3.1 Material

3.1.1 Reagents and Chemicals

Component	Vendor
Agarose	Sigma-Aldrich
Alexa Fluor 488 Isolectin B4	LifeTechnologies
BrdU (5-bromodeoxyuridine)	Invitrogen
BSA (bovine serum albumin)	AppliTech
Calcium chloride dihydratate	Roth
Desoxynucleotide (dNTP) Solution Mix	Qiagen
Dimethylsulfoxid (DMSO)	Roth
Endothelial Cell Growth medium	Promocell
Ethanol (100% (vol/vol))	AppliChem
Fetal calf serum (FCS) superior	Biochrom
Flouromount-G	Southern Biotech
Formaldehyd	AppliChem
Formamide	Sigma-Aldrich
GelRed	Biotum
GeneRuler™ DNA ladder Mix (100bp-10kb)	Fermentas
Glycerol	Sigma
Hydrochloric acid (HCl 37%(wt/vol))	AppliChem

MATERIALS & METHODS

Isopropanol	AppliChem
Lipofectamine 2000 Reagent	Invitrogen
Loading Dye PCR samples	Qiagen
Magnesium chloride hexahydrate	Qiagen
Magnesium chloride tetrahydrate	Qiagen
Nonfat-dried milk bovine	Sigma-Aldrich
Paraformaldehyde (PFA)	Sigma-Aldrich
PBS	<i>Provided by the pharmacy of "Klinikum Großhadern"</i>
Peanut oil	Sigma-Aldrich
Penicillin/Streptomycin (PS)	Sigma-Aldrich
Phalloidin-Alexa-546	Invitrogen
Protease-Inhibitor Tablet	Roche
Protein PageRuler™	Thermo Scientific
Proteinase K (RNAse free)	Sigma-Aldrich
SDS ultrapure	AppliChem
Sodium chloride (NaCl)	AppliChem
Tamoxifen free base	Sigma-Aldrich
Taq DNA polymerase	Peqlab
TO-PRO-3 iodide	Cambridge
Triton-X-100	AppliChem
Trypsin	PAN
VEGF-human (recombinant)	PeproTech
Viagen Direct PCR-tail	PEQLAB Biotechnology
β-Mercaptoethanol	AppliChem

3.1.2 Kits

Name	Vendor
BCA kit	Biorad
Enhanced chemiluminescence kit	Millipore
PCR kit	Qiagen Peqlab

3.1.3 Antibodies

Antibody	Species	Concentration	Vendor
Alexa Fluor 488 anti-rat-ab	donkey	1:200 (<i>IF</i>)	Invitrogen
Alexa Fluor 546 anti-mouse-ab	goat	1:200 (<i>IF</i>)	Invitrogen
Alexa Fluor 546 anti-rabbit-ab	donkey	1:200 (<i>IF</i>)	Invitrogen
Anti-BrdU Pure	mouse	1:50 (<i>IF</i>)	BD Bioscience
Anti-Caspase 3 – cleaved	rabbit	1:50 (<i>IF</i>)	Cell signaling
Anti-CD31	rat	1:100 (<i>IF</i>)	BD Pharmingen
Anti-Claudin 5	rabbit	1:100 (<i>IF</i>)	Invitrogen
Anti-Collagen IV	rabbit	1:50 (<i>IF</i>)	Biorad
Anti-Cy3 conjugated α SMA	rabbit	1:100 (<i>IF</i>)	Sigma
Anti-Erg1/2/3	rabbit	1:100 (<i>IF</i>)	Santa Cruz
Anti-GAPDH	mouse	1:5000 (<i>WB</i>)	Millipore
Anti-GFAP	rabbit	1:75 (<i>IF</i>)	Dako
Anti-ICAM-2	rat	1:200 (<i>IF</i>)	BD Pharmingen
Anti-ILK	rabbit	1:1000 (<i>WB</i>)	Cell Signaling
Anti-mouse IgG H&L Chain specific peroxidase conjugated	goat	1:2000 (<i>WB</i>)	Calbiotech
Anti-NG2	rabbit	1:100 (<i>IF</i>)	Chemicon
Anti-p-38	rabbit	1:1000 (<i>WB</i>)	Cell Signaling
Anti-p-Akt	rabbit	1:1000 (<i>WB</i>)	Cell Signaling
Anti-p-histone H3	rabbit	1:100 (<i>IF</i>)	Upstate
Anti-p-MAPK (42/44)	mouse	1:1000 (<i>WB</i>)	Cell Signaling
Anti-p-paxillin	rabbit	1:50 (<i>IF</i>)-1:1000 (<i>WB</i>)	Cell Signaling
Anti-Paxillin	mouse	1:1000 (<i>WB</i>)	BD Biosciences
Anti-rabbit IgG H&L Chain specific peroxidase conjugated	goat	1:2000 (<i>WB</i>)	Calbiotech
Anti-total-Akt	rabbit	1:1000 (<i>WB</i>)	Cell Signaling
Anti-total-MAPK (42/44)	rabbit	1:1000 (<i>WB</i>)	Cell Signaling
Anti-VE-Cadherin	mouse	1:100 (<i>IF</i>)	eBioscience
Anti- α -parvin	rabbit	1:100 (<i>IF</i>)-1:1000 (<i>WB</i>)	Cell signaling

3.1.4 Solutions

Solution	Ingredients
Blocking buffer for WB	1X TBS 0,1% Tween-20 5% (w/v) nonfat-dried milk
BrdU solution	3 mg/ml BrdU in PBS
DNA Lysis buffer	99% Viagen Direct PCR tail 1% Proteinase K
Fixative	PFA-PBS (4% (wt/vol))
Formamide-SSC	50% formamide 5% SSC (20x)
Laemmli sample buffer	277.8 mM Tris-HCl pH 6.8, 4,4% LDS 44.4% (w/v) glycerol 0.02% bromophenol blue
Pblec	1% Triton X-100 1mM CaCl ₂ 1mM MgCl ₂ 1mM MnCl ₂ PBS (pH6.8)
Permeabilization buffer	0.1% Triton X-100 in PBS
Radioimmunoprecipitation assay (RIPA) lysis and extraction buffer	25 mM Tris-HCl (pH 7.6) 150 mM NaCl 1% NP-40 1% sodium deoxycholate 0,1% SDS
Retina-blocking buffer	1%BSA 0,3% Triton X-100

MATERIALS & METHODS

Retina-washing buffer	0,1 % Triton X-100 in PBS
SSC (20x) (saline-sodium-citrate)	3M NaCl 300 mM sodium citrate 14N HCl (pH 7.0)
Tamoxifen solution	10% tamoxifen stock solution (10mg/ml) 90% peanut oil
Tamoxifen stock solution	10 mg/ml tamoxifen 25% ethanol (100% (vol/vol)) 75% peanut oil
1X Tris-buffered saline (TBS)	50 mM Tris-Cl 150 mM NaCl (pH 7.6)
TBST (washing buffer WB)	1X TBS 0,1% Tween-20
Transfer buffer for WB	25 mM Tris Base 192 mM glycine 20% methanol (pH 8.5)
Tris-acetate EDTA (TAE) buffer (1X)	40 mM Tris 20 mM acetic acid 1 mM EDTA (pH 8.0)
Tris-glycine/SDS (Running buffer WB)	25 mM Tris-base 190 mM glycine 0,1% SDS (pH 8.3)
1M Tris-HCl pH 8	1M Tris in ddH ₂ O pH adjusted with HCl

3.1.5 Media

Medium	Vendor
Endothelial Cell growth medium	Promocell
Medium 199	Gibco, LifeTechnologies
Opti-Mem reduced serum	Gibco, LifeTechnologies

Medium	Ingredients
HUVEC culture medium	50% Endothelial Cell growth medium + 2,5% Supplement mix 50% Medium 199 + 20% FCS + 1% PS
Freezing medium	90% FCS 10% DMSO
Starving medium (1%)	Medium 199 1% FCS 1% PS
Stimulation medium	Starving medium 50 ng/ml VEGF-A

3.1.6 Oligonucleotides

Primer	Sequence
APE2f (forward)	5'-GAAGGAATGAACGCCATCAAC-3'
APloxPf (forward)	5'-CTGAGTGACATGGAGTTTGAG-3'
APloxPr (reverse)	5'-GGACTTGTGGACTAGTTAGAC-3'
CreF (forward)	5'-GCCTGCATTACCGGTCGATGCAACGA-3'
CreR (reverse):	5'-GTGGCAGATGGCGCGGCAACACCATT-3'
siRNA (Sigma-Aldrich)	Sequence

α -pv SASI_Hs01__00165014	5'-CGACAAUGGUCGAUCCAAA-3'
α -pv SASI_Hs01__00165015	5'-GAACAAGCAUCUGAAUAAA-3'
Scrambled control	SIC001 Sigma Aldrich

3.1.7 Equipment and disposals:

Equipment	Vendor
Centrifuge	Rotina 35R Hettich-Lab-Technologies
Confocal microscope SP5	Leica SP5, Leica
Dissection forceps no.5	Fine Science Tools
Dissection microscope/Stereomicroscope	Zeiss Stemi SV11
Elisa Reader	Tecan Infinite F200
Fluorescence microscope	Zeiss Axiophot
Imaging system PCR	Intas Science Image
Incubator	Binder
Injection needle 27G x ½''	BD Microlance 3, BD Becton Dickinson
Injection needle 30G x ½''	BD Microlance 3, BD Becton Dickinson
Inverted microscope	Zeiss Axiovert 25
Microcentrifuge with rotor for 2-, 1.5 ml tubes	Eppendorf Centrifuge 5410
Rocker-Shaker (mini)	PMR 30; Grant-Bio
Short-blade scissors	Fine Science Tools
Spring scissors	Fine Science Tools
Sterile bench	Steril VBH compact
Thermoblock	Eppendorf Thermomix comfort
Thermocycler PCR	PTC-100 [®] Peltier Thermal Cycler, MJ Research
Waterbath	HAAKE SWB25
Western Blot imaging software	Wasabi software 1.4, Hamamatus Photonics

3.2 Animals

All experiments with mice were performed in accordance to German guidelines and regulations. The Committee on the Ethics of Animal Experiments of the Ludwig-Maximilians University, Munich, approved the protocols.

3.2.1 Lifeact-EGFP transgenic mice

For *ex vivo* visualization of the actin cytoskeleton Lifeact-EGFP mice have been used [10]. Lifeact is a 17 aa long peptide derived from yeast, that comprises the first 17 aa of the ABP140 in *saccharomyces cerevisiae*. To study actin dynamics in living cells it has been fused to EGFP on its C-terminal end. Through direct binding to F-actin it allows *in vitro* and *in vivo* visualization of the cytoskeleton without affecting neither actin organization nor its dynamics [38].

In 2010 Riedl et al. first generated Lifeact-EGFP mice to study F-actin dynamics in primary cells and whole animals [10]. Therefore they created a construct based on the pCAGGS vector and inserted the Lifeact-EGFP sequence. In order to obtain broad expression patterns the vector contains a cytomegalovirus (CMV) enhancer sequence upstream to a chicken actin (CAG) promoter, which drives the Lifeact-EGFP expression.

Lifeact-EGFP mice can be tested for a fluorescent signal by using a UV-lamp.



Ill.12: Vector fragment containing Lifeact-EGFP. Linearization of the vector used for pronuclear injection. The sequence comprising CMV-enhancer, CAG promoter, chimeric intron, Lifeact-EGFP and a Poly-A sequence ensures ubiquitous expression. [10]

3.2.2 Inducible α -Pv knockout mice: α -pv^{fl/fl};Cdh5(PAC)-CreERT2

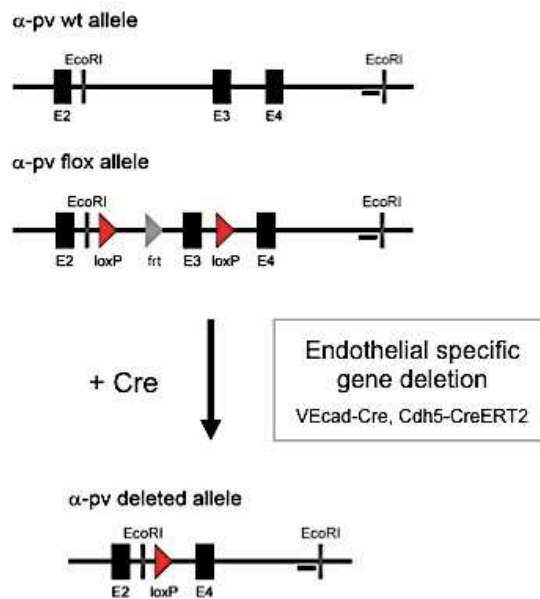
To determine the roles of α -pv in ECs during vessel sprouting, we generate specific EC deletion of α -pv in mice: α -pv^{fl/fl};Cdh5(PAC)-CreERT2 (herein referred to as α -pv^{iΔEC}).

Therefore Cdh5-CreERT2 mice [63] were bred into a background of animals carrying a *loxP*-flanked α -pv gene (α -pv^{floxed/floxed} (flox/flox)). Cre activity and respective gene deletion, was induced in newborn mice by intraperitoneal (IP) injection of 50 μ l of Tamoxifen solution (Sigma-Aldrich; 1mg/ml; generated by diluting a 10 mg/ml tamoxifen stock solution in 1:4 ethanol: peanut oil (Sigma-Aldrich) with additional peanut oil) once daily at postnatal days (P)1, P2, P3. Phenotypes of mutant mice were analyzed at days P6, P7, P8.5 or P16, as indicated. Littermate animals were used as controls.

Inducible gene deletion *in vivo*:

Up to date the best gene deletion *in vivo* is achieved with the conditional Cre-*loxP* system. It involves the insertion of two *loxP* sites flanking the gene or region of interest (α -pv in our case) by homologous recombination in cultured embryonic stem cells. A site-specific DNA recombinase Cre recognizes the marked sites as substrate, removes the DNA segment and generates a nonfunctional, truncated allele. Temporal control of the recombinase can be accomplished by the use of a Tamoxifen-inducible version of the Cre (CreERT2) (III.12, 13) [3].

EC specific expression of the inducible Cre was obtained by the use of mice carrying the Cre recombinase under the control of the cadherin-5 (Cdh5) promoter (Cdh5-CreERT2) (III.12).



III. 13 Site-specific recombinase technology used to inactivate α -pv in the postnatal endothelium. For more information see text

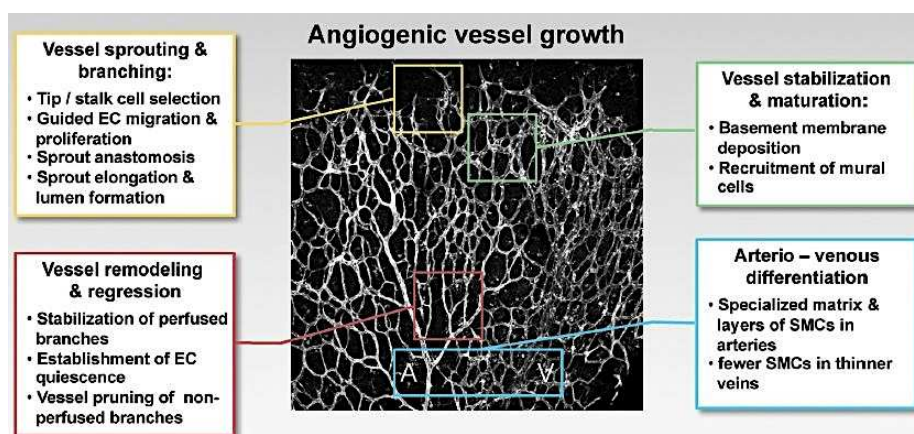
3.3 Postnatal mouse retina as an angiogenesis model

The postnatal mouse retina model is a powerful, widely used *ex vivo* system for the analysis of physiologic and pathologic angiogenesis [3]. Moreover once combined with novel tools in mouse genetics, such as the inducible *Cre-loxP* site-specific recombinase technology, it allows investigation of signaling pathways that control retinal vascular development.

Development of retinal vasculature

Blood vessels in the retina undergo extensive changes and reorganization during development. Before birth mouse pups have an immature retinal vasculature involving hyaloid vessels, which supply the inner retinal portion with oxygen and nutrients by a diffusion process. Immediately after birth hyaloid vessels regress and start to be replaced by a vascular plexus that emerges from the optic nerve. Within the first week after birth, sprouting, proliferation and directional migration of ECs from the center towards the periphery leads to the formation of a primitive vascular plexus that covers the inner layer of the retina. Thereby vessels at the growing edge are less mature than more central ones. At P8 the outer margin is reached and onwards the ECs start to grow perpendicularly in order to fuel the deeper retinal layers (Ill.14 A). After about 21 days of substantial remodeling the vasculature matures into a hierarchical network of arteries, capillaries and veins [64].

In these premise, an advantage of the postnatal mouse retina model is the possibility of capturing all mentioned stages of vascular differentiation within a single system with spatiotemporal separation. Likewise it represents a fast tool, with a two-dimensional flat primary plexus easy to image after immunohistochemistry [64] (Ill.13).

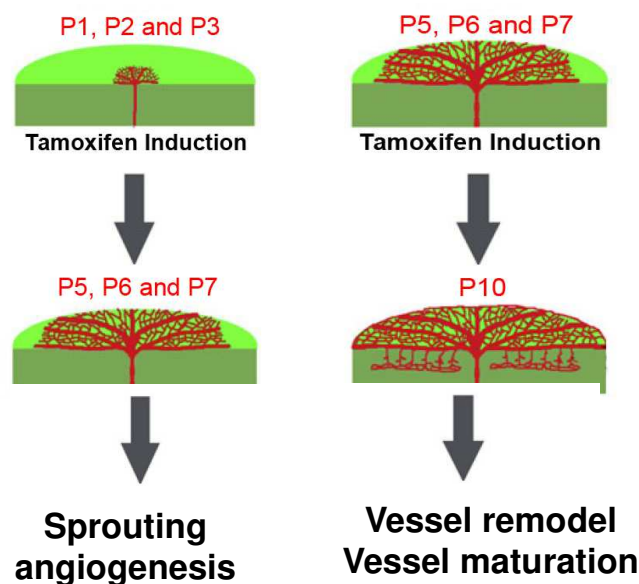


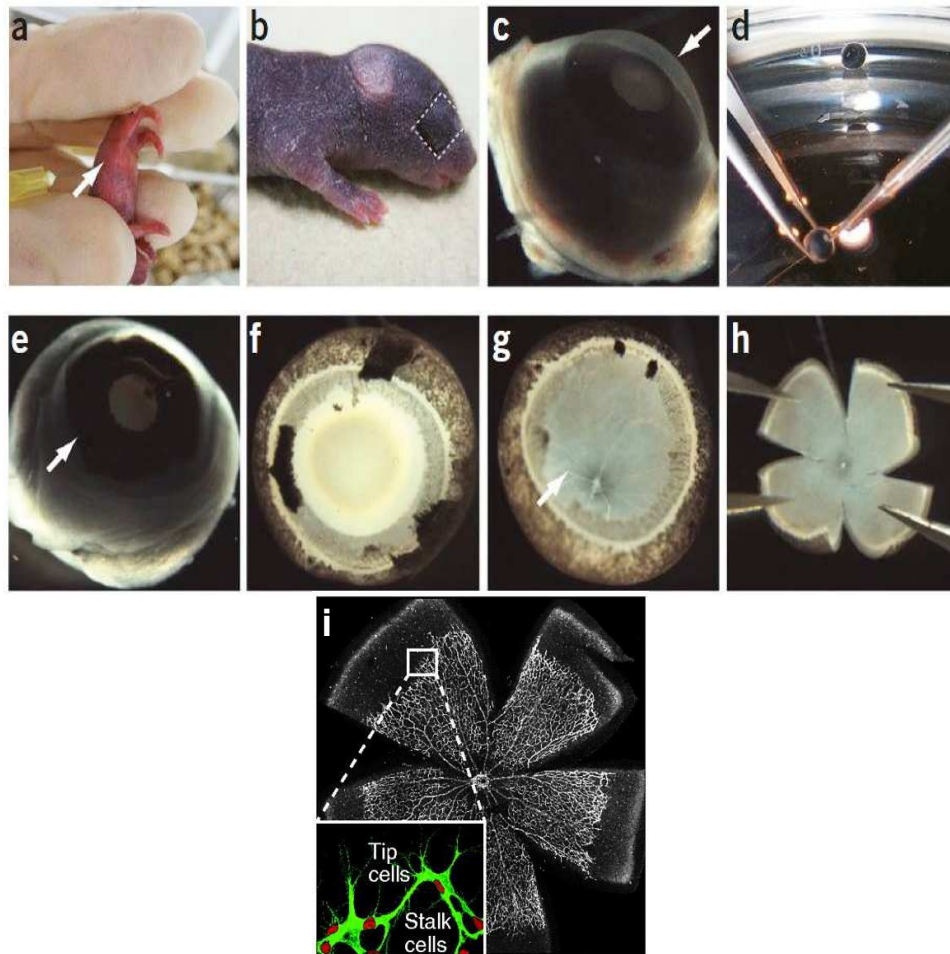
III.14: 2D-Imaging of retinal angiogenesis. Retinal vascular plexus is depicted with vessel growing direction from the bottom of the image to the top. Within the angiogenic front on top, vessel sprouting and branching can be analyzed (yellow box). Moving towards the bottom of the picture vessels get more mature and allow examination of vessel stabilization and maturation (green box). Moreover in the central plexus vessel remodeling, regression and arterio-venous differentiation can be studied (red and blue box). Image taken from [12].

The postnatal mouse retina model [3]

The procedure starts with 3 IP injections of Tamoxifen (selective estrogen receptor modulator) (III.14A, Ba) in order to induce gene deletion. According to which step of angiogenesis aims to be analyzed pups are injected and sacrificed respectively within the first 3 weeks of life, eyes removed and fixed in 4% paraformaldehyde (PFA) (III.14b). After fixation, the cornea (III.14c, d), iris (III.14e), vitreous (III.14f) and hyaloid vessels (III.14g) are removed through dissection under a stereomicroscope. Immunostaining follows blocking- and permeabilization step. Finally, 4 incisions (as indicated III.14h) are made to flatten the samples and prepare them for whole mount.

a



b

III.15: Postnatal mouse retina angiogenesis model. **A** Scheme illustrates different time points for Tamoxifen injections and corresponding stages of vascular development being affected. **B** shows single protocol steps of the postnatal angiogenesis model (a-h) and confocal image after IHC (i). Images modified from [3] and [7].

3.3.1 Whole retina immunohistochemistry:

Dissection and labeling of retinas was performed as previously described [3]. Eyes were collected from P6 onwards, as indicated, and fixed in 4% paraformaldehyde (PFA) on ice for 2 hours. Retinas were then dissected and stained as whole mounts. Therefore they were incubated in retinal blocking buffer (1%BSA and 0,3% Triton X-100), washed twice in Pblec

(1% Triton X-100, 1mM CaCl₂, 1mM MgCl₂ and 1mM MnCl₂ PBS [pH6.8]), and incubated overnight at 4°C with Isolectin-B4, in order to label the retinal endothelium. Further antibodies diluted in Pblec were added to highlight other retinal components. (For antibody information and dilutions see antibody table in materials part.)

Primary antibodies were followed by 2-hour incubation of an anti-rabbit, anti-mouse or anti-rat IgG Alexa in 488 nm, 546 nm or 633 nm (1:200). Alexa 546 nm conjugated Phalloidin (1:100) (Invitrogen) was used for visualization of the actin cytoskeleton.

Whole mount of retinas was performed by the use of a low-intensity stereomicroscope light (Zeiss STEMI SV11). 4 incisions were made to flatten the retinas and Fluoromount-G (Southern Biotech) pipetted drop wise onto them.

3.3.2 Proliferation assay

Proliferating cells were labeled using Bromodeoxyuridine (BrdU) proliferation assay as described in [3]. BrdU is a thymidine analog that replaces thymidine during S-phase of dividing cells. The experiment was started with IP-administration of 300 µg BrdU (Invitrogen) per pup, 4 hours prior to sacrifice and eye collection. Subsequent to retinal labeling with Erg1/2/3 (Santa Cruz) to tag the nucleus and isolectin-B4 (LifeTechnologies) staining to highlight the vasculature, retinas were post-fixed in 4% PFA for 30 minutes, washed 3 times with PBS and incubated for 1 hour in formamide- sline sodium citrate (SSC) solution (50% formamide (Sigma Aldrich), 5% 20x SSC with additional ddH₂O) to denature and expose the BrdU-labeled DNA. Further 30 minutes of incubation in a 6M HCl and 0,1% Triton X-100 solution completed the exposure of the halogenated nucleotide antigen, which then could be visualized after overnight incubation at 4°C with an anti-BrdU antibody (BD Bioscience).

Quantification was carried out by comparison of BrdU-positive Erg1/2/3-positive EC and BrdU-negative Erg1/2/3-positive EC in high-resolution confocal images (Leica TCS SP5 II microscope).

3.4 Immunohistochemistry in other tissues

3.4.1 Whole embryo immunohistochemistry

Embryos were dissected in PBS at embryonic day (E) 10.5, yolk sacs and skin fixed overnight in fixation buffer (80% methanol, 20% DMSO). Samples were rehydrated in 0,1% Tween-20 in PBS, incubated in blocking buffer (10% goat serum, 5% BSA in PBS) for 2 hours and exposed to primary antibodies overnight at 4°C. After 5-7 hours of washing with 0.1% Tween-20 in PBS samples were incubated with secondary antibodies overnight at 4°C and thereafter whole mounted [2].

3.4.2 Skin immunohistochemistry

Samples were collected fixed and stained as previously described [65]. Tail and ear skin was cut into small pieces and incubated in 5mM EDTA in PBS at 37°C for four hours.

3.4.3 Skeletal muscle immunohistochemistry/ Cremaster - in vivo microscopy

Mice were anesthetized by IP injection of a ketamine/xylazine mixture (100 mg/kg ketamine and 10 mg/kg xylazine). The right cremaster muscle was exposed through ventral incision of the scrotum. Muscle then was opened ventrally in a poorly vascularized zone, using careful electrocautery to stop any bleeding, and spread over the pedestal of a custom-made microscopy stage. Epididymis and testicle were detached from the cremaster muscle and placed into the abdominal cavity. Throughout the procedure and after surgical preparation, the muscle was superfused with warm buffered saline. Tissue was fixed in 2% PFA and immunostained a whole mount following to *in vivo* microscopy [66].

3.5 Molecular biological methods:

3.5.1 DNA isolation of mouse ear biopsies

A 0,3 cm tip of mouse ear was cut, placed into a microcentrifuge tube and 250 µl of lysis buffer (Viagen Direct PCR-tail; PEQLAB Biotechnology) and proteinase K (Sigma-Aldrich) (1:100 dilution) were added. Samples were incubated at 55°C overnight with gentle shaking. Next, samples were centrifuged for 10 minutes at 5000 RPM in a bench top microcentrifuge (Eppendorf centrifuge 5410) to pellet residual hair. The supernatant was carefully aspirated and transferred to a new tube. 1µl of each sample was used for PCR analysis. DNA was stored at 4°C.

3.5.2 Polymerase chain reaction (PCR):

For PCR, a thermocycler (PTC-100[®] Peltier Thermal Cycler, MJ-Research) was used to amplify the target sequences and so allowed genotyping of the mice. Amplification reaction involved the sample of template DNA, two/three oligonucleotide primers, 1mM deoxynucleotide triphosphates (dNTPs, Qiagen), 10x reaction buffer (Qiagen), magnesium and a thermostable DNA polymerase (Taq-polymerase, PeQlab).

PCR reactions started with a pre-incubation step, which denatures the template DNA at 95-100°C. The second step was carried out at a lower temperature and enabled the oligonucleotide primers to anneal to the denatured DNA. Reaction proceeded with elongation of the primers at 72°C, the optimal temperature for the Taq-polymerase.

For genotyping of α -pv-floxed mice, a PCR with three-primer system was used:

APE2f (forward): 5'-GAAGGAATGAACGCCATCAAC-3'

APloxPf (forward): 5'-CTGAGTGACATGGAGTTTGAG-3'

APloxPr (reverse): 5'-GGACTTGTGGACTAGTTAGAC-3'

Presence of the Cdh5-CreERT2 transgene was determined by PCR using the primers:

CreF (forward): 5'-GCCTGCATTACCGGTCGATGCAACGA-3'

CreR (reverse): 5'-GTGGCAGATGGCGCGGCAACACCATT-3'

3.5.3 Agarose gel electrophoresis:

Agarose gel electrophoresis enables the visualization of the size fractionated PCR products. Prior to gel casting, dried agarose is dissolved in 1x TAE buffer by heating and is then poured into a mold, into which a comb is fitted until the mixture containing 1% agarose (Sigma-Aldrich) is still wet. Gel Red (Ethidium-bromide-equivalent, Biotium) was added to the mixture according to manufacturer's instructions in order to allow fluorescent visualization of the DNA fragments under UV light. Gels were then submerged in electrophoresis buffer (1xTAE), samples were mixed with 2 μ l of Loading Dye (Qiagen) and loaded into the sample wells. Gene ruler 1kDa (Fermentas) was used as a size marker. Electrophoresis then started by applying 100 mA for at least 60 minutes at room temperature (RT) (Biorad Power Pac 300 and associated electrophoresis gel box). Thereafter gel was placed on a UV light box and DNA pictured by using the imaging system Gel iX20 Imager (Intas Science Imaging), allowing the discrimination of wildtype (wt) (1.1kb and 186bp), flox (240bp) and Cre-mediated-recombined (595bp) alleles.

3.6 Cells culture methods

Cell culture was carried out in a sterile bench (Steril VBH compact) applying sterile working techniques. Cells were cultivated at 37°C, 5% CO₂ and 95% humidity (incubator, Binder). Cells were centrifuged at 900-1000 RPM for 5 minutes, using a Rotina 35 R centrifuge (Hettich-Lab Technologies).

3.6.1 Freezing and thawing of cells:

Cells were stored at -80°C for short term (up to 6 months) or in liquid nitrogen for longer term. Regarding the freezing procedure, cells were centrifuged and medium was completely aspirated before re-suspending them in ice-cold freezing medium, transferring them to Cryotubes and placing them on ice.

For thawing, cell-tubes were put in a 37°C waterbath (Haake SWB25). Cells were then immediately transferred into 6 ml of medium, centrifuged and resuspended in medium before plating them on culture plates.

3.6.2 Cell lines

Human umbilical endothelial cells (HUVECs) were purchased from Promocell (C-12203) and cultured with EC growth medium (Promocell): Medium 199 (Gibco, LifeTechnologies) 1% Penicillin/Streptomycin (PS, Sigma-Aldrich), 20% Fetal Calf Serum (FCS, Biochrom);1:1.

3.6.3 siRNA transfection

HUVECs were transfected with a siRNA duplex against α -pv (Sigma, SASI_Hs01__00165014 and SASI_Hs01_00165015) and scrambled control (Sigma SIC001) using Lipofectamine 2000 (Invitrogen) according to manufacturer's protocol. Briefly, Lipofectamine 2000 and siRNAs were diluted in reduced serum medium (OptiMem, Gibco, LifeTechnologies) and incubated on the cells. After 6 hours the Optimem medium was removed and replaced by HUVEC culture medium (Endothelial cell growth medium: Medium 199 (1:1)). All experiments were carried out 48 hours after transfection.

3.6.4 Cell lysis

Cells were lysed in protein lysis buffer (150 mM NaCl, 50 mM Tris pH 7,4, 1 mM EDTA, 1% Triton-X100, supplemented with protease inhibitors (Roche)). They were scraped off the plate, then transferred to a microcentrifuge-tube and sonicated twice for 3 seconds to shear the DNA and so reduce sample viscosity. Following, cells were centrifuged at 12000 RPM for 10 minutes at 4°C. The pellet was removed and either continued with protein quantification or sample storage at -20°C.

3.6.5 Protein quantification: Bicinchoninic acid assay (BCA)

The biochemical assay was used to determine the total protein concentration in a solution. Reagents were prepared according to manufacturer's instruction of BCA-kit (Biorad). After pipetting them upon the samples, protein concentration was exhibited by a color change of the sample solution from green to purple in proportion to the protein concentration, which was then measured using colorimetric techniques. The color change relies on a biochemical reaction where two molecules of bicinchoninic acid chelate a single Cu^+ ion, forming a purple water-soluble complex. The amount of protein was quantified by measuring the absorption spectra of the sample solutions (Tecan, Infinite F200), which were compared with solutions of known protein concentration.

3.6.6 SDS page

Protein samples were homogenized in Laemmli sample buffer (277.8 mM Tris-HCl pH 6.8, 4.4% LDS, 44.4% (w/v) glycerol, 0.02% bromophenol blue) and boiled for 5 minutes before lysates were loaded and resolved by 10% sodium dodecyl polyacrylamide gels (SDS-PAGE). The gel electrophoresis principle relies on electric potential, which, if applied to both ends of a gel, allows protein migration depending on size and charge, from the anode to the cathode, resulting in fractionation of the probe with specific protein locations within the gel. In order to estimate protein size a protein standard (Protein PageRuler™ Thermo Scientific) was loaded in the first slot of the gel. Proteins then were separated by application of 90 Volt (V) for at least 60 min to the SDS-PAGE fully surrounded by running buffer (25 mM Tris-base, 190 mM glycine, 0.1% SDS (pH 8.3)).

3.6.7 Immunoblot

Proteins were electrophoretically transferred from gels onto nitrocellulose membranes by using a transfer buffer (25 mM Tris Base, 192 mM glycine, 20% methanol (pH 8.5)) and applying amperage according to protein sizes. After the blotting process membranes were washed in washing buffer (Tris-buffered saline (TBS) and 0.1% Tween-20 (TBST)) and incubated for 1 hour at RT in nonfat-dried milk (Sigma-Aldrich) in order to prevent non-

specific binding reactions. Primary antibodies (for antibodies and dilutions see table in materials part) were diluted in TBST and incubated on the membrane overnight at 4°C. After 1 hour incubation with respective secondary antibodies (for antibodies and dilution see table in materials part) and further membrane-washing steps, bound antibodies were detected the following day using enhanced chemiluminescence (Millipore) and Wasabi software 1.4 (Hamamatsu, Photonics). GAPDH was used a housekeeping gene.

3.6.8 Immunofluorescence-staining of cells

HUVECs were grown on coverslips in multi-well plates, where they were directly fixed using 4% PFA. After 15 minutes of incubation at RT, the fixative was removed and washed out by rinse the cells twice in PBS for 5 min. Cells were then covered with PBS-0.1% Triton X-100 for permeabilization. A 1-hour blocking step followed (HUVEC blocking buffer: 3% FBS, 1% BSA, 1% Triton in PBS and thereafter the cells were incubated overnight with the primary antibody (for antibodies and dilution see table in materials). Fluorescently labeled secondary antibody incubation followed. Slides then were analyzed by confocal microscopy or long-term stored at 4°C, protected from light.

3.7 Microscopic models

3.7.1 Confocal Microscopy

Images were acquired and processed using a Leica TCS SP5 II microscope, LAS Montage Imaging software (Leica) and the IMARIS Digital Imaging software (Biplane). Wide-field images were acquired using DeltaVision OMX V3 microscope (Applied Precision) in conventional mode and Cascade II:512 EMCCD cameras (Photometrics). SoftWoRx software (Applied Precision) was used for deconvolving the images with enhanced additive method.

3.7.2 *In vivo* Microscopy

The setup for *in vivo* microscopy was centered on an AxioTech-Vario 100 Microscope (Zeiss), equipped with LED excitation light (Zeiss) for fluorescence epi-illumination. Microscopic images were obtained with a water dipping objective (20x, NA 0.5) and acquired with an AxioCam Hsm camera and Axiovision 4.6 software.

3.8 Statistical analysis

Samples were collected independently of one another for each experimental series. All measurements were performed with $N \geq 7$ mice per genotype, obtained from minimum of three independent litters three times for each experimental series; the mean of the three repeats was used. The data shown are mean \pm s.e.m.. All quantitative data were analyzed using unpaired Student's t-Test using Excel (Microsoft) software after testing for normal distribution of the data. Error probabilities (P-values) lower than 0.05 (*), 0.01 (**), or 0.001 (***) were considered significant.

Qualitative microscopic data were not statistically tested. Descriptions on experimental microscopic observation are always based on minimum three independent experiments.

4 RESULTS:

4.1 Imaging of endothelial Actin cytoskeleton

4.1.1 Lifeact-EGFP: Vascular expression pattern

Lifeact is ubiquitously expressed during embryogenesis

I started by analyzing Lifeact-EGFP expression in the mouse embryo. Therefore, I performed whole-mount immunostaining of E10.5 embryos with an antibody against cluster of differentiation (CD) 31 in order to visualize ECs. After confocal imaging and 3-dimensional reconstruction I found ubiquitous Lifeact-EGFP expression. Epithelial- and mesenchymal- as well as neuronal actin structures were demarked, precluding adequate imaging of F-actin structures in ECs (Fig.1).

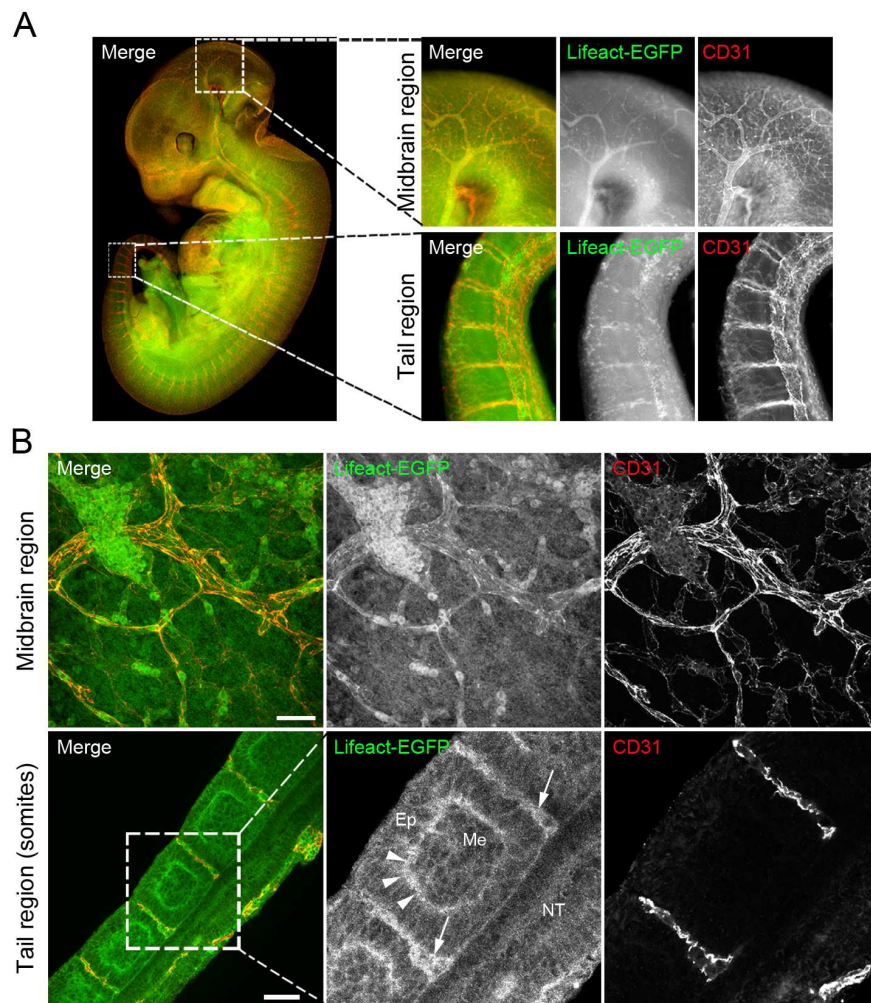


Fig.1: Lifact-EGFP is ubiquitously expressed during embryogenesis. E10.5 Lifact-EGFP transgenic embryo whole-mounts with CD31 (in red) immunostaining and Lifact-EGFP depicted in green. (A) 3D reconstruction. (B) Confocal sections. Arrows point to intersomitic vessels; arrowheads indicate epithelial actin-rich apical site. Scale bars: 50 μ m. Ep: Epithelial cell; Me: Mesenchymal cell; NT: Neural tube.

Lifact-EGFP is mainly expressed in EC in the postnatal mouse retina

Next I studied Lifact-EGFP in postnatal retinas of P5 and P10 Lifact-EGFP mice. In the retina the vascular plexus develops in close association with a pre-existing network of retinal astrocytes (ACs). Therefore I combined Isolectin B4 (IB4) staining – for EC labeling - with an antibody against glial fibrillar protein (GFAP) to visualize ACs. The analysis revealed an overlap of Lifact-EGFP expression with IB4 staining and absence of Lifact-EGFP signal in GFAP tagged ACs, indicating that Lifact-EGFP is highly expressed in ECs and almost absent in ACs. (Fig.2A, B, D). To further verify EC-identity of Lifact-EGFP expressing cells, I performed immunostaining with the endothelial specific-marker VE-Cad and found co-localization with Lifact-EGFP expression. (Fig.2C, D)

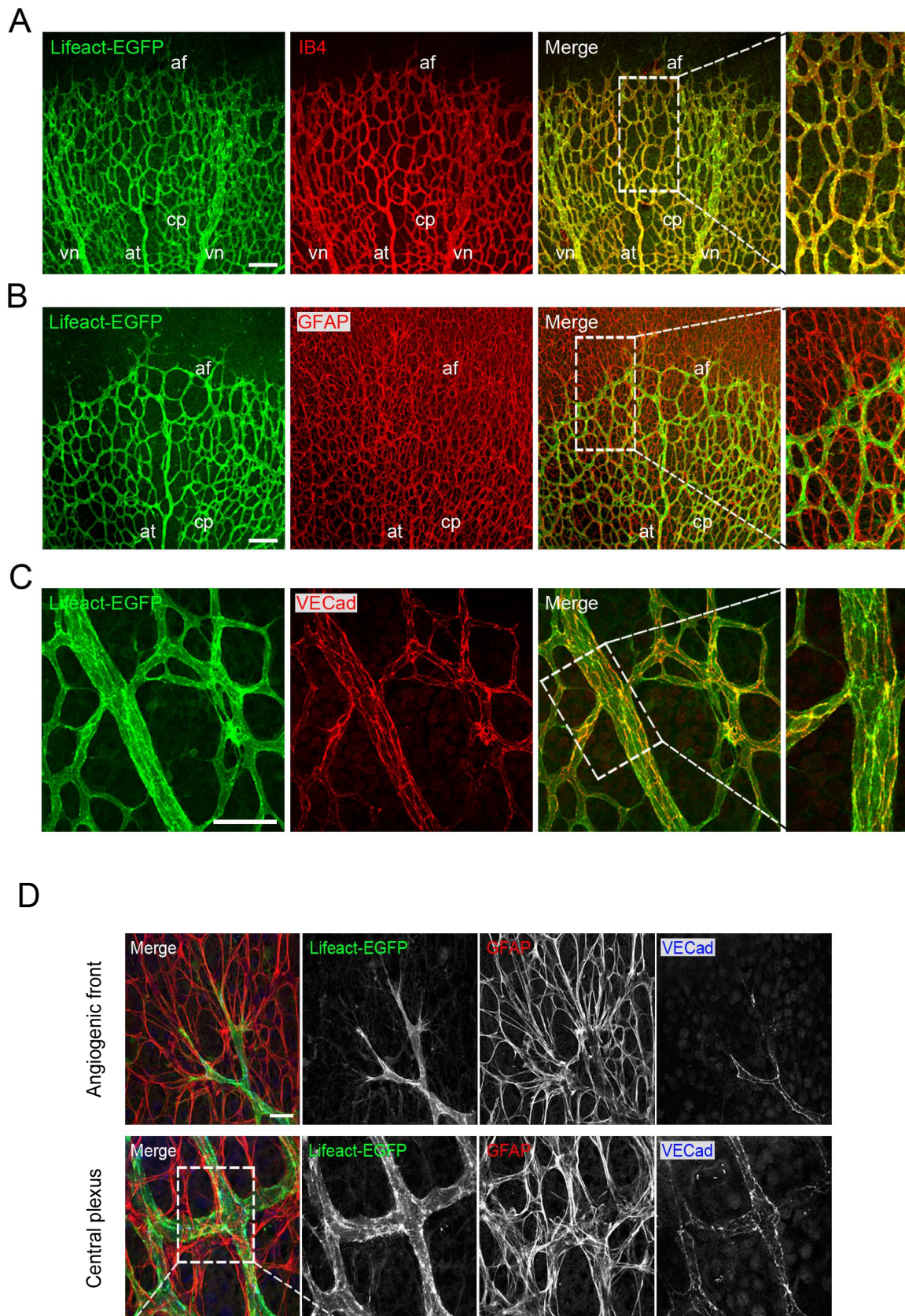


Fig.2: Lifeact-EGFP is highly expressed in EC but practically absent from AC in the postnatal retina of Lifeact-EGFP mice. Immunostaining of whole-mounted P5 retinas: IB4 (A in red), GFAP (B in red), VE-Cad (C in red). (D) pictures the angiogenic front and the central plexus (Lifeact-EGFP in green, GFAP in red, VE-Cad in blue). Scale bars: A: 100 μ m, B: 100 μ m, C: 50 μ m. af: angiogenic front; cp: central plexus; at: artery;

The analysis also showed low Lifact-EGFP expression in retinal tissue macrophages (TMs) (Fig.3).

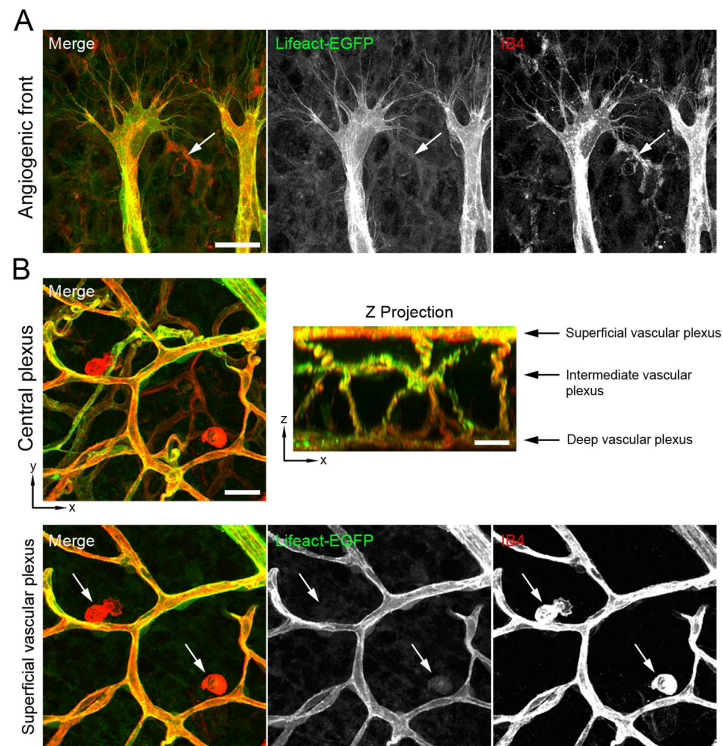


Fig.3: Lifact-EGFP expression is nearly absent in retinal tissue macrophages. IB4 (in red) staining of whole-mounted P5 (A) and P10 (B) retinas. Lifact EGFP: green. Arrows point to IB4 positive tissue macrophages. Scale bars 20 μ m.

Next, I determined whether Lifact-EGFP was expressed in retinal vascular mural cells (vMCs). To do this, I performed immunostaining of Lifact-EGFP retinas with antibodies against alpha-smooth muscle actin (α -SMA) to mark vascular smooth muscle cells (vSMCs) and neuron glial antigen 2 (NG2) to visualize pericytes (PCs) (Fig. 4). I found weak Lifact-EGFP expression in vSMCs and PCs.

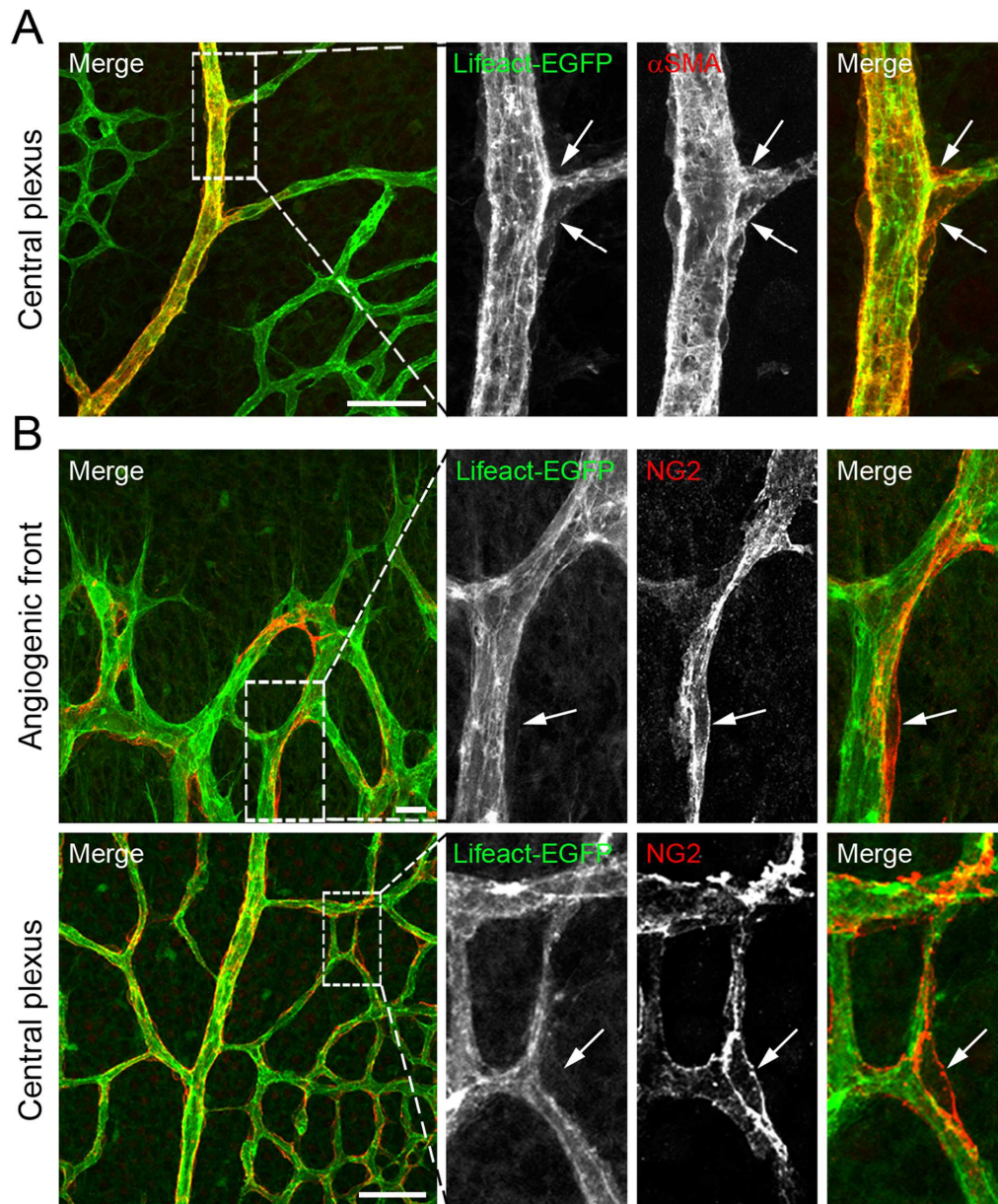


Fig.4: Lifact-EGFP is weakly expressed in vMC of the retinal vasculature. α -SMA (A in red) or NG2 (B in red) staining of whole-mounted P5 retinas. Lifact-EGFP in green. Arrows point to α -SMA-positive cells (A) and NG2-positive PC (B). Scale bars: A: 50 μ m, B: 20 μ m and 50 μ m.
Lifact-EGFP is mainly expressed in vMC in skin and skeletal muscle

Having obtained results that indicated that Lifact-EGFP is highly expressed in the endothelium of postnatal retinas, I analyzed Lifact-EGFP expression in vascular and lymphatic vessels in skin and skeletal muscle of Lifact-EGFP mice.

Skin

To characterize Lifeact-EGFP expression in the skin I performed immunofluorescence stain using antibodies against CD31 and α -SMA on ear - and tail-skin (Fig.5) in two-month old mice.

In contrast to the retina, I found that in the skin, Lifeact-EGFP was highly expressed in vMCs and weakly expressed in ECs. Moreover, I was not able to detect Lifeact-EGFP in lymphatic ECs, suggesting that Lifeact-EGFP is almost absent within those cells.

Skeletal muscle

In terms of skeletal muscle analysis, I analyzed Lifeact-EGFP expression in the cremaster-muscle and found that Lifeact-EGFP expression was highly expressed in vMCs and almost absent in ECs (Fig.5B, D).

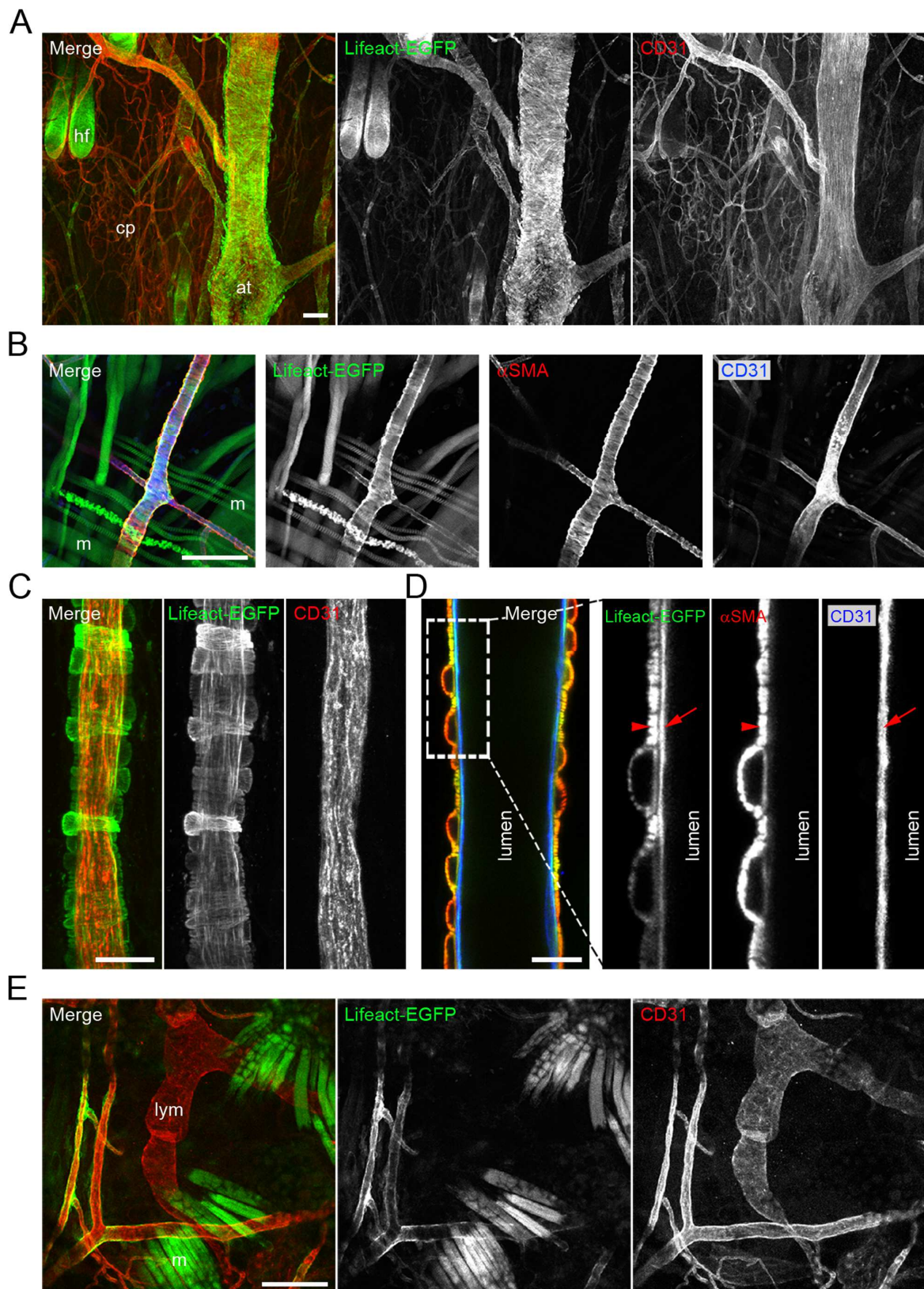


Fig.5: Lifeact-EGFP mice allow visualization of F-actin structures in vMC in skin and cremaster muscle. CD31 (in red) staining of whole-mounted tail skin (A) and ear (C and E). Lifeact-EGFP: green. (B and D) α -SMA (in red) and CD31 (in blue) double labeling of blood vessels in the cremaster muscle. Lifeact-EGFP: green. Arrows point to endothelium and arrowheads point to vMC. Scale bars: A: 100 μ m, B: 100 μ m, C: 20 μ m, D: 15 μ m, E: 100 μ m. at: artery; cp capillaries; hf: hair follicle; lym: lymphatic endothelium; m: muscle.

As the cremaster muscle is a well-established *in vivo* model to study leukocyte-EC interactions and leukocyte extravasation [67], we analyzed whether Lifact-EGFP was expressed in leukocytes. We observed that leukocytes expressed Lifact-EGFP, enabling *in vivo* visualization of rolling and adherent leukocytes at the vessel walls of postcapillary venules (Fig.6).

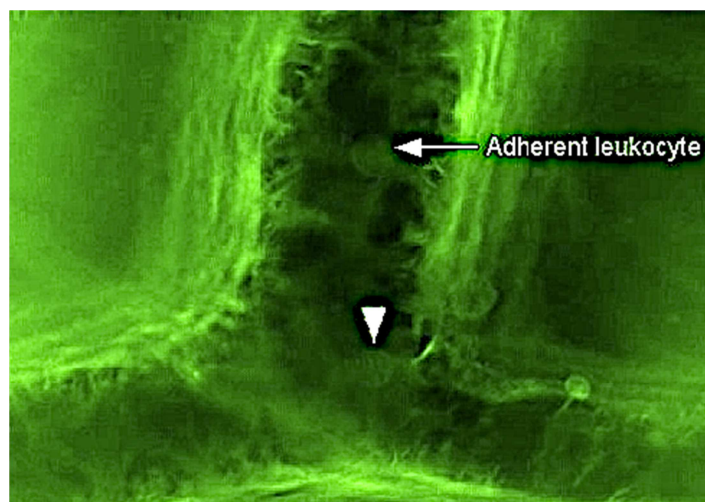


Fig.6: Postcapillary venules in the cremaster muscle from Lifact-EGFP mouse. Arrow marks adherent leukocyte. Arrowbar marks rolling leukocyte.

Lifact-EGFP an EC-specific actin marker in the retina

My results indicate that in postnatal retinas of Lifact-EGFP mice, Lifact-EGFP is mainly expressed in the vascular endothelium, allowing imaging of the endothelial actin cytoskeleton with excellent contrast. Another widely used actin marker is fluorescent Phalloidin. Whole mount immunostaining of Lifact-EGFP and WT retinas was performed and compared. (Fig.6)

Phalloidin is not EC specific [17]. In the retinal vascular plexus phalloidin presented an unequal distribution of actin labeling. In line with previous data I confirmed that phalloidin mainly stained the angiogenic front of the vascular plexus where it highlighted leading edges and filopodia of tip cells (Fig.6) [17]. On the other hand, in the central plexus, phalloidin staining in ECs was weak. It labeled non-vascular structures, thus making it difficult to visualize and analyze endothelial actin cytoskeleton in consolidated vessels.

Lifeact-EGFP signal overlapped with phalloidin at the leading edges of the vascular front and filopodia of tip cells. Besides that, it was bright all over the entire vascular plexus, enabling visualization of F-actin in all types of specialized ECs, in various stages of the angiogenic process with almost no background (Fig.7).

Taken together, these results show that in the retina Lifeact-EGFP labels endothelial F-actin in higher grade and better signal-to-noise-ratio compared to Phalloidin.

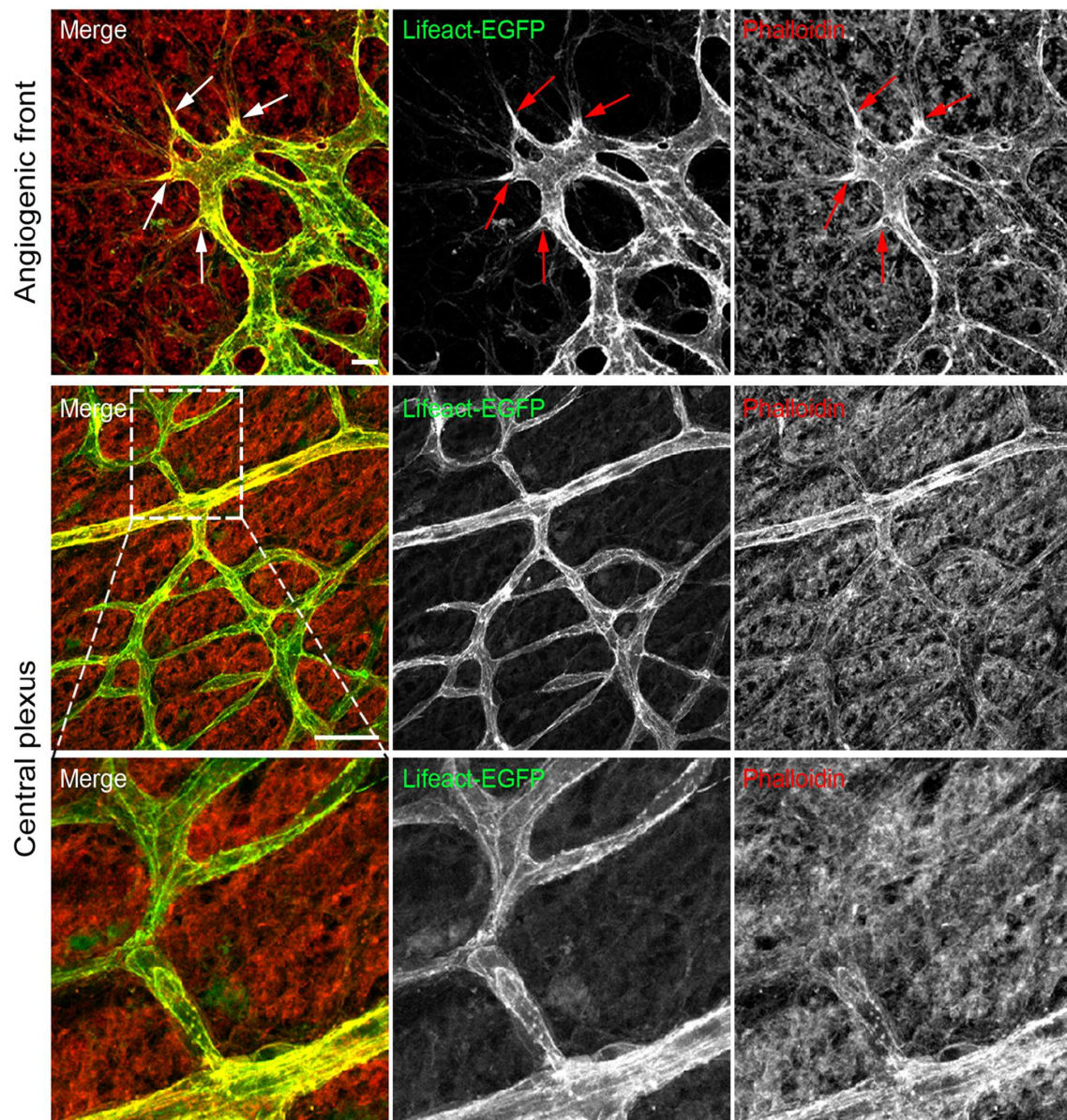


Fig.7: Lifeact-EGFP colocalizes with phalloidin. Whole-mounted P6 retinas with Phalloidin staining (in red). Lifeact-EGFP in green. Arrows point to the leading edges of tip cells that are highly enriched in actin filaments.

Visualization of single F-actin structures *in situ*

The planar outgrowth of the inner vasculature in the retina allows high-resolution three-dimensional (3D) imaging of the endothelium. Hence, all stages of the sprouting process can be efficiently analyzed in a single sample owing to spatiotemporal sequence of angiogenic network formation. Up to date, there is no tool able to show cytoskeletal details of the sprouting process within the angiogenic front. Our results indicated an extraordinary potential of Lifeact-EGFP in the visualization of endothelial specific F-actin in the postnatal mouse retina. Therefore we performed high-resolution confocal laser scanning microscopy and high-power deconvolution imaging of sprouting vessels in P6 retinas of Lifeact-EGFP mice. Indeed, we found that in the migrating tip cells, Lifeact-EGFP brightly labeled cortical actin, filopodia as well as long and thin actin bundles in the cytoplasm, most likely representing stress fibers (Fig.8A, B, D).

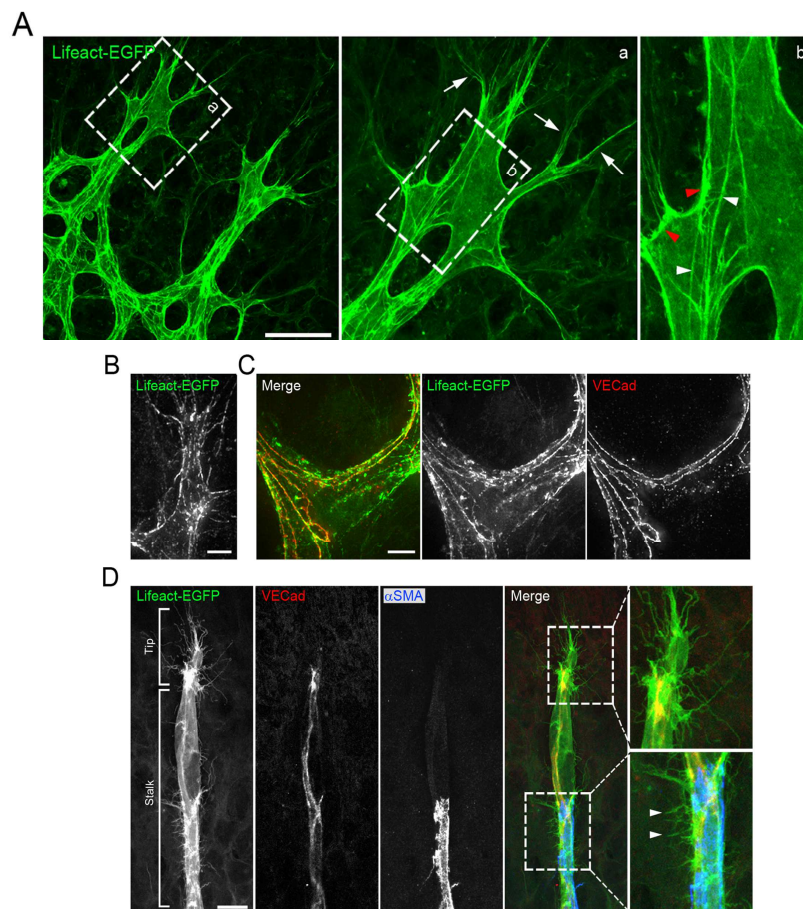


Fig.8: Lifact-EGFP labels cortical actin, filopodia and stress fibers in retinal tip and stalk EC. (A) Migrating tip cells. Arrows indicate filopodia, white arrowheads point to actin filaments in the cytoplasm and red arrowheads point to cortical actin. High-magnification deconvolution images of tip (B) and stalk cells (C) showing details of cytoskeletal organization (Lifact-EGFP: green), with fine actin-rich filopodia protrusions and cortical actin cables, running along adherens junctions (VE-Cad: red) (D) VE-Cad (in red) and α -SMA (in blue) double labeling of vascular sprout. Lifact-EGFP: green. Arrowheads indicate short actin filament protrusions in stalk cells.

The analysis also revealed that in stalk cells, Lifact-EGFP highlighted endothelial junctions and short filopodia-like protrusions along the cell membrane (Fig.8 C, D). Similar protrusions were also observed in EC in the established plexus and in anastomosing tip cells at the fusion points (Fig.9).

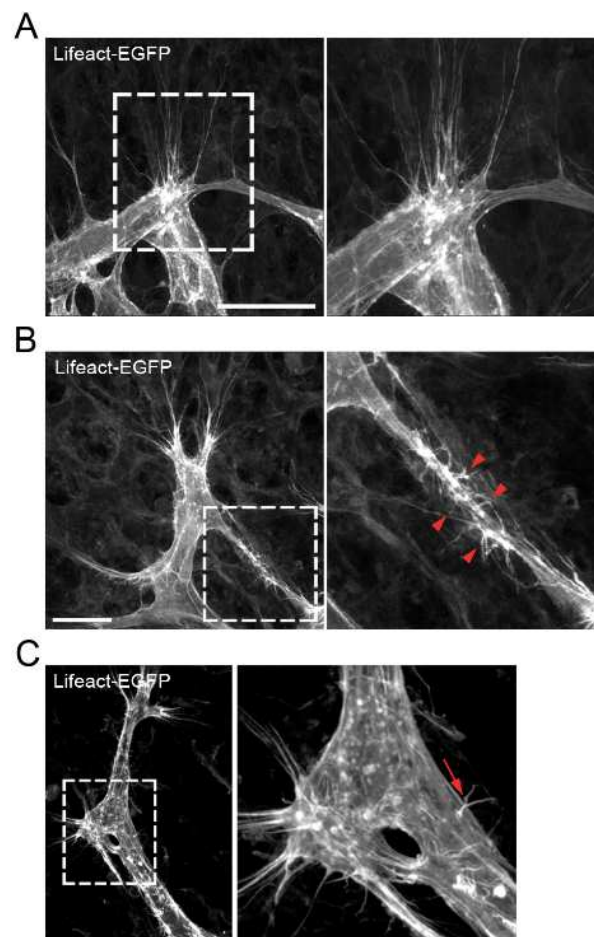


Fig.9: Visualization of endothelial actin cytoskeleton in a sprout during anastomosis of tip cells (A;B) (Lifact-EGFP: white) Arrowheads point to short actin filament protrusions during fusion. 3-dimensional reconstruction of an EC sprout (C) (Lifact-EGFP: white). Arrow points to actin filament protrusions.

Lifact-EGFP a marker for apical-basal-polarity

Lumen formation requires EC polarity. The actin cytoskeleton reorganizes and allows the formation of a luminal and abluminal side of an EC.

I whole-mounted retinas of Lifact-EGFP mice and stained them with an antibody against intercellular adhesion molecule 2 (ICAM-2) (Fig.10), a marker allowing visualization of lumenized vessels by marking the apical EC membrane. High-resolution confocal images revealed a Lifact-EGFP signal partially adjacent to ICAM-2 positive structures. Furthermore, Lifact-EGFP expression was not simply restricted to the luminal site, but highlighted abluminal F-actin structures as well.

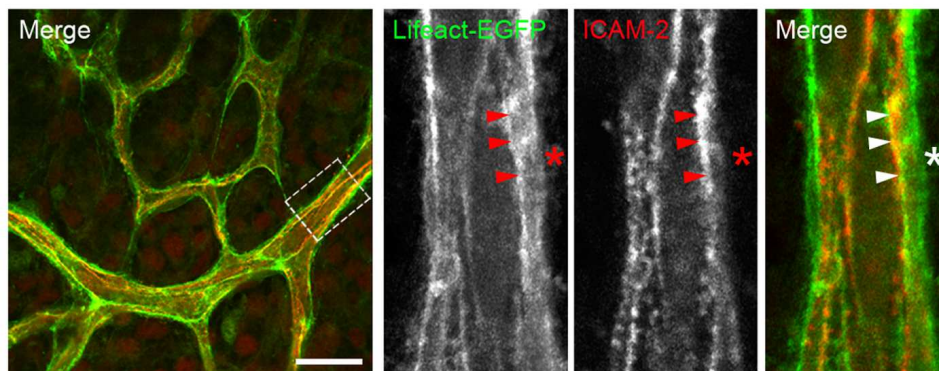


Fig.10: Lifact-EGFP is a marker for apical-basal cell polarity. Optical section of retinal vasculature of P5 Lifact-EGFP transgenic mouse retinas. ICAM-2 staining (in red), Lifact-EGFP (in green). Arrowheads point to the luminal endothelial membrane and the asterisk marks the abluminal side of the vessel. Scale bar: 20 μ m.

4.2 Functional α -parvin characterization:

To gain insights in the function of endothelial α -pv *in vivo*, our group intercrossed mice carrying a *loxP*-flanked α -pv gene (α -pv^{fl/fl}) (unpublished data) with Cadh5(PAC)-CreERT2 mice and induced α -pv gene deletion in ECs by administering three consecutive IP injections of Tamoxifen in newborns starting at P1. Cre-expression was confirmed by PCR on ear DNA (Fig.11a). Furthermore Western blot analysis of lung lysates from P7 α -pv^{fl/fl}; Cadh5(PAC)-Cre^{ERT2} (referred to herein as α -pv^{i Δ EC}) confirmed downregulation of α -pv expression when compared with lysates from Cre-negative control littermates (Fig.11b).

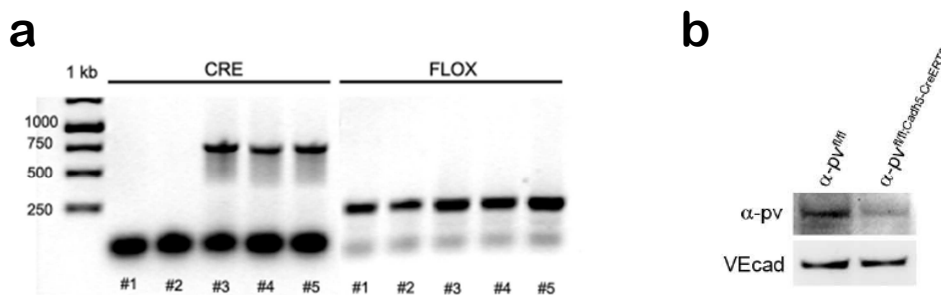


Fig.11: Identification of α -pv^{i Δ EC} mice. (a) PCR on ear DNA for CRE (750 bp) and FLOX (250 bp). (b) Western blot analysis of lung lysates from P7 control and α -pv^{i Δ EC} mice, three days after tamoxifen administration. VE-Cad was used as loading control.

IB4 staining of control and α -pv^{i Δ EC} retinas showed significant reduction in radial expansion of the vascular plexus from the center towards the periphery (Fig.12 a, b). Migratory length in α -pv^{i Δ EC} retinas was 17% lower than in littermate control mice, indicating a decreased retinal sprouting angiogenesis (Fig.12 a, b).

Furthermore, the number of branch points was compared between α -pv^{i Δ EC} and control mice to gather information about vessel density. The latter was significantly reduced in α -pv^{i Δ EC} retinas compared to control retinas (Fig.12 a, b). Next, I quantified vessel sprouting at the angiogenic front by counting the number of sprouts per vessel length and found a significant decrease in mutant retinas (Fig.12 a, b). Interestingly number of filopodia presented no difference in the absence of α -pv (Fig.12 c, d).

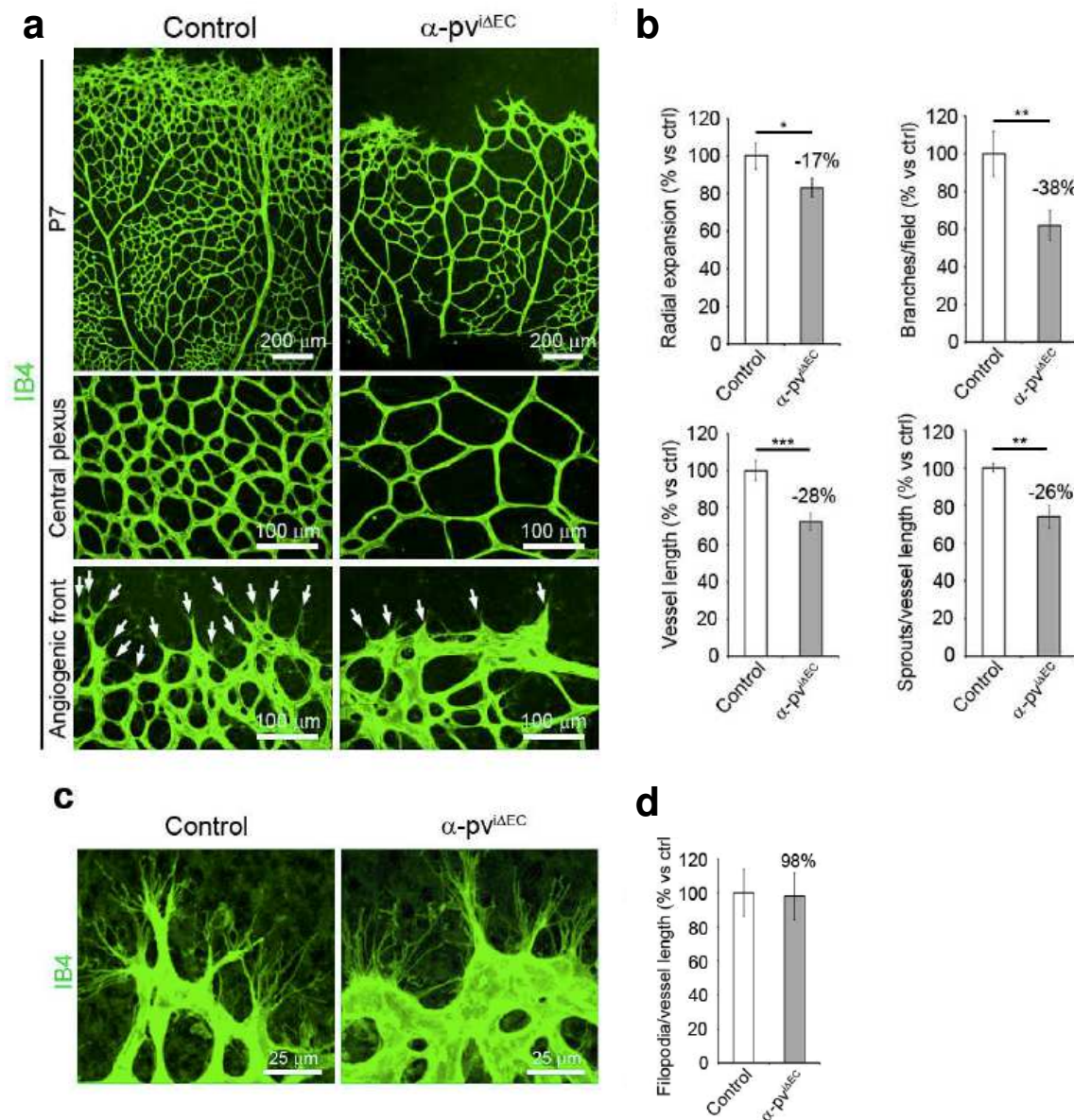
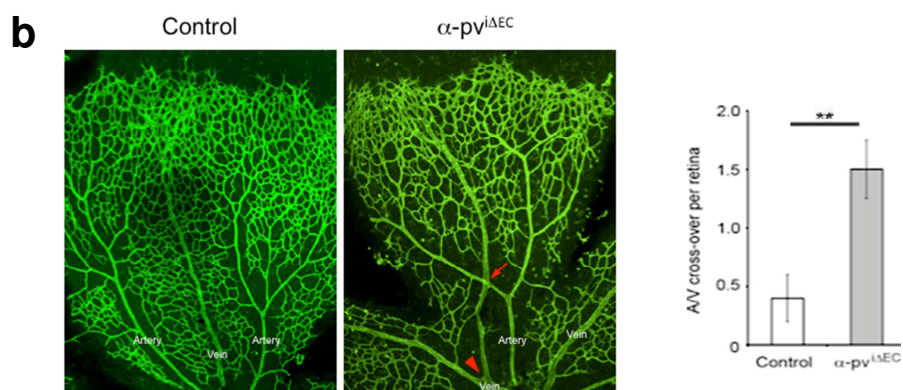
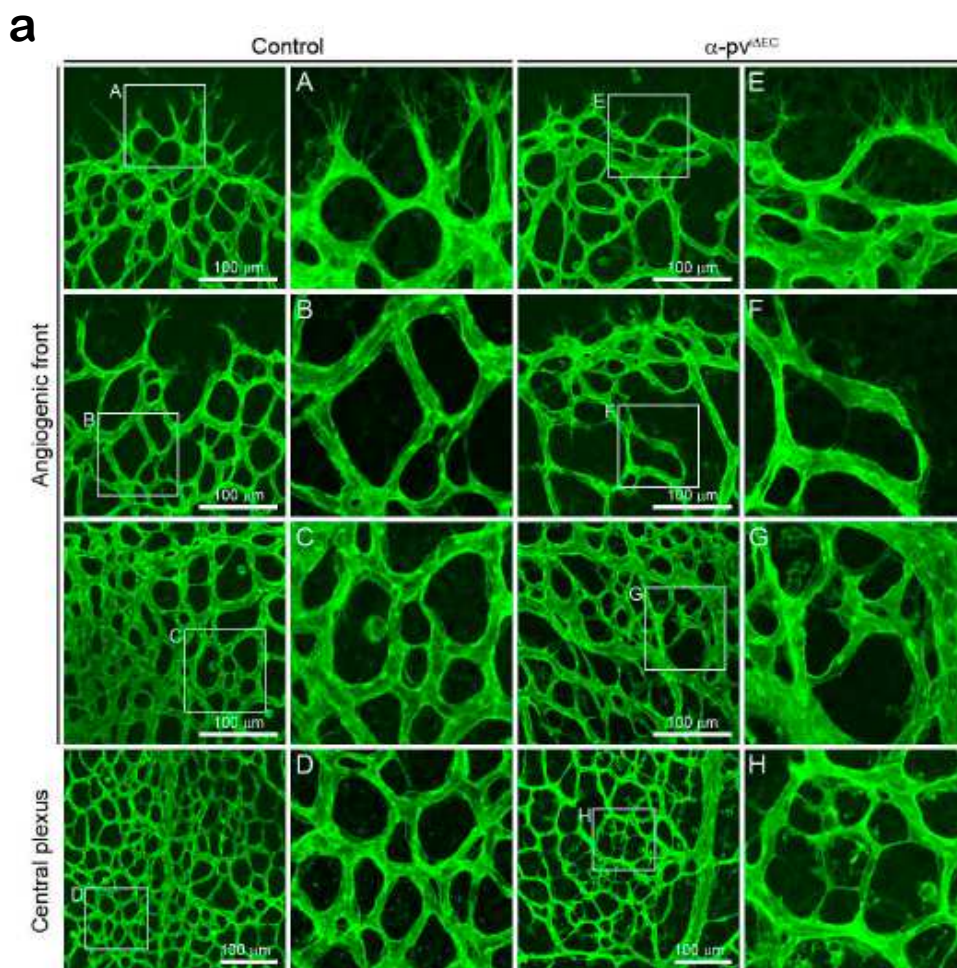


Fig.12: Loss of endothelial α -pv leads to impaired vessel sprouting and hypovascularization. (a) IB4 staining of whole-mounted P7 retinas from control and α -pv^{iΔEC} mice. Arrows point to vessel sprouts. (b) Quantification of vascular parameters as indicated. Values represent percentages of means versus (vs) respective controls \pm s.e.m. P values are 0.024, 0.002, 0.001 and 0.004, respectively. (c) High magnification confocal image of tip cells and filopodia at the angiogenic front in control and α -pv^{iΔEC} P7 retinas. (d) Quantification of number of filopodia per vessel length. Values represent percentages of means vs controls \pm s.e.m. ($n \geq 7$ mice per genotype)

Loss of endothelial α -pv alters vessel morphology and impacts on vessel patterning.

Further analysis of IB4 labeled P6 retinas showed differences in vessel morphology between α -pv^{iΔEC} and control retinas. Whereas α -pv^{iΔEC} vessels displayed irregular shapes, with caliber

fluctuation and unstable appearance, control vessels showed regular shapes (Fig.13 a). Moreover vessel patterning in α -pv^{iΔEC} retinas was abnormal compared to control. I found an increased number of arterial-venous (AV) cross-overs per retina (Fig. 13 b). Further I observed higher occurrence of small caliber vessel segments (IB4-labeled connections between two branch points) in α -pv^{iΔEC} retinas compared to control retinas. ICAM-2 staining showed no signal of the apical/luminal side marker on the small caliber vessel segments (Fig.13 c).



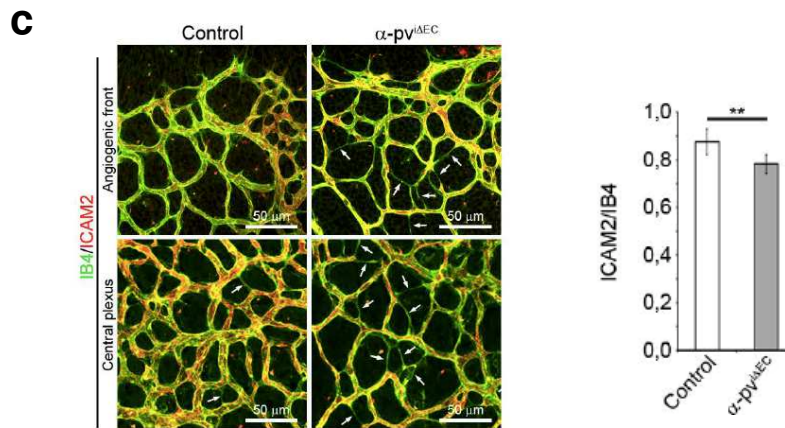


Fig.13: Depletion of α -pv alters vessel morphology and patterning. (a) P7 control and α -pv^{iΔEC} retinas labeled for IB4. (b) P7 control and α -pv^{iΔEC} retinas labeled for IB4. Arrows point to A/V cross-overs. A/V cross-overs per retina. Values represent percentages of means \pm s.e.m. P value is 0.01 (c) P6 control and α -pv^{iΔEC} retinas labeled for IB4 and ICAM2. Ratio of ICAM2-positive vessel segments to IB4-positive vessel segments. Values represent percentages of means \pm s.e.m. P value is 0.01. $n \geq 7$ mice per genotype.

Postnatal deletion of endothelial α -pv compromises EC proliferation.

Angiogenic growth of blood vessels requires proliferation of ECs [6]. To investigate whether the observed defects in vessel density were due to defects in cell proliferation, I performed BrdU incorporation assay in control and α -pv^{iΔEC} mice followed by co-labeling of BrdU, the EC-specific transcription factor Erg1/2/3 and IB4. I found a reduced number of proliferating ECs in α -pv^{iΔEC} retinas compared to control retinas, indicating that α -pv positively controls proliferation of ECs (Fig.14).

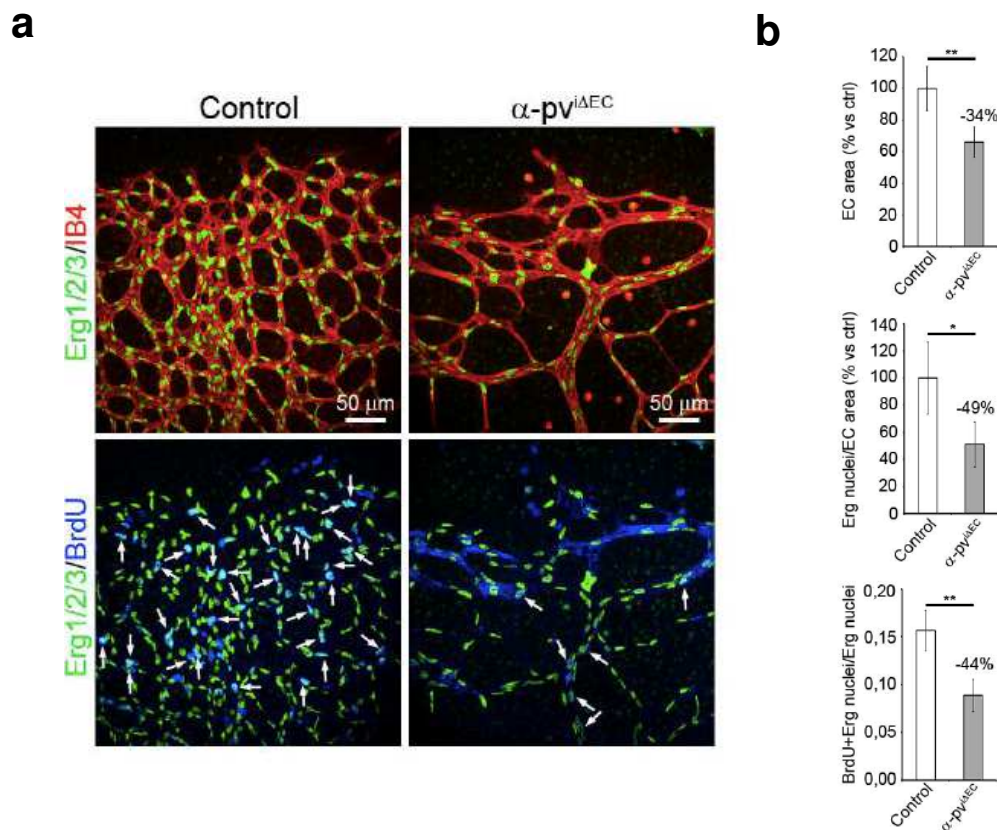


Fig.14: Loss of endothelial α -pv results in a proliferation deficit. (a) P6 control and α -pv^{iAEC} retinas labeled for Erg1/2/3, IB4 and BrdU. (b) Quantification of EC area (IB4 positive area), EC nuclei (Erg1/2/3 positive nuclei) per EC area and ratio of EC/BrdU- positive nuclei to total EC nuclei. Values represent percentages of means \pm s.e.m. P values are 0.007, 0.014 and 0.002, respectively. $n \geq 7$ mice per genotype.

Loss of endothelial α -pv results in ectopic vessel regression.

Next, I analyzed whether depletion of α -pv from ECs impaired vessel integrity by performing whole-mount immunostaining of control and α -pv^{iAEC} retinas using an antibody against collagen IV (Coll IV) and IB4, taking advantage of the fact that regressing ECs leave empty basal membrane sleeves rich in Coll-IV [3]. Confocal microscopy analysis showed a significant increase in Coll-IV segments lacking IB4 in α -pv^{iAEC} retinas compared to control retinas (Fig.15 a, b), indicating compromised vessel stability in α -pv^{iAEC} mice. Furthermore to analyse survival, I performed immunostaining of control and mutant retinas with an antibody against cleaved Caspase-3. Microscopic sample evaluation showed a significant increase in EC-apoptosis in absence of α -pv (Fig.15 c, d).

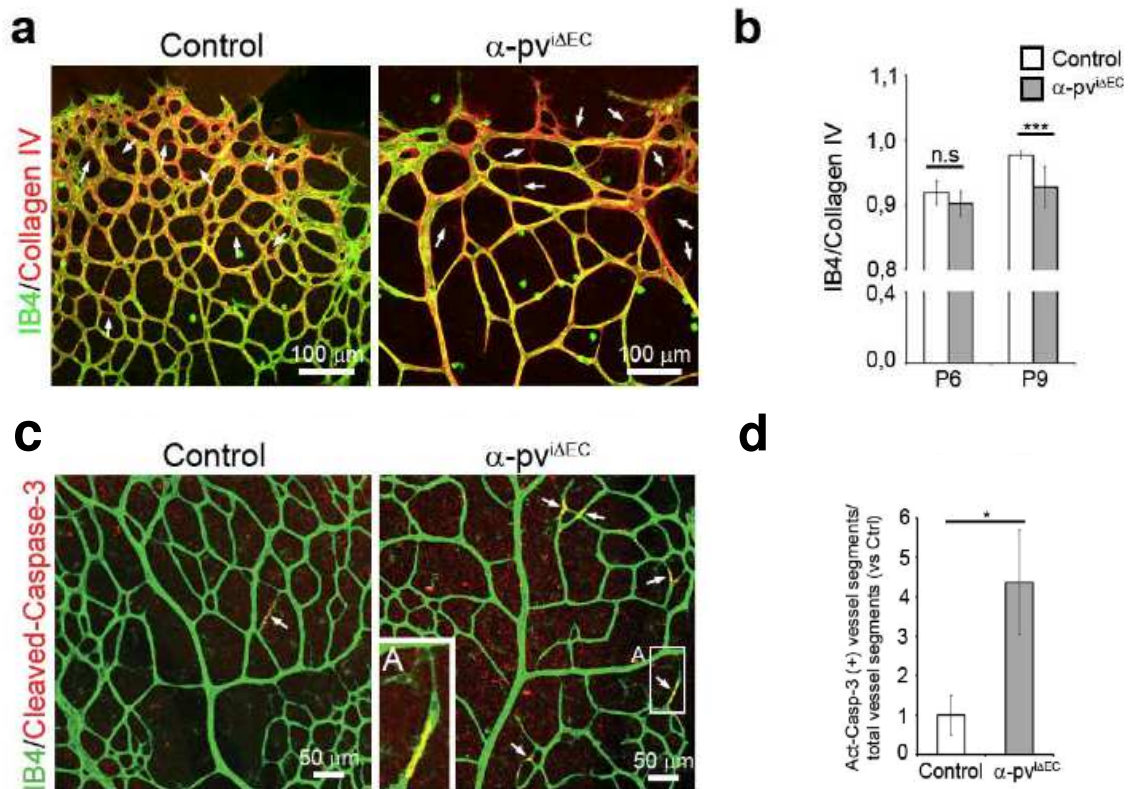


Fig.15: Loss of endothelial α -pv^{iAEC} results in increased vessel regression. (a) P8 control and α -pv^{iAEC} retinas labeled for IB4 and collagen IV. Arrows point to empty collagen IV sleeves. (b) Ratio of IB4-positive vessel segments to collIV-positive vessel segments. Values represent means \pm s.e.m. P values are 0.18 and 0.0004, respectively. (c) P7.5 control and α -pv^{iAEC} retinas labeled for IB4 and cleaved-(active)-caspase-3. Arrows point to cleaved caspase-3-positive vessel segments. (d) Relative ratio of cleaved (active)-caspase-3 positive vessel segments to total vessel segments. Values represent means versus control \pm s.e.m. P-value is 0.05. $n \geq 7$ mice per genotype.

Depletion of α -pv affects vascular integrity by interfering with junctional formation.

Blood vessel stability and maintenance of vascular integrity greatly depend on cell-cell junctions between ECs [23]. Therefore I performed whole-mount immunostaining for the junctional marker VE-Cad in α -pv^{iAEC} and control retinas and found a diffuse and discontinued stain around cell boundaries in vessels of α -pv^{iAEC} retinas compared to the sharp and continuous stain observed in vessels of control retinas (Fig. 16 a). Closer morphologic analysis revealed cytoplasmic dotted VE-Cad stain within several vessel segments of mutant mice as well as fragments of vessels partially disconnected from the vascular bed. The analysis also revealed a higher incidence of gaps between ECs in α -pv^{iAEC} vessels compared to control vessels.

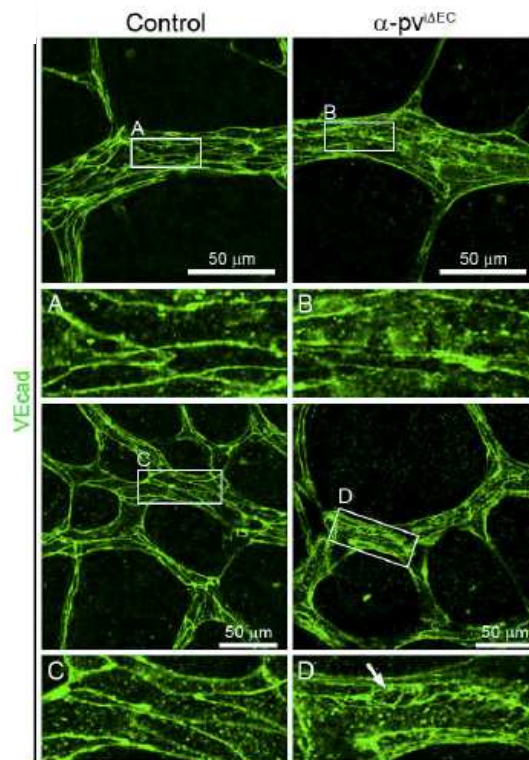


Fig.16: Abnormal vessel integrity in absence of endothelial α -pv. P7 and α -pv^{i Δ EC} retinas labeled for VE-Cad. Arrow highlights gaps between ECs. (b) Altered cell junction morphology in α -pv^{i Δ EC} mice. P6 control and α -pv^{i Δ EC} retinas labeled for VE-Cad, IB4 and claudin-5. Arrows highlight vessel segments with diffuse punctuated VE-Cad stain.

Vascular MC are recruited to newly formed vessels to reinforce and stabilize blood vessel [68]. Previous publications showed that α -pv is crucial for the recruitment of MCs to the vessel wall in embryos [2]. Therefore, I analyzed the coverage of retinal vessels by MCs in α -pv^{i Δ EC} mice. Whole-mount immunostaining of control and α -pv^{i Δ EC} retinas using antibodies against α -SMA and NG2 (Fig.17) showed that the MC coverage of the retinal vessels lacking α -pv was comparable to control vessels, suggesting that depletion of α -pv did not have a significant effect on the recruitment of vascular SMCs and PCs to the vessel wall and the so imparted stability.

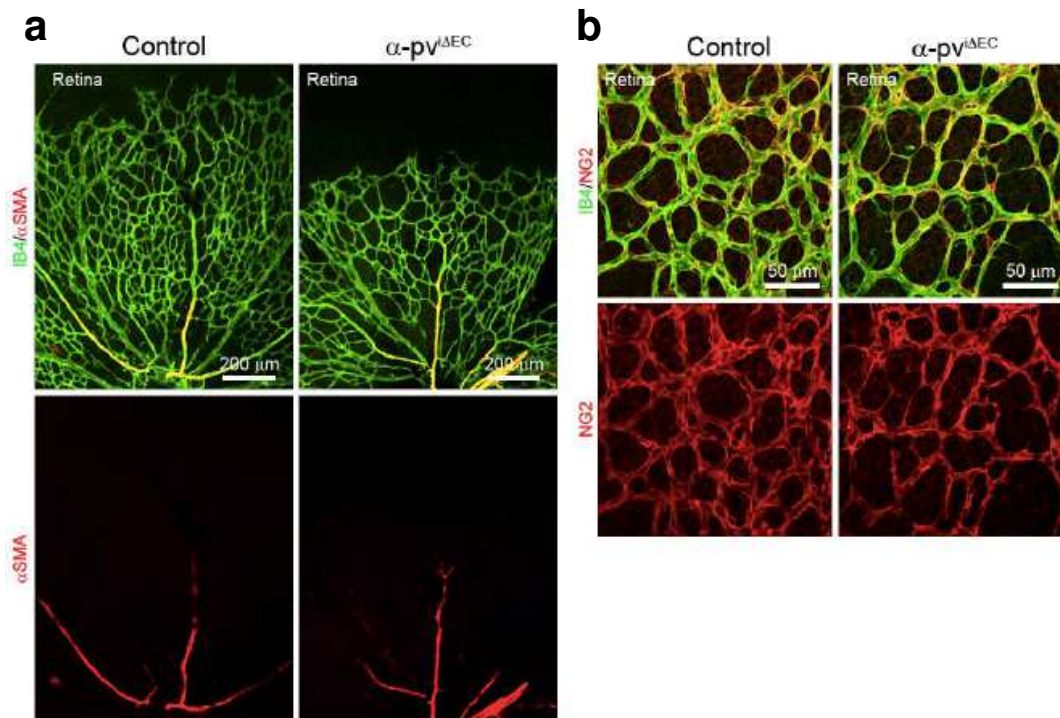


Fig.17: Mural cell coverage of retinal vessels in α -pv^{iΔEC} mice. (a) Whole-mount labeling of P6 control and α -pv^{iΔEC} retinas for IB4 and α SMA. (b) IB4 and NG2 labeled α -pv^{iΔEC} retinas.

Endothelial α -pv is not required for the stability and maintenance of established vessels.

To ascertain whether α -pv is required for stability of formed vessels, investigation of vascular remodeling and maturation has been completed through concurrent analysis of superficial and deep vascular plexus in the retina. Therefore I deleted α -pv gene with three consecutive Tamoxifen injections starting from day P5, and performed retina dissection at P10 [3]. The majority of the superficial vascular plexus could form in the presence of α -pv (radially expanding from P1-P7), the formation of the deep vascular layer instead occurred in absence of α -pv (spreading perpendicularly from P8 onwards before forming a planar deeper layer [64]) (Fig. 18). Examination of the superficial vascular plexus showed no difference in migratory length or vessel density (quantified by branch points per field and EC-area per field) between control and α -pv^{iΔEC} retinas, indicating no necessity of α -pv in the preservation of consolidated vessels. EC migration though was compromised as we observed a delay in deep plexus formation, the latter displaying the same defects we observed prior in P7 α -pv^{iΔEC} retinas (Fig. 18).

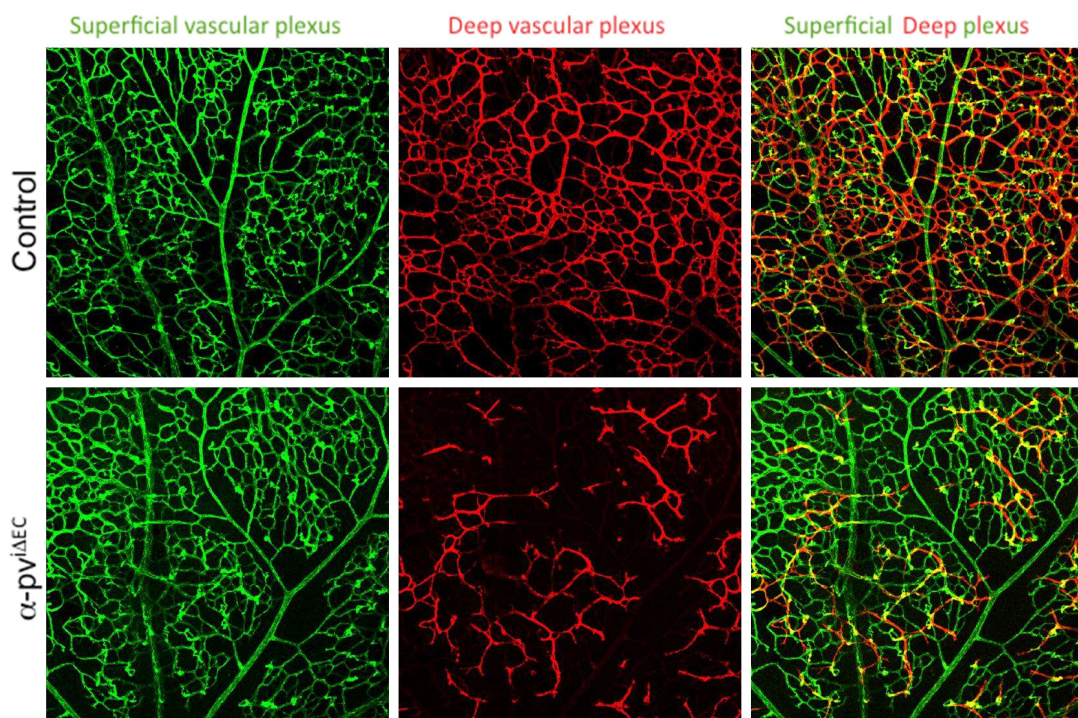


Fig.18: Depletion of endothelial α -pv does not affect stability or maintenance of established vessels. IB4 labeled P10 control and α -pv^{iΔEC} retinas. Superficial plexus conformation shows no difference between KO and WT mice, formation of the deep plexus is delayed in α -pv^{iΔEC} mice.

Deletion of α -pv in postnatal EC leads to severe persistent retinal angiopathy.

In order to appreciate whether the retinal sprouting defects in α -pv^{iΔEC} mice were transient or persistent we analyzed the retinal vascular network at a later developmental stage, too. At P16, we repetitively found a delay in radial expansion as well as reduced vascular density indicating migration defects (Fig. 19). Intriguingly, nearly all sprouts in α -pv^{iΔEC} mice consisted of large clusters of tip cells lacking filopodia protrusions. They appeared ballooned, substantially enlarged most likely resembling to saccular aneurysms (Fig 19 a). Vascularization of the deeper retinal layer was severely affected, and very few vessels were formed compared to control littermate retinas (Fig 19 b, c). Some areas of mutant retinas completely missed deep plexus establishment, indicating an impaired development of the primary plexus until late stages of retinal vascularization. Quantification of the ratio between EC-area in the superficial plexus vs. EC-area in the deep plexus, using 40x confocal images and *ImageJ*-software shows significant decrease of EC-area (superficial/deep) in α -pv^{iΔEC} retinas (Fig 19 d).

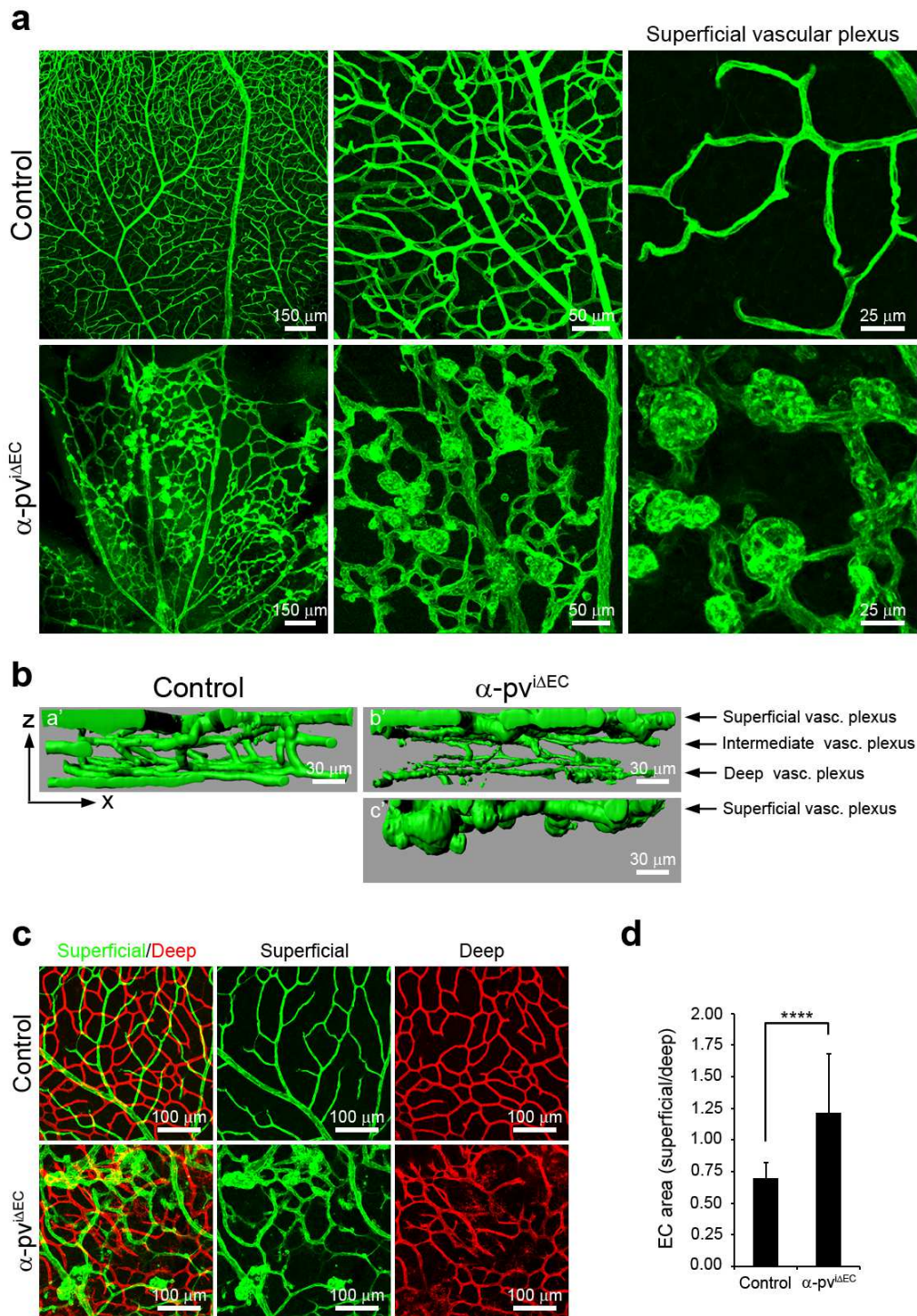


Fig.19: Severe persistent retinal vascular pathology in α -pv^{iAEC} mice. (a) IB4 staining of P16 α -pv^{iAEC} and control retinas, depicting the superficial vascular plexus with balloon-like sprout structures in mutant retinas, secondary invading deeper retinal layers. (b) Z-projection of a 3D reconstruction using Imaris. (c) IB4 stain showing the superficial and the deep vascular plexus. The deep vascular plexus in the mutants are immature (based in the number of tip cells) compared to controls and show a high number of tissue macrophages. (d) Quantification of the ratio between EC-area in the superficial plexus vs. EC-area in the deep plexus. Data is shown as mean (SD). P-value **** $n \geq 3$ mice per genotype.

Depletion of α -pv in ECs leads to reduced FX formation and impaired cell spreading.

To investigate the role of α -pv in the regulation of EC migration on a cellular level, we depleted α -pv in primary HUVECs by siRNA and first compared spreading and polarization of control and α -pv deficient HUVECs. When plated on gelatin, control cells underwent progressive spreading, developed multiple filopodial protrusions and polarized. F-actin labeling through phalloidin staining showed long and thin stress fibers across the cytoplasm and strong membrane ruffling (Fig. 20). There was no significant difference in spreading rates between α -pv deficient and control cells, when compared after 45 minutes on gelatin, indicating that α -pv is not required for initial spreading of EC. However, after 12 hours in culture, α -pv deficient cells had irregular shapes with aberrant membrane protrusions and had failed to polarize (Fig. 20). F-actin staining revealed a poorly organized F-actin cytoskeleton, characterized by an increase in staining of short actin bundles at the periphery of the cell and multiple filopodia-like structures around the cell borders (Fig. 20 c).

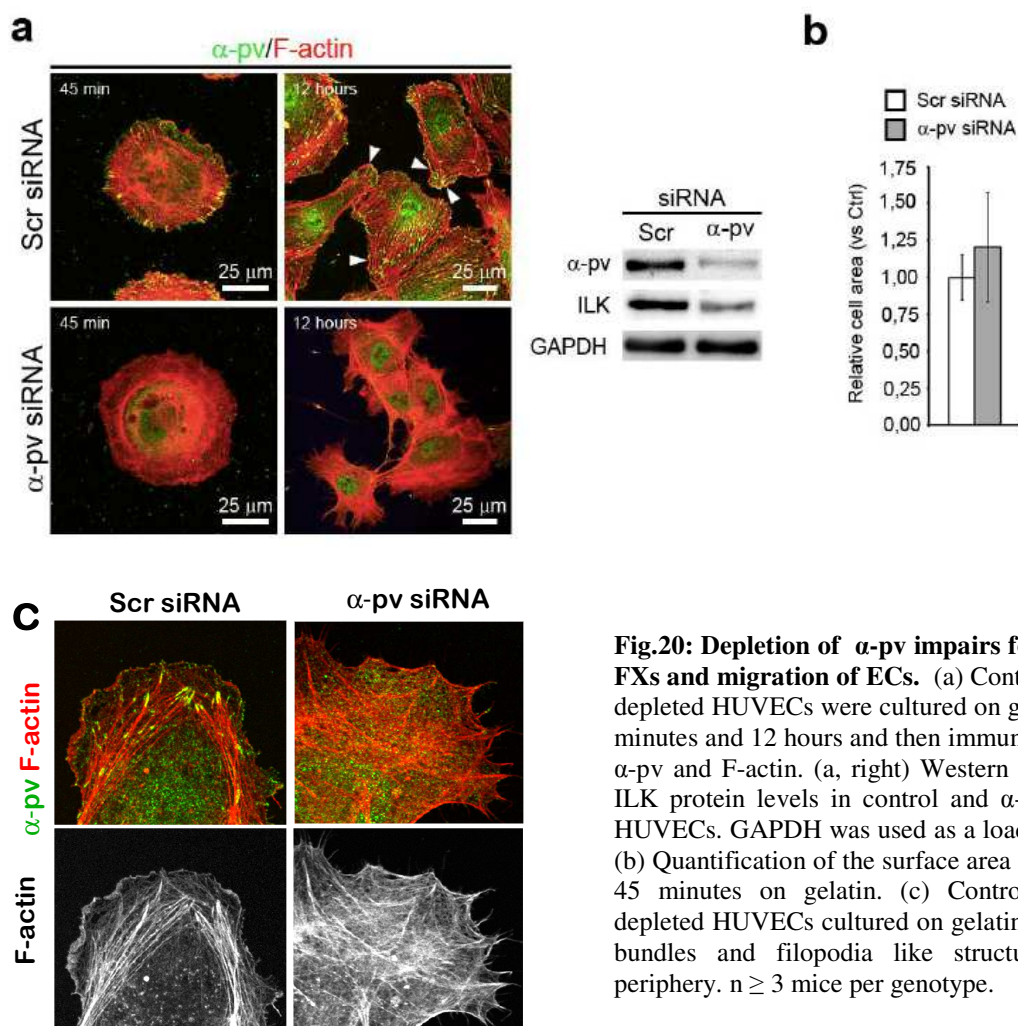


Fig.20: Depletion of α -pv impairs formation of FXs and migration of ECs. (a) Control and α -pv depleted HUVECs were cultured on gelatin for 45 minutes and 12 hours and then immunolabeled for α -pv and F-actin. (a, right) Western blot of α -pv ILK protein levels in control and α -pv depleted HUVECs. GAPDH was used as a loading control. (b) Quantification of the surface area of cells after 45 minutes on gelatin. (c) Control and α -pv depleted HUVECs cultured on gelatin; short actin bundles and filopodia like structures in the periphery. $n \geq 3$ mice per genotype.

Unchanged VEGF-A mediated ERK-activation in the absence of α -pv

To further examine proliferation we investigated α -pv's role in the MAPK/ERK pathway. Therefore we performed a time course experiment, stimulating HUVECs - priorly transfected with either scrambled (scr) RNA or α -pv depleting siRNA - with the angiogenesis inducing mitogen VEGF-A. After 4 hours of starvation, HUVECs were stimulated with VEGF-A (50 ng/ml) for 10 minutes. Control and α -pv depleted HUVECs showed no difference in ERK activation levels, measured by western blot analysis and respective quantification of phospho-ERK protein levels, suggesting that α -pv is not required for VEGF-A mediated ERK-activation (Fig.21).

These results are comparable to ILK regarding the VEGF-A dependent MAPK/ERK pathway, which remains unaffected by the loss of IPP-complex partners [55].

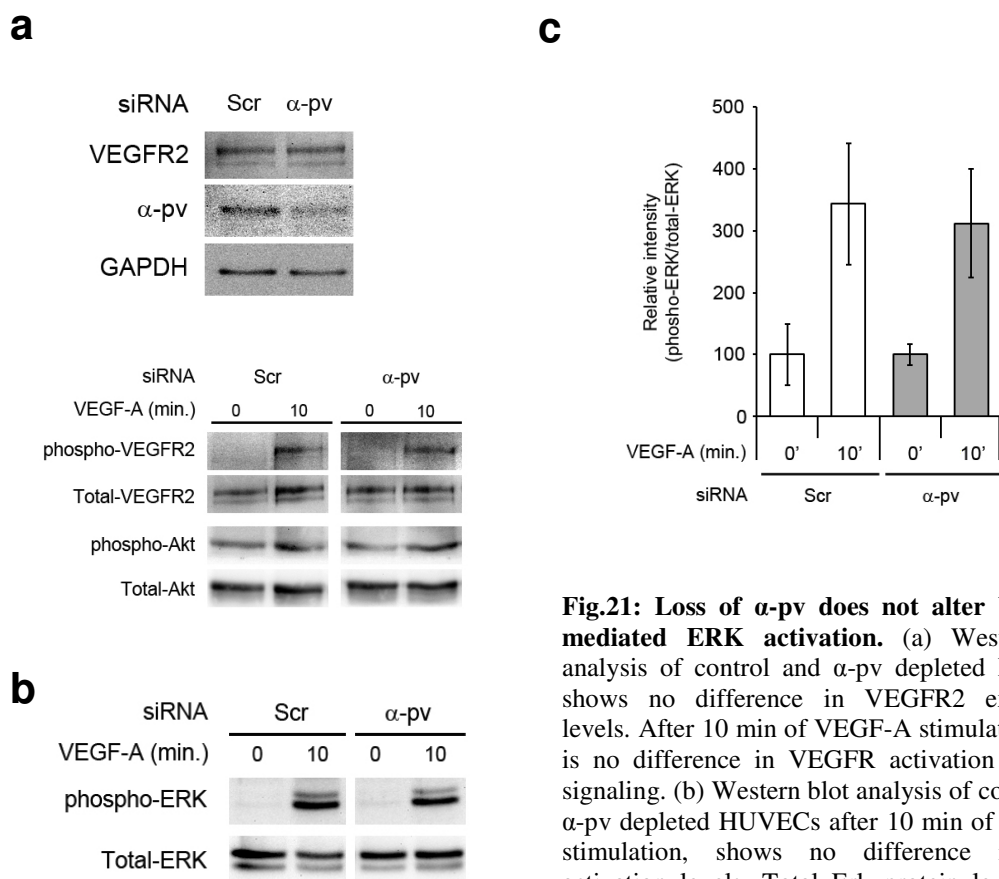


Fig.21: Loss of α -pv does not alter VEGF-A mediated ERK activation. (a) Western blot analysis of control and α -pv depleted HUVECs shows no difference in VEGFR2 expression levels. After 10 min of VEGF-A stimulation there is no difference in VEGFR activation and Akt signaling. (b) Western blot analysis of control and α -pv depleted HUVECs after 10 min of VEGF-A stimulation, shows no difference in ERK activation levels. Total Erk protein levels were used as loading control. (c) Quantification of relative intensities. $n \geq 3$.

5 STATEMENT OF CONTRIBUTIONS:

To give a complete picture of all the results during my thesis, I also mentioned some experiments where other people collaborated. Contributions are listed below.

Experiment	Person
Tie2 embryo IHC	Bettina Pitter
Cremaster model	Markus Rehberg
OMX microscopy	Claudio Franco

6 DISCUSSION :

6.1 Angiogenesis: a therapeutic target in disease

As listed in the Angiogenesis foundation web page (<https://www.angio.org/learn/angiogenesis/>), angiogenesis-based therapies are a unifying, wide-ranging approach for fighting disease. By restoring the organism's natural balance through use of new medical treatments that either inhibit or stimulate angiogenesis, cancer progression can be arrested, limb amputations might be prevented, vision loss can be restored and general health thereby is improved. Over the past decades these angiogenesis therapies represented a heavily funded area of medical research, where millions have been invested for the development of new therapeutics. Over 300 angiogenesis interfering drugs were discovered so far, but most of them failed in demonstrating clinical benefit in trials, because of significant systemic adverse events and unacceptable toxicities occurring during their use. In summary, the drugs that entered actual clinical practice either function as (1) anti-VEGF (e.g. Bevacizumab) or – VEGFR antibodies, (2) immunomodulatory drugs with antiangiogenic properties, or receptor tyrosine kinase inhibitors targeting downstream VEGF signaling pathways [69]. However, over time cells develop resistance mechanisms to these drugs, not least through upregulation of compensatory pathways resetting the drug's efficacy. Facing this current challenge, recent scientific efforts focus on simultaneous multiple pathway blockage as well as on finding new targetable effector molecules [69].

Aiming at analyzing the principles underlying the regulation of angiogenesis patterns, the cytoskeleton itself gained more and more attention as the cell's framework is involved in virtually all physiological and pathological processes including the cellular activities in angiogenesis [70]. It is essential for cell-cell interactions as well as cell shape rearrangement triggered by outside stimuli [70]. Alterations in structure result in disease characterized by abnormal migration, proliferation and cellular function [71].

6.1.1 Visualization of endothelial actin cytoskeleton in the mouse retina during angiogenesis: an important approach to understand the mechanisms behind structural cell regulation

Angiogenesis requires coordinate changes in shape of ECs, orchestrated by the actin cytoskeleton [6]. The mechanisms that regulate this rearrangement *in vivo*, however, are poorly understood, mostly due to the difficulty to visualize F-actin structures with sufficient resolution. Our knowledge regarding endothelial actin dynamics during angiogenesis is predominantly based on *in vitro* studies using compounds as the fungal toxin phalloidin, which, however, do interfere with actin dynamics [17], or transfection of GFP-actin to visualize the cytoskeletal changes in a cell. Yet, there is no possibility to visualize F-actin structures without affecting its organization *in situ* [38, 39]. As many biological processes rely on the actin cytoskeleton, gaining insights into actin dynamics through better visualization tools of actin filaments in certain cells *in vivo/in situ* might add important new information to our understanding of cell adhesion, motility, proliferation and survival processes.

To allow the visualization of F-Actin in intact, living cells, in 2010 a new mouse line was generated by Riedl et al. [10], meant to express Lifeact-EGFP ubiquitously. In order to obtain broad expression patterns, the vector upstream to the promotor driving Lifeact-EGFP expression contains a cytomegalovirus (CMV) enhancer sequence, so allowing visualization of F-actin in tissues and whole animals without affecting actin dynamics, cell physiology or tissue organization.

These mice therefore are widely used in various disease models [10, 40], though up to now, the Lifeact-EGFP mouse-strain's usability for vascular research remains unclear, as Lifeact-

EGFP expression level and cellular expression patterns in the vascular system have not been studied, yet. Hence, we hypothesized that Lifeact-EGFP is sufficiently expressed in vascular

cells allowing a closer analysis of the vascular expression patterns of Lifeact-EGFP mice and might add important insights in the study of actin dynamics in vascular research.

For vascular actin analysis in Lifeact-EGFP mice we used IHC of embryos (as described in material and methods) and the postnatal retinal angiogenesis model [3].

In accordance to previously published data our analysis showed that in the mouse embryo, Lifeact-EGFP is ubiquitously expressed, precluding adequate and selective imaging of F-actin structures in ECs during early organogenesis [10]. Briefly, the ubiquitous expression of Lifeact-EGFP impedes a detailed analysis of F-actin dynamics in vascular cells, which would be required for the understanding of how ECs regulate their actin cytoskeleton analogously to angiogenic stimuli.

In contrast, the role of F-actin in postnatal angiogenesis could be more easily analyzed using the retina model as an established tool [3, 64]. Through the use of confocal microscopy, we found that Lifeact-EGFP expression in the retina was mainly restricted to the endothelium, with no Lifeact-EGFP expression in other retinal cell types as ACs or vMCs. This allowed us to get a static frame of actin rearrangement to filopodial structures as well as the established vascular plexus selectively focusing on actin filament arrangement with excellent contrast.

Contrary to the retina, we found that in the skin and the skeletal cremaster muscle, Lifeact-EGFP was only weakly expressed by ECs, though vSMCs showed remarkable expression, as well as some blood cells as leukocytes, enabling the visualization of leukocyte-vessel wall interactions, rolling, chemotaxis, phagocytosis and extravasation of leukocytes. Moreover, in the lymphatic endothelium of those organs, Lifeact-EGFP was almost absent.

Variegated GFP actin expression patterns are a well-known problem in GFP transgenic mouse strains and were already described earlier in literature [40, 42, 72]. The reason for this selective patterning remains unclear, though we think it might be attributable to different promotor dependent activation in each cell type and tissue, as described previously by Oertel et al. in hepatoblasts, where GFP silencing *in vitro* occurred if GFP expression was driven by the CMV promotor/enhancer but not if driven by the albumin promotor [72]. Still, the reason for selective GFP expression through GFP silencing remains an unresolved quest. In other transgenic mouse lines, as the CMV-GFP strain, loss of GFP expression was shown to be lost with differentiation of the tissue. We did not perform a respective analysis in the Lifeact-EGFP mice, though we assume that this might also influence Lifeact-EGFP expression in our case. Furthermore, it was speculated that epigenetic modification of the CMV regulatory

elements might be involved in the loss of GFP expression in the different mouse tissues, resulting in variegating expression patterns [42].

Further studies are needed to unravel the exact functional background of these selective patterning. It was not an aim of this thesis to get deeper functional understanding concerning this issue.

Through descriptive analysis of the postnatal retina model on Lifeact-EGFP mice, our data indicate, that imaging of the endothelial actin cytoskeleton *in situ* during vascular plexus formation can easily be performed and so acts as an excellent tool for vascular cell biology research regarding selective endothelial actin imaging.

Up to now, actin visualization was mostly done using fluorescently labeled phalloidin. To validate our findings we compared Lifeact-EGFP and phalloidin staining and, to this end performed whole mount immunostaining of respective retinas. The analysis showed that phalloidin mainly stained the angiogenic front of the vascular plexus where it highlighted leading edges and filopodia of tip cells [17]. On the contrary, in the central plexus, phalloidin staining of ECs was weak. Moreover, it labeled non-vascular structures, thus making it difficult to visualize and analyze endothelial actin cytoskeleton in consolidated vessels. These results are consistent with previously published data, showing similar phalloidin staining patterns [17]. The more homogeneous immunostaining in Lifeact-EGFP retinas might be due to the different binding properties of the compared compounds. Whereas Phalloidin coupled to different fluorophores selectively binds along the sides of actin filaments and inhibits their polymerization, Lifeact-EGFP directly binds to F-actin via an ABP-sequence, so probably allowing actin visualization more precisely [17, 38].

A further advantage we observed in Lifeact-EGFP animals was the faster actin imaging of the cytoskeleton, the omission of additional treatment for further immunostaining and hence, reduced susceptibility for errors or methodological failure throughout the experiment. Pretreatment of the retinas as for example the permeabilization for the compound could be dismissed in Lifeact-EGFP retinas. The necessary pretreatment procedures might be a further reason for unselective, inhomogeneous immunostaining of phalloidin labeled retinas.

Regarding *in vivo* studies, several transgenic mouse lines expressing the GFP-actin gene under the control of tissue specific promoters have been created and described. Among them there are the GFP-actin mice (CBA-GFP strain), GFP expression being under the control of a

CAG promoter and CMV enhancer [40, 41]. Compared to Lifeact-EGFP mouse strains though, tissue specific actin visualization is impaired in GFP actin mice, because ubiquitous promoters control the GFP expression. Moreover it has been argued that there is clear variability in GFP-expression patterns within the transgenic mouse strains, none of them giving reproducible or ubiquitous GFP-expression making it difficult to analyze the cytoskeleton reliably *in vivo* [42]. Both mouse strains are susceptible for bleaching after UV-light exposure. CBA-GFP mice were originally constructed for transplantation experiments. Numerous studies have been made to validate their GFP expression in various tissues. In 2007 Swenson et al. [42] analyzed three different mouse strains, in which GFP was considered ubiquitously expressed. Similar to Lifeact-EGFP mice, GFP expression was variable within the different organ tissues. CBA-GFP mice for instance had strong but variegated expression of GFP in adult liver, kidney, small intestine, and blood. The author attributed it to the high proportion of GFP expressing peripheral blood cells, interfering with single organ tissue visualization. None of the mouse lines tested showed ubiquitous GFP expression in Swenson's study [42]. These results are in line with our study showing selective, but different Lifeact-EGFP expression patterns in different cells according to the analyzed organ. In our study we took advantage of the variegated expression, showing its benefits in endothelial actin visualization within the postnatal mouse retina model.

Compared to previously used tools, our results for the first time demonstrate that Lifeact-EGFP can be used for the visualization of endothelial specific F-actin structures in the retina during the various angiogenic steps *in situ*. We demonstrated that they allow to selectively study ECs' actin cytoskeleton: filopodia protrusion during the initiation of the sprouting process, cell spreading, cell polarization with demarcation of luminal and abluminal actin bundles, establishment of cell-cell contacts and lumen formation by highlighting F-actin structures at the luminal and abluminal side [6]. To our knowledge there is no other tool described in literature, which allows selective endothelial actin imaging with such great contrast. Combined to the postnatal retinal angiogenesis mouse model it allows to depict endothelial actin dynamics *in situ* as a static frame in sequence and accordance to angiogenesis hallmarks.

Regarding vascular biology research, this novel tool might add important information to the current knowledge about how the cytoskeleton rearranges according to the influences of growth factors and integrin signaling. Deeper understanding of the processes involved might

eventually allow to specifically target actin dynamics in order to stop allied disease as local progression of cancer through spreading and burking blood supply.

6.1.2 α -parvin in vascular development

The establishment and maintenance of a functional blood-supplying network involves a series of events requiring collective cell migration, coordinated sprouting and pruning as well as dynamic cell-cell contact remodeling between ECs in order to ensure effective vessel formation and firmness [6, 24]. Mechanisms involved in the tight regulation of angiogenesis rely on actin cytoskeleton dynamics whose regulation among others involves the $\beta 1$ integrins and especially their downstream regulator and actin anchor, α -pv.

As shown in previous publications ubiquitous deletion of α -pv gene in mice leads to late embryonic lethality (E10.5) caused by severe cardiovascular defects, hemorrhages and decreased vascular density [2]. In line with these results, mice lacking vascular endothelial $\beta 1$ integrins (Tie2-cre $\beta 1$ Int^{fl/fl} mice) showed a similar vascular phenotype[50, 73]. Early *in vivo* studies in the latter showed defective angiogenesis with a reduced number of blood cells, who led to early embryonic death (E9.5) [50]. In our analysis of mouse embryos lacking α -pv gene in ECs (Tie2-cre α -pv^{fl/fl}), lethality occurred later during embryonic development (E13.5). Leading death causes in both were hemorrhages; torturous vascular plexuses and an overall reduced vascular density. Hence, we speculate that the longer embryonic survival at the presence of similar defects occurring in embryonic development in Tie2-cre α -pv^{fl/fl} mice might indicate that not all integrin functions related to endothelial action during vascular development are compromised in the absence of α -pv.

We then looked at postnatal angiogenesis in α -pv^{i Δ EC} mice, with inducible EC-selective gene silencing through tamoxifen injections (P1-P3). Endothelial specific deletion of the adapter protein α -pv in mice - at P7 - resulted in decreased vascular density mostly due to excessive vessel regression and reduced vessel sprouting in the retina.

In sprouting angiogenesis tip and stalk cell specification is a key aspect in the establishment of a blood supplying vessel network and it is crucial for synchronized cell sprouting as well as

migration and proliferation of ECs. The selection of tip and stalk cells is regulated by the Dll4/Notch signaling pathway. The promotion of Dll4 expression by VEGF-A on certain ECs leads to their differentiation into tip cells, and these then activate Notch in the neighboring cells, which makes them turn into stalk cells [6]. To limit tip cell formation thereby preventing excessive vessel sprouting, Dll4 expression in this case must be controlled through $\beta 1$ integrin signaling [74]. Laminin (LN)/integrin signaling is necessary to induce physiologically functional levels of DLL4 expression and thus regulating branching frequency during sprouting angiogenesis *in vivo*. Loss of LN/integrin signaling results in insufficient Notch activation with excessive filopodia extension and increased tip cell formation as reflected by a hypersprouting, dense vascular phenotype [74]. In contrast to that, the reduced vessel sprouting together with the normal filopodia formation in α -pv^{iAEC} retinas suggest that endothelial α -pv is not required for the integrin mediated regulation of tip cell specification, but it is essential for the elongation of sprouts and their radial expansion.

Moreover, there are *in vitro* studies on cultured ECs lacking $\beta 1$ integrins demonstrating a reduced migration and elongation capacity of ECs, so mechanistically explaining the defective vascularization process [73]. Although it is an *in vivo* vs *in vitro* comparison, this again confirms similar angiogenesis defects in $\beta 1$ integrin- and α -pv missing ECs, suggesting that α -pv may not be the key player in the migration process [73].

Vessel growth depends on EC proliferation via cell division and intercalation of ECs. According to the results presented in this thesis, α -pv positively regulates proliferation of ECs *in vivo* and their survival. In line with our results Huang et al. [75] showed that in an adenocarcinoma cell line of the lungs cell overexpression of α -pv led to tumor cell growth *in vivo* and *in vitro* through elevated proliferation. Therefore we speculate that α -pv's influence on proliferation occurs EC-independently, making it a more universal function of α -pv.

The reduced EC proliferation and EC apoptosis rates in developing vessels of α -pv^{iAEC} mice led to a severe and persistent retinal angiopathy. Vessels displayed impaired cell-cell junction morphology as well as increased intercellular spaces between ECs, resulting in altered vessel morphology. Vessel networks of α -pv^{iAEC} retinas displayed irregular shapes, with heterogeneity in vessel diameters and had a collapsing appearance. These vessel segments were characterized by failure of lumen formation as assessed through ICAM-2 negative immunostaining and leakiness of the immature vascular plexus.

Leakiness in vessel originating from different sources occurs in many eye diseases [15] and lately was also reported to occur in tumor vessels, showing these structural and functional abnormalities thereby facilitating metastasis seeding [76]. Leakiness especially in eye disease is attributable to insufficient MC recruitment to the vessel walls [77]. Although previous publications were able to show that α -pv indeed is crucial for the recruitment of MCs to the vessel wall in embryos [2], here we discovered no difference in PC and vSMC coverage in the retinas of α -pv^{iΔEC} mice compared to WT retinas, indicating an EC autonomous role α -pv in vessel stabilization.

However, α -pv^{iΔEC} mouse strains showed a phenotype characterized by leaky vessels displaying impaired cell-cell junction morphology, increased intercellular spaces between ECs, which may explain the severe persistent retinal angiopathy found in our studies.

Cell-cell junctions are fundamental to maintain the integrity of newly formed vessels along with the stability provided by vascular mural cells, reinforcing the vessel wall. Impaired remodeling of junctions leads to vessel regression and ultimately culminates into vessel rupture and hemorrhages [23, 68, 78]. Cell junctions as visualized through VE-cad immunostaining showed a diffuse and discontinuous stain around cell boundaries in vessels of α -pv^{iΔEC} retinas compared to the sharp and continuous stain observed in vessels of control retinas, with fragments of vessels partially disconnected from the vascular bed. Therefore, we assume that endothelial α -pv loss in developing vessels weakens the integrity of VE-cadherin junctions. This finding is consistent with recently published data, showing that β 1 integrins control blood vessel stability in the growing vasculature by preserving cell-cell junction integrity via cell-ECM adhesion. [79]. Interestingly we found that, if deletion of α -pv in ECs occurred at later time points (Tamoxifen injections at P5-P7) of development, already established vessels showed no compromised stability or patterning, indicating that endothelial α -pv is not required for the stability and maintenance of established vessels.

In summary it can be stated, that α -pv deficient ECs display reduced integrin-mediated cell-ECM adhesion structures, altered cell-cell junctions, and reduced cell migration. These findings indicate that α -pv controls sprouting angiogenesis by regulating integrin-mediated processes required for the elongation of endothelial sprouts. The immature nature of the vascular plexus and matches with an inability of α -pv lacking ECs to effectively intercalate, as cell intercalation involves collective cell migration, which requires dynamic regulation of integrin-mediated cell-ECM adhesions and VE-cadherin-mediated cell-cell junctions [24].

Upon EC specific deletion of α -pv (Tamoxifen injections at P1-P3), postnatal retinal defects of the vascular plexus persisted at P16 and were not compensated throughout development. Vessels were incapable to assert their shape generating avascular zones and distal microneurysms in the primary plexus, partially missing deep plexus formation. A similar phenotype was described upon postnatal ablation of MRTF-SRF [36] and showed strong similarities to human disease including Norrie disease (ND) [80]. So far the genetic lesions identified in ND affect the Wnt signaling pathway. This might elucidate the existence of a cross-talk between Wnt and actin-signaling in guaranteeing proper EC function during retinal angiogenesis.

We showed that targeting endothelial α -pv and inhibiting its functions in ECs severely compromises angiogenesis. It interrupts stability and sprouting of a vascular network, leading to oxygen and nutrient deficit of the tissue next in-line. Similar results were shown recently by a taiwanese group analyzing α -pv role in adenocarcinoma of the lungs [75]. They overexpressed α -pv in ECs and found a larger number of branch points, increased vessel lengths and upregulation of VEGF-A expression as α -pv effects on sprouting angiogenesis. [75].

Of note in a study done in an adenocarcinoma cell line of the lungs, pv showed an important function in promoting tissue invasion of cancer cells, too, so promoting metastases formation [75]. In osteosarcoma and breast cancer cells pv phosphorylation was shown to be of central importance in matrix degradation through Src and MMPs for promotion of cell invasion [81]. α -pv blockage therefore might not just compromise angiogenesis, but might additionally block tumor progression directly through growth and metastasis inhibition [81], thereby representing an effective target for cancer therapy.

7 SUMMARY:

Sprouting angiogenesis, the formation of new blood vessels from pre-existing ones, is not only required for organogenesis and homeostasis, but also contributes to the progression of many diseases including tumor growth. It involves coordinated ECs differentiation, migration and proliferation, as well as vascular stability relying on adhesion of ECs to adjacent ECs and to the ECM.

Key pathways directing the molecular machinery underlying EC dynamics and organization, involve the rearrangement of the endothelial actin cytoskeleton.

The first part of my work consisted in an extensive study of the expression patterns of Lifeact-EGFP – an actin marker - in the vascular system of Lifeact-EGFP mice. The results presented here show that 1) the Lifeact-EGFP mouse represents an excellent system to visualize and to characterize the actin cytoskeleton in individual EC *in situ* during vessel growth the early postnatal retinal angiogenic model is and 2) in the skin and skeletal cremaster muscle, Lifeact-EGFP is a powerful tool for imaging vMCs as PCs or vSMCs. Moreover, the postnatal retinal angiogenesis model in Lifeact-EGFP mice could be used as a tool in the investigation of actin in regulating morphogenic angiogenic processes such as migration, polarization and anastomosis of ECs, as well as lumen formation.

In the second part, α -pv as one of the main regulators of the actin cytoskeleton dynamics was studied. Integrins, which cluster various adapter proteins and so allow the formation of FAs, influence and rearrange the endothelial actin organization α -pv localizes to FAs and facilitates the interaction of the integrins with the actin cytoskeleton, coupling integrin signaling to the RTK signaling. Here we show that selective inducible gene deletion of α -pv in ECs of mice

results in hemorrhages due to leaky vessels and decreased vascular density. Postnatal EC-specific deletion of α -pv leads to retinal hypovascularization due to reduced vessel sprouting and excessive vessel regression. In absence of endothelial α -pv vessels display impaired cell-cell junction morphology, increased intercellular gaps, reduced EC proliferation and increased EC apoptosis. *In vitro* analysis of α -pv depleted HUVECs confirmed reduced cell motility, compromised formation of integrin-mediated cell-ECM adhesion structures, and alterations of the actin cytoskeleton.

Our results underline the importance of α -pv, for the actin cytoskeleton changes which are required for the coordinated changes of EC-shape required for cell migration, the maintenance of intercellular junctions and FA formation. This thesis discloses new mechanisms by functionally analyzing α -pv as an essential endothelial regulator protein involved in blood vessel growth and vessel stabilization. This functional characterization might eventually lead to new therapeutic targets for the cure of angiogenesis allied disease.

8 Zusammenfassung:

Die Angiogenese subsumiert Spross- und Spaltungsvorgänge, welche zur Bildung neuer Blutgefäße aus bereits existierenden führen. Es handelt sich um einen komplexen Prozess, welcher die koordinierte Differenzierung, Adhäsion, Polarisierung, Migration und Proliferation entsprechender Endothelzellen (EZ) beinhaltet und durch physikalische Interaktionen zwischen EZ und der extrazellulären Matrix (EZM), sowie durch lösliche angiogene Wachstumsfaktoren reguliert wird. Fehlfunktionen der einzelnen Prozesse führen zu Störungen in der Organogenese und unterhalten das Fortschreiten zahlreicher Krankheiten, darunter vieler Tumorarten und Augenerkrankungen.

Eine zentrale Rolle in der Entwicklung und Erhaltung der Blutgefäße nimmt das Aktin-Zytoskelett ein.

Im ersten Abschnitt dieser Dissertation wurden gentechnisch veränderte Mauslinien (Lifeact-EGFP Mauslinie) untersucht, in welchen das Aktin-Zytoskelett fluoreszierend markiert ist. Die hier vorgestellten Ergebnisse zeigen, dass 1) Lifeact-EGFP Mäuse eine exzellente Visualisierung und Charakterisierung des endothelialen Aktin-Zytoskeletts der einzelnen Zellen *in situ* während des Wachstumsvorgangs in dem Modell der postnatalen Maus-Retina-Angiogenese ermöglichen, und 2) dass in Haut und Cremastermuskel Lifeact-EGFP vor allem Aktinfilamente gefäßassoziierter glatter Muskelzellen markiert. Aus eben diesen Gründen wird hier die Kombination dieser Methoden zur Analysierung morphologischer angiogener Prozesse, wie beispielsweise Migration, Polymerisation, Anastomose sowie der Ausbildung des Lumens empfohlen.

Von besonderer Bedeutung in der Regulation des Aktin Zytoskeletts ist die Integrin-vermittelte Signaltransduktion und Adhäsion dieser Rezeptoren an ihren Liganden, die EZM. Integrine übermitteln Signale, indem sie Signal- und Adaptorproteine in fokale Adhäsionsstrukturen rekrutieren und dadurch die Neuorganisation des Aktinzytoskeletts regulieren. α -pv stellt eines dieser Adaptorproteine dar, welches in fokalen Adhäsionen lokalisiert ist und an der Wechselwirkung zwischen Integrin und Wachstumsfaktor-vermittelten Signalwegen beteiligt ist. Auch kann α -pv an F-Aktin und Aktin-regulierende Proteine binden und so den Aktinfluss, Zellpolarität und Zellmigration beeinflussen.

Der zweite Teil dieser Dissertationsarbeit charakterisiert α -pv's Funktionen in der Angiogenese und zeigt, dass bei der induzierten Deletion von α -pv in der neonatalen Phase, die Gefäßentwicklung kompromittiert ist. Das Gefäßnetz ist in seiner Dichte reduziert. Es kommt gehäuft zu Blutungen durch Leckagen in der Gefäßwand, letztendlich resultierend in Letalität. Als Folge postnataler endothelspezifischer α -pv Deletion kommt es in den entsprechenden Mäusen zu eingeschränkter Gefäßaussprossung und übermäßiger Gefäßregression. Die Gefäße weisen eine eingeschränkte Ausbildung von Zell-Zell-Kontakten mit weiten Interzellularspalten zwischen den einzelnen Endothelzellen auf. Insgesamt zeigt sich eine verminderte Proliferation, sowie eine gesteigerte Apoptoserate in den untersuchten retinalen Gefäßen. Auch *in vitro* konnte in α -pv depletierten Nabelschnurothelzellen (HUVECs) eine reduzierte Zellmotilität, sowie eine eingeschränkte Ausbildung von Integrin-vermittelten Zell-EZM-Adhäsionsstrukturen nachgewiesen werden, welche zusammenfassend in einer gestörten Verankerung sowie einer veränderten Zellmorphologie und verändertem Zellverhalten resultierten.

In der Zusammenschau unterstreichen die Ergebnisse die Bedeutung eines engen Zusammenspiels zwischen α -pv, Integrinen und Aktin-Zytoskelett in der koordinierten EZ-Veränderung, welche für Prozesse wie Migration und Aufrechterhaltung von Zell-Zell Kontakten notwendig ist. Diese Doktorarbeit gewährt Einblick in die Funktion von α -pv bei der Regulation des Verhaltens von EZ während der Angiogenese und wird uns ein besseres Verständnis darüber ermöglichen, wie die vaskuläre Morphogenese reguliert wird, und dadurch möglicherweise den Weg für eine zukünftige Entwicklung neuer therapeutischer Strategien zur Kontrolle von pathologischer Angiogenese inklusive entsprechender Krankheiten, wie beispielsweise Krebs, ebnet.

9 REFERENCES:

1. Legate, K.R., et al., *ILK, PINCH and parvin: the tIPP of integrin signalling*. Nat Rev Mol Cell Biol, 2006. **7**(1): p. 20-31.
2. Montanez, E., et al., *Alpha-parvin controls vascular mural cell recruitment to vessel wall by regulating RhoA/ROCK signalling*. Embo j, 2009. **28**(20): p. 3132-44.
3. Pitulescu, M.E., et al., *Inducible gene targeting in the neonatal vasculature and analysis of retinal angiogenesis in mice*. Nat Protoc, 2010. **5**(9): p. 1518-34.
4. Eliceiri, B.P. and D.A. Cheresh, *The role of alphav integrins during angiogenesis: insights into potential mechanisms of action and clinical development*. J Clin Invest, 1999. **103**(9): p. 1227-30.
5. Pipes, G.C., E.E. Creemers, and E.N. Olson, *The myocardin family of transcriptional coactivators: versatile regulators of cell growth, migration, and myogenesis*. Genes Dev, 2006. **20**(12): p. 1545-56.
6. Potente, M., H. Gerhardt, and P. Carmeliet, *Basic and therapeutic aspects of angiogenesis*. Cell, 2011. **146**(6): p. 873-87.
7. Geudens, I. and H. Gerhardt, *Coordinating cell behaviour during blood vessel formation*. Development, 2011. **138**(21): p. 4569-83.
8. De Smet, F., et al., *Mechanisms of vessel branching: filopodia on endothelial tip cells lead the way*. Arterioscler Thromb Vasc Biol, 2009. **29**(5): p. 639-49.
9. Phng, L.K. and H. Gerhardt, *Angiogenesis: a team effort coordinated by notch*. Dev Cell, 2009. **16**(2): p. 196-208.
10. Riedl, J., et al., *Lifect mice for studying F-actin dynamics*. Nat Methods, 2010. **7**(3): p. 168-9.
11. Fraccaroli, A., et al., *Visualization of endothelial actin cytoskeleton in the mouse retina*. PLoS One, 2012. **7**(10): p. e47488.
12. Oellerich, M.F. and M. Potente, *FOXOs and sirtuins in vascular growth, maintenance, and aging*. Circ Res, 2012. **110**(9): p. 1238-51.
13. Hynes, R.O., *Integrins: bidirectional, allosteric signaling machines*. Cell, 2002. **110**(6): p. 673-87.
14. Folkman, J., *Angiogenesis: an organizing principle for drug discovery?* Nat Rev Drug Discov, 2007. **6**(4): p. 273-86.
15. Carmeliet, P., *Angiogenesis in health and disease*. Nat Med, 2003. **9**(6): p. 653-60.
16. Carmeliet, P. and R.K. Jain, *Molecular mechanisms and clinical applications of angiogenesis*. Nature, 2011. **473**(7347): p. 298-307.
17. Gerhardt, H., et al., *VEGF guides angiogenic sprouting utilizing endothelial tip cell filopodia*. J Cell Biol, 2003. **161**(6): p. 1163-77.

18. Gaengel, K., et al., *Endothelial-mural cell signaling in vascular development and angiogenesis*. *Arterioscler Thromb Vasc Biol*, 2009. **29**(5): p. 630-8.
19. Jakobsson, L., et al., *Endothelial cells dynamically compete for the tip cell position during angiogenic sprouting*. *Nat Cell Biol*, 2010. **12**(10): p. 943-53.
20. Lamalice, L., F. Le Boeuf, and J. Huot, *Endothelial cell migration during angiogenesis*. *Circ Res*, 2007. **100**(6): p. 782-94.
21. Bayless, K.J. and G.A. Johnson, *Role of the cytoskeleton in formation and maintenance of angiogenic sprouts*. *J Vasc Res*, 2011. **48**(5): p. 369-85.
22. Hotulainen, P. and P. Lappalainen, *Stress fibers are generated by two distinct actin assembly mechanisms in motile cells*. *J Cell Biol*, 2006. **173**(3): p. 383-94.
23. Giannotta, M., M. Trani, and E. Dejana, *VE-cadherin and endothelial adherens junctions: active guardians of vascular integrity*. *Dev Cell*, 2013. **26**(5): p. 441-54.
24. Bentley, K., et al., *The role of differential VE-cadherin dynamics in cell rearrangement during angiogenesis*. *Nat Cell Biol*, 2014. **16**(4): p. 309-21.
25. Huveneers, S., et al., *Vinculin associates with endothelial VE-cadherin junctions to control force-dependent remodeling*. *J Cell Biol*, 2012. **196**(5): p. 641-52.
26. Pollard, T.D. and G.G. Borisy, *Cellular motility driven by assembly and disassembly of actin filaments*. *Cell*, 2003. **112**(4): p. 453-65.
27. Defilippi, P., et al., *Actin cytoskeleton organization in response to integrin-mediated adhesion*. *Microsc Res Tech*, 1999. **47**(1): p. 67-78.
28. Bustelo, X.R., V. Sauzeau, and I.M. Berenjano, *GTP-binding proteins of the Rho/Rac family: regulation, effectors and functions in vivo*. *Bioessays*, 2007. **29**(4): p. 356-70.
29. Riento, K. and A.J. Ridley, *Rocks: multifunctional kinases in cell behaviour*. *Nat Rev Mol Cell Biol*, 2003. **4**(6): p. 446-56.
30. Goley, E.D. and M.D. Welch, *The ARP2/3 complex: an actin nucleator comes of age*. *Nat Rev Mol Cell Biol*, 2006. **7**(10): p. 713-26.
31. Garcia-Mata, R. and K. Burridge, *Catching a GEF by its tail*. *Trends Cell Biol*, 2007. **17**(1): p. 36-43.
32. DerMardirossian, C. and G.M. Bokoch, *GDI: central regulatory molecules in Rho GTPase activation*. *Trends Cell Biol*, 2005. **15**(7): p. 356-63.
33. Huveneers, S. and E.H. Danen, *Adhesion signaling - crosstalk between integrins, Src and Rho*. *J Cell Sci*, 2009. **122**(Pt 8): p. 1059-69.
34. Franco, C.A., et al., *SRF selectively controls tip cell invasive behavior in angiogenesis*. *Development*, 2013. **140**(11): p. 2321-33.
35. Vartiainen, M.K., et al., *Nuclear actin regulates dynamic subcellular localization and activity of the SRF cofactor MAL*. *Science*, 2007. **316**(5832): p. 1749-52.
36. Weinl, C., et al., *Endothelial SRF/MRTF ablation causes vascular disease phenotypes in murine retinae*. *J Clin Invest*, 2013. **123**(5): p. 2193-206.
37. Faulstich, H., et al., *Virotoxins: actin-binding cyclic peptides of Amanita virosa mushrooms*. *Biochemistry*, 1980. **19**(14): p. 3334-43.
38. Riedl, J., et al., *Lifeact: a versatile marker to visualize F-actin*. *Nat Methods*, 2008. **5**(7): p. 605-7.
39. Lemieux, M.G., et al., *Visualization of the actin cytoskeleton: different F-actin-binding probes tell different stories*. *Cytoskeleton (Hoboken)*, 2014. **71**(3): p. 157-69.
40. Okabe, M., et al., *'Green mice' as a source of ubiquitous green cells*. *FEBS Lett*, 1997. **407**(3): p. 313-9.
41. Gurniak, C.B. and W. Witke, *HuGE, a novel GFP-actin-expressing mouse line for studying cytoskeletal dynamics*. *Eur J Cell Biol*, 2007. **86**(1): p. 3-12.

42. Swenson, E.S., et al., *Limitations of green fluorescent protein as a cell lineage marker*. *Stem Cells*, 2007. **25**(10): p. 2593-600.
43. Hynes, R.O., *Cell-matrix adhesion in vascular development*. *J Thromb Haemost*, 2007. **5 Suppl 1**: p. 32-40.
44. Wegener, K.L., et al., *Structural basis of integrin activation by talin*. *Cell*, 2007. **128**(1): p. 171-82.
45. Choi, C.K., et al., *Actin and alpha-actinin orchestrate the assembly and maturation of nascent adhesions in a myosin II motor-independent manner*. *Nat Cell Biol*, 2008. **10**(9): p. 1039-50.
46. Geiger, B., et al., *Transmembrane crosstalk between the extracellular matrix--cytoskeleton crosstalk*. *Nat Rev Mol Cell Biol*, 2001. **2**(11): p. 793-805.
47. Wolfenson, H., I. Lavelin, and B. Geiger, *Dynamic regulation of the structure and functions of integrin adhesions*. *Dev Cell*, 2013. **24**(5): p. 447-58.
48. Zaidel-Bar, R., et al., *Functional atlas of the integrin adhesome*. *Nat Cell Biol*, 2007. **9**(8): p. 858-67.
49. Eliceiri, B.P. and D.A. Cheresh, *Adhesion events in angiogenesis*. *Curr Opin Cell Biol*, 2001. **13**(5): p. 563-8.
50. Tanjore, H., et al., *Beta1 integrin expression on endothelial cells is required for angiogenesis but not for vasculogenesis*. *Dev Dyn*, 2008. **237**(1): p. 75-82.
51. Francavilla, C., L. Maddaluno, and U. Cavallaro, *The functional role of cell adhesion molecules in tumor angiogenesis*. *Semin Cancer Biol*, 2009. **19**(5): p. 298-309.
52. Stiegler, A.L., et al., *Purification and SAXS analysis of the integrin linked kinase, PINCH, parvin (IPP) heterotrimeric complex*. *PLoS One*, 2013. **8**(1): p. e55591.
53. Fukuda, T., et al., *PINCH-1 is an obligate partner of integrin-linked kinase (ILK) functioning in cell shape modulation, motility, and survival*. *J Biol Chem*, 2003. **278**(51): p. 51324-33.
54. Guo, L., et al., *Targeting of integrin-linked kinase with a small interfering RNA inhibits endothelial cell migration, proliferation and tube formation in vitro*. *Ophthalmic Res*, 2009. **42**(4): p. 213-20.
55. Xie, W., et al., *Targeting of integrin-linked kinase with small interfering RNA inhibits VEGF-induced angiogenesis in retinal endothelial cells*. *Ophthalmic Res*, 2013. **49**(3): p. 139-49.
56. Wong, R.P., et al., *The role of integrin-linked kinase in melanoma cell migration, invasion, and tumor growth*. *Mol Cancer Ther*, 2007. **6**(6): p. 1692-700.
57. Rosenberger, G., et al., *Interaction of alphaPIX (ARHGEF6) with beta-parvin (PARVB) suggests an involvement of alphaPIX in integrin-mediated signaling*. *Hum Mol Genet*, 2003. **12**(2): p. 155-67.
58. D'Amico, M., et al., *The integrin-linked kinase regulates the cyclin D1 gene through glycogen synthase kinase 3beta and cAMP-responsive element-binding protein-dependent pathways*. *J Biol Chem*, 2000. **275**(42): p. 32649-57.
59. Gimona, M., et al., *Functional plasticity of CH domains*. *FEBS Lett*, 2002. **513**(1): p. 98-106.
60. Olski, T.M., A.A. Noegel, and E. Korenbaum, *Parvin, a 42 kDa focal adhesion protein, related to the alpha-actinin superfamily*. *J Cell Sci*, 2001. **114**(Pt 3): p. 525-38.
61. Yamaji, S., et al., *Affixin interacts with alpha-actinin and mediates integrin signaling for reorganization of F-actin induced by initial cell-substrate interaction*. *J Cell Biol*, 2004. **165**(4): p. 539-51.

62. Nikolopoulos, S.N. and C.E. Turner, *Molecular dissection of actopaxin-integrin-linked kinase-Paxillin interactions and their role in subcellular localization*. J Biol Chem, 2002. **277**(2): p. 1568-75.
63. Wang, Y., et al., *Ephrin-B2 controls VEGF-induced angiogenesis and lymphangiogenesis*. Nature, 2010. **465**(7297): p. 483-6.
64. Fruttiger, M., *Development of the retinal vasculature*. Angiogenesis, 2007. **10**(2): p. 77-88.
65. Jensen, U.B., S. Lowell, and F.M. Watt, *The spatial relationship between stem cells and their progeny in the basal layer of human epidermis: a new view based on whole-mount labelling and lineage analysis*. Development, 1999. **126**(11): p. 2409-18.
66. Rehberg, M., et al., *Quantum dots modulate leukocyte adhesion and transmigration depending on their surface modification*. Nano Lett, 2010. **10**(9): p. 3656-64.
67. Khandoga, A.G., et al., *In vivo imaging and quantitative analysis of leukocyte directional migration and polarization in inflamed tissue*. PLoS One, 2009. **4**(3): p. e4693.
68. Adams, R.H. and K. Alitalo, *Molecular regulation of angiogenesis and lymphangiogenesis*. Nat Rev Mol Cell Biol, 2007. **8**(6): p. 464-78.
69. Petrovic, N., *Targeting Angiogenesis in Cancer Treatments: Where do we Stand?* J Pharm Pharm Sci, 2016. **19**(2): p. 226-38.
70. Stevenson, R.P., D. Veltman, and L.M. Machesky, *Actin-bundling proteins in cancer progression at a glance*. J Cell Sci, 2012. **125**(Pt 5): p. 1073-9.
71. Stehn, J.R., et al., *A novel class of anticancer compounds targets the actin cytoskeleton in tumor cells*. Cancer Res, 2013. **73**(16): p. 5169-82.
72. Oertel, M., et al., *Repopulation of rat liver by fetal hepatoblasts and adult hepatocytes transduced ex vivo with lentiviral vectors*. Hepatology, 2003. **37**(5): p. 994-1005.
73. Malan, D., et al., *Endothelial beta1 integrins regulate sprouting and network formation during vascular development*. Development, 2010. **137**(6): p. 993-1002.
74. Stenzel, D., et al., *Endothelial basement membrane limits tip cell formation by inducing Dll4/Notch signalling in vivo*. EMBO Rep, 2011. **12**(11): p. 1135-43.
75. Huang, A.H., et al., *PARVA promotes metastasis by modulating ILK signalling pathway in lung adenocarcinoma*. PLoS One, 2015. **10**(3): p. e0118530.
76. Carmeliet, P. and R.K. Jain, *Principles and mechanisms of vessel normalization for cancer and other angiogenic diseases*. Nat Rev Drug Discov, 2011. **10**(6): p. 417-27.
77. Vahatupa, M., et al., *Lack of R-Ras Leads to Increased Vascular Permeability in Ischemic Retinopathy*. Invest Ophthalmol Vis Sci, 2016. **57**(11): p. 4898-4909.
78. Phng, L.K., et al., *Nrarp coordinates endothelial Notch and Wnt signaling to control vessel density in angiogenesis*. Dev Cell, 2009. **16**(1): p. 70-82.
79. Yamamoto, H., et al., *Integrin beta1 controls VE-cadherin localization and blood vessel stability*. 2015. **6**: p. 6429.
80. Berger, W., *Molecular dissection of Norrie disease*. Acta Anat (Basel), 1998. **162**(2-3): p. 95-100.
81. Pignatelli, J., et al., *Actopaxin (alpha-parvin) phosphorylation is required for matrix degradation and cancer cell invasion*. J Biol Chem, 2012. **287**(44): p. 37309-20.

DANKSAGUNG:

Ich möchte mich an erster Stelle recht herzlich bei Prof. Ulrich Pohl bedanken, welcher mir durch die Annahme als Doktorandin am Walter-Brendel-Zentrum für experimentelle Medizin, die Möglichkeit gegeben hat, dort wissenschaftlich unter seiner Leitung tätig zu werden.

Ein ganz besonderer Dank sei Dr. Eloi Montanez ausgesprochen, welcher mir mit seinem Fachwissen und seinen ausgezeichneten Ideen immer zur Seite stand, mit mir ausgiebig diskutiert hat, mir in privaten Gesprächen sehr geholfen hat und mir das breite Spektrum der Laborarbeit und wissenschaftlichen Tätigkeit geduldig gelehrt und vermittelt hat.

Mein Dank geht auch an Brigitte Bergner, unsere MTA, und Bettina Pitter, meine Mitdoktorandin, für ihre tatkräftige Unterstützung, sowie den restlichen Doktoranden des Walter-Brendel-Zentrums, u.a. Julian Kirsch, für die wundervolle und freundschaftliche Unterstützung während unserer gemeinsamen Zeit.

Für die bedingungslose Unterstützung möchte ich mich nicht zuletzt bei meiner Familie und meinen Freunden bedanken, die mich das ganze Studium über unterstützt haben und mir immer ein Rückhalt waren.